JOURNAL OF THE
AERO/SPACE SCIENCES

VOLUME 26 MARCH, 1959 NUMBER 3

MECHANICAL ENGINEERING
MAR 16 1959
LIBRARY
PURDUE UNIVERSITY
MAR 17 1959
LIBRARY

CONTENTS

Some Significant Developments in Aerodynamics Since 1946 (The First Daniel and Florence Guggenheim Memorial Lecture).....THEODORE VON KÁRMÁN 129

Direct-Analog Method of Analysis of the Influence of Aerodynamic Heating on the Static Characteristics of Thin Wings.....MICHAEL A. BASIN, RICHARD H. MACNEAL, AND JOHN H. SHIELDS 145

Investigation of Normal Force Distributions and Wake Vortex Characteristics of Bodies of Revolution at Supersonic Speeds.....J. F. MELLO 155

On the Flow of a Sonic Stream Past an Airfoil Surface.....COLIN S. SINNOTT 169

On the Base Pressure Resulting From the Interaction of a Supersonic External Stream With a Sonic or Subsonic Jet.....W. L. CHOW 176

Readers' Forum..... 181

Published by
INSTITUTE OF THE AERONAUTICAL SCIENCES, INC.

JOURNAL OF THE AERO/SPACE SCIENCES

Editor: W. R. SEARS
Director, Graduate School of Aeronautical Engineering, Cornell University

Associate Editor: ROBERT R. DEXTER *Managing Editor:* RITA J. TURINO
Editorial Assistant: CAROLINE TAYLOR

Editorial Committee

Aerodynamics and Fluid Mechanics

H. Julian Allen
Holt Ashley
Dean R. Chapman
Francis H. Clauser
Hugh L. Dryden
John C. Evvard
Antonio Ferri
Alexander Flax
Wallace D. Hayes
R. T. Jones
Carl Kaplan
H. W. Liepmann
C. C. Lin
H. F. Ludloff
Harold Luskin
Clark B. Millikan
Henry T. Nagamatsu
H. J. E. Reid
George S. Schairer
G. B. Schubauer
John Stack
Theodore Theodorsen
Arthur N. Tifford
Th. von Kármán

Flight Testing

R. R. Gilruth
Melvin N. Gough
W. L. Howland
W. F. Milliken, Jr.

Rotating Wing Aircraft

F. B. Gustafson
K. H. Hohenemser
Bartram Kelley
R. B. Maloy
Ralph McClarren
R. H. Miller
R. H. Prewitt
Igor I. Sikorsky

Structures

John E. Duberg
R. R. Heldenfels
N. J. Hoff
Samuel Levy
J. F. McBrearty
W. Ramberg
E. E. Sechler
F. R. Shanley
C. R. Strang
S. Timoshenko

Meteorology

C. F. Brooks
D. M. Little
F. W. Reichelderfer
K. C. Spengler

Vibration and Flutter

Lee Arnold
M. A. Biot
R. L. Bisplinghoff
Harold A. Cheilek
I. E. Garrick
Martin Goland

Aircraft Design

W. E. Beall
E. H. Heinemann
Hall L. Hibbard
Richard Hutton
C. L. Johnson
A. A. Kartveli
F. K. Teichmann

Electronics

K. C. Black
M. V. Kiebert, Jr.
David S. Little
Paul Rosenberg
Giles J. Strickroth

Physiologic Problems

H. G. Armstrong
Louis H. Bauer
Robert J. Benford
W. Randolph Lovelace, II
Ross A. MacFarland

Flight Propulsion

William Bollay
George W. Brady
R. P. Kroon
Frank E. Marble
Abe Silverstein
E. S. Taylor

Instruments

Alan G. Binnie
Charles H. Colvin
Frank R. Cook
C. S. Draper
S. G. Eskin
C. F. Savage
R. C. Sylvander

SUBSCRIPTION RATES

JOURNAL OF THE AERO/SPACE SCIENCES (formerly Journal of the Aeronautical Sciences), Published Monthly. United States and Possessions: 1 Year, $15.00; Single Copies, $1.50. Foreign Countries Including Canada (American Currency Rates): 1 Year, $16.00; Single Copies, $1.50.

AERO/SPACE ENGINEERING, Published Monthly. United States and Possessions: 1 Year, $5.00; Single Copies, $0.50. Foreign Countries Including Canada (American Currency Rates): 1 Year, $6.00; Single Copies, $0.50.

Notices of change of address should be sent to the Institute at least 30 days prior to actual change of address.

Manuscripts for publication, proofs, and all correspondence should be addressed to the Editorial Office of the JOURNAL.

Publication Office, 20th and Northampton Sts., Easton, Pa. Correspondence regarding subscriptions may be addressed to the Editorial Office of the JOURNAL OF THE AERO/SPACE SCIENCES, 2 East 64th Street, New York 21, N.Y.

© Copyright, 1959, by the Institute of the Aeronautical Sciences, Inc.

Second-Class Mail Privileges Authorized at Easton, Penna. Acceptance for mailing at a special rate of postage provided for in Section 1103, Act of October 3, 1917, authorized April 29, 1937

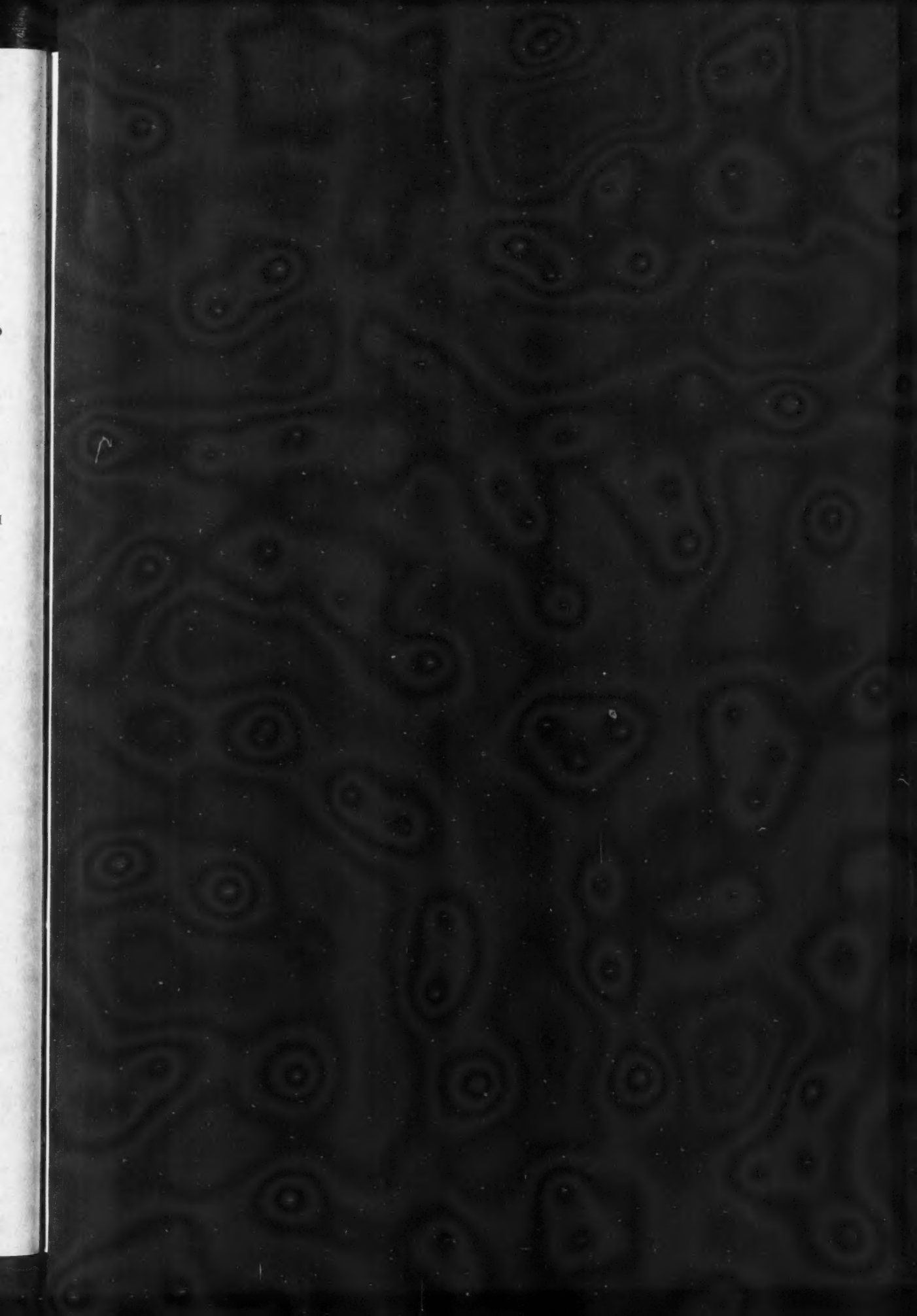

JOURNAL OF THE AERO/SPACE SCIENCES

VOLUME 26 MARCH, 1959 NUMBER 3

Some Significant Developments in Aerodynamics Since 1946

The First Daniel and Florence Guggenheim Memorial Lecture

THEODORE VON KÁRMÁN*

IT IS A GREAT HONOR and pleasure for me to give the first Daniel and Florence Guggenheim Memorial Lecture before this distinguished international gathering. The name Guggenheim will be connected forever in the history of aviation with the development of the aeronautical sciences. In fact, the Daniel Guggenheim Fund for the Promotion of Aeronautics, which Daniel Guggenheim established in 1926, gave a great impetus to education and research at a number of American universities. I am personally indebted to the Guggenheim family by the fact that my change of continents from Europe to America originated with Daniel Guggenheim and Robert A. Millikan, world-famous physicist and then head of the California Institute of Technology. The story, as I learned it from R. A. Millikan, was that, in 1926, as the Daniel Guggenheim Fund started to distribute grants to several colleges for the purpose of forming graduate schools for aeronautics, Millikan undertook a trip to Long Island where Mr. Guggenheim lived. During his visit with Mr. Guggenheim, Millikan told him that he would make the greatest mistake of his life if a sizable chunk of the money of the Fund did not go to California. California would be, Millikan insisted, in the near future, the most important center of American aircraft production, due to climatic conditions and availability of space for flying establishments. Mr. Guggenheim answered that he would provide the funds for a graduate school if Millikan would bring to Pasadena from Europe someone familiar with and active in aeronautical research, and especially familiar with the theoretical side of research. In this way I received a call to come to the United States. I was told later that Robert A. Millikan said, "First I aimed at Prandtl—then I settled on Kármán." Prandtl was, without doubt, the leading genius in the early development of modern aerodynamics.

Daniel Guggenheim was a man of great vision and lively interest in progress in aeronautics. I remember that after I went through the United States visiting all the places where Guggenheim funds were invested for the promotion of aeronautical science, he asked me what he should do in addition to supporting the schools, so that aeronautical science would flourish in the United States as it had grown and brought ripe fruits in several European countries during the first two decades of our century. I suggested that it would be extremely desirable to have a kind of Handbook of Aerodynamic Theory that would lay down the present state of fundamental aeronautical knowledge, so that young American scholars would know from which point to start. Then I said jokingly, "In Europe it was very helpful that young scientists could meet in quiet cafés for informal discussions. Unfortunately there is no equivalent institution in the United States." Mr. Guggenheim answered, "All right, I shall provide the money for the book." (As a matter of fact, this was the origin of Durand's "Aerodynamic Theory," a collective work based on international authorship which has had a great influence on the development of American scientific literature in the field of Aerodynamics.) "However," he continued, "I will not go into the cafeteria business—even for science's sake!"

Daniel Guggenheim, born in Philadelphia in 1856, was of the second generation in the leadership of the large Guggenheim enterprises in mining and affiliated industries. His son, our great friend Harry, once told me jokingly that, in his grandfather's time, a really good man, in order to be recognized as such, had to create a great fortune. When his father was in business, the main duty was to broaden the scope and to maintain

Presented before the First International Congress of the Aeronautical Sciences, Madrid, Spain, September 8, 1958.

* Chairman, AGARD, NATO. Also, Honorary President, International Council of the Aeronautical Sciences.

the level of the enterprises. "Of me," he said, "they only expect that I spend the money usefully and gracefully."

I am sure that this formulation of Harry F. Guggenheim's activities is extremely modest. He has an impressive record of public service; he was a successful ambassador of the United States to Cuba. There is no doubt that his interests in aeronautics and his personal experience in aviation, especially as a naval aviator during the first World War, were the decisive factor for Daniel Guggenheim's donations being directed toward the promotion of the aeronautical sciences. Also, the organization of the Safe Aircraft Competition in 1930, the active support of Professor Goddard's early efforts in rocket research, and the establishment of the Daniel and Florence Guggenheim Jet Propulsion Centers at C.I.T. and Princeton University, the Institute of Flight Structures at Columbia University, and the Center for Aviation Health and Safety at Harvard are far beyond the qualification "spend the money usefully and gracefully." They are proofs of an extraordinary vision for the kind of education and research needed for the progress of aviation. And last but not least, this "First International Congress for the Aeronautical Sciences" owes its birth not only to the donation of funds by the Daniel and Florence Guggenheim Foundation, but in the first place to the initiative and desire of Harry F. Guggenheim to spend the money for the organization of an international congress open to scientists and engineers of all the nations of the globe which have an association or group devoted to the aeronautical sciences.

I shall now proceed to the technical part of my lecture.

For my review of progress in aerodynamics I would like to choose as a point of departure my Wright Brothers lecture delivered on December 17, 1946. I wrote at that time:

"I believe we have now arrived at the stage where knowledge of supersonic aerodynamics should be considered by the aeronautical engineer as a necessary prerequisite to his art. This branch of aerodynamics should cease to be a collection of mathematical and half-digested, isolated, experimental results. The aeronautical engineer should start to get the same feeling for the facts of supersonic flight as he acquired in the domain of subsonic velocities by a long process of theoretical study, experimental research, and flight experience."

I have the impression that this goal has generally been achieved. There has been rapid progress in the theory of supersonic wings, bodies, and wing-body combinations exposed to supersonic flow, and this progress has been reported in the scientific literature. Experimental work has been carried out in newly created facilities in governmental and industrial laboratories. Finally, advanced students have had improved training at our aeronautical schools. As a result of these developments, a number of engineering firms now have at their disposal large staffs with the necessary grasp and appreciation of the main features of supersonic aerodynamics. As a matter of fact, some of our supersonic bombers have been designed on the basis of more detailed aerodynamic calculations than was possible in the case of the best subsonic aircraft.

However, the honeymoon was short. Soon, new problems were facing the aeronautical engineer, who nowadays is pleased to call himself a missile engineer or even a space technologist.

The problem of ballistic missiles led us to the range of hypersonic speeds, to speeds which are not only comparable with sound velocity but are greater by an order of magnitude than the velocity of sound. At first sight, the hypersonic range introduces certain simplifications into the flow problem; as a matter of fact, it was pointed out as early as 1931 by P. S. Epstein, in a paper devoted to the problem of the drag of artillery projectiles, that for very large Mach Numbers the classical Newtonian law of air resistance becomes valid. At that time, and even at the time of the memorable Volta Congress for High Speed, held at Rome, in 1935, high Mach Numbers belonged to the realm of academic speculation.

The simplification introduced by very high Mach Numbers is largely overbalanced by the complications due to the high temperatures caused by shock and friction. The production of heat, an annoyance in flight at moderate Mach Numbers, becomes a major problem at hypersonic speeds. Furthermore, and as a new complication, one has to take into account the chemical changes in the air, such as dissociation and recombination. No longer are we dealing with pure aerodynamics, nor aerothermodynamics; fluid mechanics must now be combined not only with thermodynamics, but also with chemistry.

I suggested the term *aerothermochemistry* for the combination of these three disciplines. I had mainly in mind problems related to combustion, like flame theory, the theory of quenching, and the like. Hypersonics has now made it necessary to consider chemical reactions which occur without having been planned by the chemical engineer.

Recently, another combination of various disciplines has attracted considerable attention—fluid mechanics and the theory of the electromagnetic field. Some aspects of the motion of conducting liquids acted upon by electromagnetic forces were investigated several decades ago. I also remember that Albert Einstein gave some thought to a thoroughly practical problem in this field: he proposed the design of a refrigerator in which the coolant, for example a liquid metal, would be kept in circulation by an imposed electromagnetic field. He wanted to avoid the use of machinery which needs lubrication. However, the main interest in "magnetofluidmechanics" arose from celestial problems, such as the structure and the motions of galaxies, wave motions and turbulence in cosmic systems and the like. Questions of space flight and problems related to the possible utilization of thermonuclear reactions led to increasing interest in "plasmadynamics." I believe that a systematic nomenclature and classification of these new

branches of combined fluidmechanics, electromagnetic theory and thermodynamics is still lacking. Nevertheless, I believe that in a review of advances of aerodynamics, they should at least be mentioned.

A detailed list of references is appended hereto. I now want to restrict myself to making some comments on some accomplishments in aerodynamics which, I believe, are most significant. One general remark may precede this. It is remarkable how far one can go with the so-called linear theory of supersonic flow, and how many useful conclusions for aircraft design can be derived from this simplified theory which, after all, is nothing else than "acoustics"—i.e., it is based on the assumption that the flow is composed of a uniform parallel flow and a perturbation flow of small magnitude.

(I) Wing Theory

In a paper published in 1946, A. E. Puckett applied the method of singularities, which I had introduced jointly with N. B. Moore, into the first theory of supersonic flow around axially symmetric bodies. We used supersonic sources distributed along the axis of the body. H. S. Tsien introduced doublets (dipoles) in order to include lift in the theory for the case of a body of revolution with angle of attack. These supersonic sources and doublets are formulated in such a way that their effect is restricted to the interior of a Mach cone, the apex of which is the point of singularity. Thus, the solution is essentially identical with the solution of a time-dependent two-dimensional acoustic problem, where the length coordinate in the flow direction replaces the time coordinate of the acoustic phenomena.

Subsonic wings are mostly calculated by means of the concept of the lifting line. Only in a few cases did it prove possible to solve the problem of the lifting surface. However, for the supersonic case, the situation is more favorable. Especially if both the leading and trailing edges are of the supersonic type—i.e., if the components of the flight speed normal to the edges are greater than sound velocity—the local slope of the wing determines directly the required distribution of sources over the wing plan form. These singularities, together with the condition that in undisturbed flow the pressure is equal to the ambient pressure, completely determine the disturbance potential.

Two complications occur if some portions of the perimeter of the wing plan form are edges of the subsonic type:

For the case of a subsonic leading edge, the flows on the upper and the lower surfaces near the edge are no longer independent. The fluid flows around the edge with subsonic velocity, and one obtains a leading-edge suction which has to be calculated. Furthermore, in the sector enclosed between leading edge and limiting Mach line, the pressures resulting from the upper and lower half spaces must be balanced.

In the case of a subsonic trailing edge the Kutta-Joukowski condition has to be satisfied; in other words, the velocity components normal to the edge on the upper and the lower surface must be equalized. This makes it necessary to compute and compensate the velocities induced by the trailing vortices in certain sectors of the plan form.

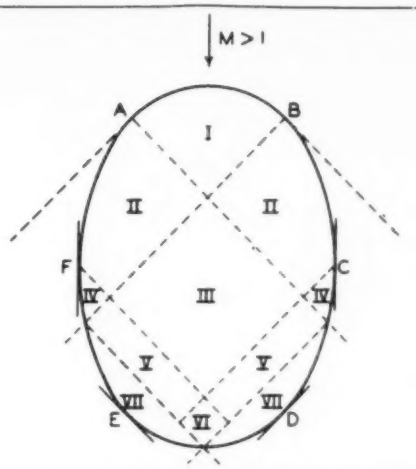

Fig. 1. Plan form of elliptic supersonic wing.

Fig. 1 is reproduced from an excellent review of the supersonic wing theory published by R. T. Jones and Doris Cohen in Volume VII of the Princeton series "High Speed Aerodynamics and Jet Propulsion." The Figure shows, for the case of an elliptic plan form, the various domains which have to be treated in different ways. Sector I has a supersonic leading edge and is not influenced by any other portion of the wing plan form. Hence, the Puckett method can be applied directly. Sector II has subsonic leading edges; Sectors IV, V, VI, and VII are evidently influenced by the trailing vortices leaving the subsonic trailing edges $\overline{FE}$ and $\overline{CD}$. The vortex wake can be built up by superposition of horseshoe vortices (Fig. 2). The Figure also shows the domain in which the flow is influenced by such a vortex.

The problem of the partially subsonic leading edge was resolved in an ingenious way by a method apparently independently proposed by J. C. Evvard in the United States and E. A. Krasilshchikova in the USSR.

Before that, H. J. Stewart treated the special case of the delta wing with subsonic straight leading edges by means of the method of conical flows. This method, originally suggested by A. Busemann, became one of the most powerful methods of supersonic aerodynamics. It reduces the problem of three-dimensional flow to a two-dimensional problem which can be solved by means of Laplace's equation.

For example, R. Legendre of France and M. C. Adams, C. E. Brown, W. H. Michael, and R. H. Edwards of the United States treated the case of delta wings with flow separation at the apex as an example of conical flow.

The linearized wing theory made it possible for R. T. Jones to arrive at a series of important results concerning the minimum drag of supersonic wings. He made very ingenious use of the concepts of the reverse flow and the combined flow. In earlier studies I had found that the drag of a thin wing due to thickness remains

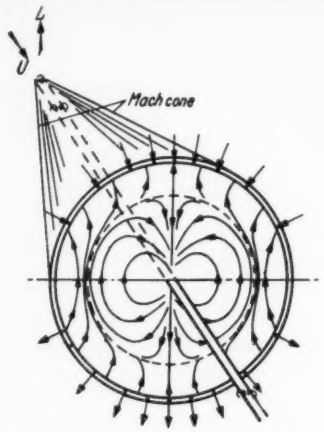

FIG. 2. Horseshoe vortex in supersonic flow.

unchanged if we reverse the flight direction. If we superpose both perturbations, which correspond to the two opposite flight directions, on one parallel uniform flow we arrive at a so-called combined flow. Using this concept and the fact that the drag is independent of the flight direction, R. T. Jones has shown that the drag of a symmetric flat wing of given plan form reaches a minimum if the thickness is distributed over the plan form in such a way that the drag per unit volume is equal for every wing element.

Jones also investigated the condition for the minimum of the drag caused by lift. He found that the optimum lift distribution over a given plan form is such that the downwash is constant over the plan form. It is evident that this result is a kind of generalization of Munk's rule for the optimum distribution of lift along a lifting line, which leads to the elliptical distribution in classical subsonic wing theory.

Many special cases have been investigated from the viewpoint of minimizing drag. Thus, Doris Cohen has shown that, for triangular wings with subsonic edges, the minimum drag due to lift is obtained by using negative spanwise camber over most of the plan form. It is interesting that the idea of conical chamber was used in the design of the wing of the Convair B-58 bomber (also called the Hustler). This development is attributed to C. F. Hall (Ames Laboratory). It is seen from the experimental results represented on Fig. 3 that the conical camber produces leading-edge suction and thus essentially reduces drag.

(II) Slender Wings and Aircraft

With the increase of the speeds of flight, aircraft in general became more and more slender; large aspect ratios disappeared, and present-day aircraft mostly consist of long bodies and wings of small aspect ratios. For such cases, the application of the linearized theory had to be revised. Considerable confusion had been caused by formal application of the Prandtl-Glauert rules for compressibility effects to bodies of revolution and slender wings and bodies in general. This question was clarified by Goethert and others in a satisfactory way. It was shown that the similarity theory of compressible flow which was correct for wings of large aspect ratio gives false results for slender bodies. It was also shown by M. J. Lighthill and G. N. Ward that the computation of the pressure based on the axial component of the disturbance velocity is inexact, since, for example, in the case of axisymmetric bodies, the influence of the radial velocity is often larger. Hence, it became necessary to describe the flow by the appropriate singularities and to compute the pressure including the quadratic terms of the disturbance velocities. In

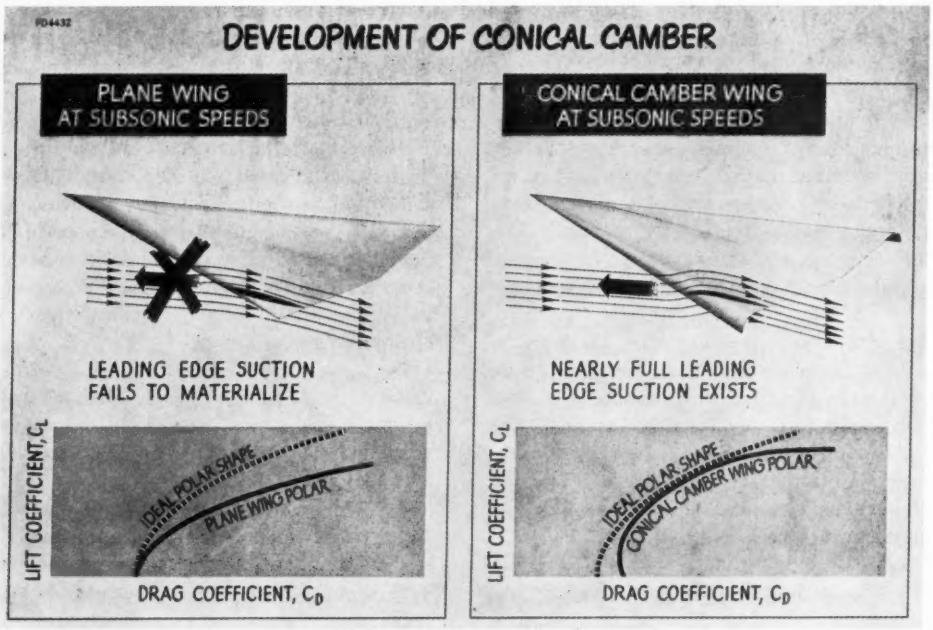
DEVELOPMENT OF CONICAL CAMBER
PLANE WING AT SUBSONIC SPEEDS
LEADING EDGE SUCTION FAILS TO MATERIALIZE
IDEAL POLAR SHAPE
PLANE WING POLAR
LIFT COEFFICIENT, C_L
DRAG COEFFICIENT, C_D
CONICAL CAMBER WING AT SUBSONIC SPEEDS
NEARLY FULL LEADING EDGE SUCTION EXISTS
IDEAL POLAR SHAPE
CONICAL CAMBER WING POLAR
LIFT COEFFICIENT, C_L
DRAG COEFFICIENT, C_D

FIG. 3. Development of conical camber.

order to simulate the flow around bodies which are neither thin wings nor axisymmetric bodies, multipoles have to be introduced.

A great simplification was achieved by extension of Munk's classical airship theory to slender bodies in general both for subsonic or supersonic speeds by R. T. Jones. This theory assumes that the flow around a slender body (wing or aircraft) can be considered as a superposition of a parallel uniform flow and a sequence of two-dimensional flows in planes perpendicular to the flight direction as shown in Fig. 4. To some extent this is the opposite of Prandtl's classical assumption for his wing theory. As a matter of fact, for wings of large aspect ratios it was assumed that the flow in planes perpendicular to the wing axis can be identified with a two-dimensional flow with circulation around the wing section.

The slender-body theory in general gives a better approximation to the pressure, forces, and moments acting on the system than the pure linearized theory.

(III) Interference Effects

We shall now consider interference effects between the wing and the body structures of the airplane which are necessary to carry payload, passengers, or fuel. The most significant example of favorable interference is the arrangement popularly known as the *area rule*. W. D. Hayes has shown in his doctoral thesis at the California Institute of Technology that the resulting flow around a system consisting of bodies and thin wings can, at large distances, be represented as originating from singularities distributed along the axis. At Mach Numbers near one the drag is that caused by a single equivalent body of revolution. Now we know—for example, according to the theories of W. Haack and W. R. Sears—the shape of the most favorable bodies of revolution as far as minimum drag is concerned. Thus, the components of the aircraft can be arranged so that, at least for a given Mach number, the equivalent body of revolution approaches the shape corresponding to minimum drag. This principle of equivalence was clearly stated by Hayes and was extended by K. Oswatitsch to the nonlinear case; the extension is important because of the limitations of linearized theory near sonic speed. The principle leads, for example, to the conclusion that in the case of nacelles arranged near the fuselage the additional drag of the nacelles can be compensated by a reduction of the diameter of the fuselage in the appropriate section. We obtain in this way the shape of the fuselage known popularly as the "Marilyn Monroe body." The name "area rule" originates from the fact that for a flow near Mach one the section of the equivalent body of revolution is simply equal to the sum of the areas cut out by a plane laid through the section considered. The agreement of these theoretical ideas with drag measurements was conclusively shown by Richard Whitcomb.

Another class of interference phenomena makes it possible to create favorable interference by reflection of

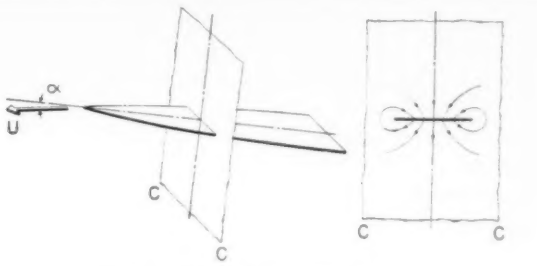

Fig. 4. Wing of low aspect ratio.

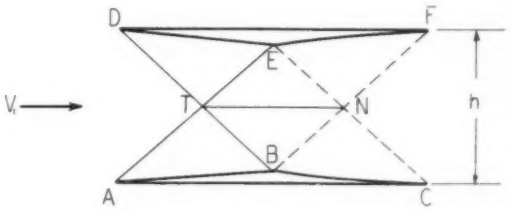

Fig. 5. Busemann biplane.

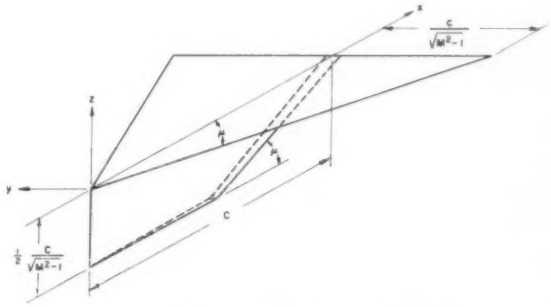

Fig. 6. Wedge-wing lifting configuration.

compression and expansion waves on components of a lifting system.

The oldest example for such a procedure is the so-called Busemann biplane (see Fig. 5). In this case we may transfer pressure from one wing to the rear portion of the other wing (for example, from $\overline{AB}$ to $\overline{EF}$ and from $\overline{DE}$ to $\overline{BC}$), so that the pressures acting on the forward and rear portions of the inner surface are balanced. Thus, the drag due to thickness effect can be eliminated, and we gain volume without additional drag.

An interesting example of similar favorable interference effects is represented by a combination of a horizontal delta wing and a vertical surface of wedge shape arranged below the wing parallel to the flight direction (Fig. 6). One can transfer the pressure created on the surface of the vertical wedge to the lower surface of the wing. Thus the total lift is increased, and one can show that the resulting lift/drag ratio is more favorable than for the case of a simple horizontal wing that would furnish the same lift.

(IV) Aeroelastic Theories

Concerning aeroelastic problems like flutter at high flying speeds, we have to mention the so-called "piston theory" initiated by M. J. Lighthill and worked out by

Holt Ashley and others. This theory assumes that the magnitude of the reaction of a high-speed flow on a wing surface can be approximated at every instant by considering the one-dimensional motion of an air column under the action of a moving piston. It seems that for Mach Numbers superior to $M = 1.5$ this approximate theory furnishes usable results and greatly simplifies the computations.

(V) Nonlinear Theories—Higher-Order Approximations

It is not possible to enter into exact discussion of the highly intricate mathematical problems connected with the development of higher-order approximations for a solution of the equations of supersonic flow even for the cases of plane and axisymmetric motions. However, the main trends of the pertinent approaches will be indicated.

For the purpose of a two-dimensional airfoil theory, Ackeret's fundamental and simple results correspond to a linearized theory. At a relatively early date (1935), Busemann showed the possibility of obtaining a correction of second order in the perturbance velocities, and in 1948 K. Friedrichs provided a means for obtaining shock shapes to the same degree of approximation. Therefore, a rather complete and accurate theoretical treatment of the two-dimensional airfoil problem is available. This applies as long as the effects of entropy changes are relatively unimportant. For practical airfoil shapes the condition seems to be satisfied up to Mach Numbers of 5 or 6. Above this limit, temperature and real-gas effects make the application of ideal-gas laws illusory anyway.

The attempts to develop higher approximations for three-dimensional flows, at least for specific cases, are reviewed by M. J. Lighthill in his article "Higher Approximations" published in Section E, Vol. VI of the Princeton series.

In the linearized theory, simplifications are introduced in three aspects of the problem: first the equation of motion is only approximately correct; second, the boundary conditions at the body are simplified; and third, the pressure is computed on the basis of a simplified relation between pressure and velocity components. The simplest idea is to keep the linearized character of the equation of motion, but to correct the boundary conditions and the pressure-velocity relations. One is tempted to call such theories "hybrid" theories. In general, the procedure leads to results which are in better agreement with exact solutions and/or the experimental evidence, but it can work also in the opposite sense.

J. B. Broderick and M. D. Van Dyke worked out second-order solutions on the basis of this general idea; Van Dyke uses the first-order linearized solutions as a starting point, whereas Broderick starts from the slender-body solution.

One of the main weaknesses of the linearized theory is the fact that it describes the flow quite inexactly at a certain distance from the body or wing In fact, according to the linearized theory the characteristic lines are always straight lines, and their inclination corresponds to the Mach Number of the undisturbed flow. G. B. Whitham has provided a relatively simple procedure for improving the flow-field representation. He assumes that the flow variables predicted by the linearized theory are satisfactorily exact as far as their magnitude is concerned, but must be relocated spatially according to a corrected Mach wave shape. He uses the first-order corrections obtained from the linearized theory for the local sonic velocity and the values for the total velocity obtained from the same theory, and uses these data to construct corresponding Mach waves, including eventual shock surfaces.

The Whitham theory, in which the positions of the Mach waves are changed without changing the values of the flow variables, can be considered as a special case of the general method or "technique" introduced by Lighthill, which he calls a "technique for rendering approximate solutions to physical problems uniformly valid." In this technique—which is based on the methods used by H. Poincaré in his investigations on celestial mechanics—in addition to developing the dependent unknowns in series of successive terms as functions of some parameters, the independent variables or a number of independent variables are also developed as functions of the same parameters. By this trick, in domains where the dependent variables have a singular behavior as functions of the independent variables, they become easy to handle as functions of the new parameter which is used for a series development of the independent variable itself. This technique has proved especially useful in some boundary-layer problems which we shall mention later. As far as applications to nonviscous problems are concerned, the treatment of the mixed flow (hyperbolic and elliptic) about a sharp-edged conical wing by R. Vaglio-Laurin is worth mentioning.

In connection with higher-order approximations, we have to mention also the so-called linearized method of characteristics used by A. Ferri to build up three-dimensional flow fields from nonlinear two-dimensional flow fields which are known by application of classical characteristic methods as used in two-dimensional supersonic aerodynamics since the fundamental works of Prandtl. Ferri finds that the characteristic surfaces of the three-dimensional flow field can be approximated by the envelopes of the characteristic surfaces of the system of two-dimensional flow fields. Hence the analysis of the three-dimensional flow is reduced to that of a flow field with given characteristic surfaces.

(VI) Transonic Flow

The transonic case is characterized by the fact that the difference between flight velocity U and sound velocity c; i.e., the quantity $(U - c)$; is small in comparison with either U or c. It is known that, at least in the case of a two-dimensional flow, for the disturbance po-

tential we arrive at a relatively simple nonlinear equation called Tricomi's equation:

$$(1 - M_\infty^2(\partial^2\varphi/\partial x^2) + (\partial^2\varphi/\partial y^2) = (\gamma + 1)\,(M_\infty/c_\infty)\,(\partial\varphi/\partial x)\,(\partial^2\varphi/\partial x^2)$$

where M_∞ denotes the Mach Number of the main flow, C_∞ the sound velocity at infinity, and γ the ratio of the specific heats. The nonlinear term of this equation contains the product $(\partial\varphi/\partial x)\,(\partial^2\varphi/\partial x^2)$; Oswatitsch and Keune proposed to replace the derivative of the u component of the horizontal velocity, $\partial^2\varphi/\partial x^2$, by a value which is taken as independent of the coordinate y, but may vary stepwise as we proceed along the flow.* They arrived in this way at very useful results for computation of transonic flows around wings and bodies.

To a certain extent, useful results have been achieved for transonic flow calculations by the so-called Kármán-Tsien method, which introduced a "hypothetic fluid" with a simplified pressure-density relation, valid in a limited Mach number range. This idea was further developed and improved by S. Tomotika and K. Tamada.

On the other hand, theoretical studies concerning exact solutions of the Tricomi equation—such as the problem of uniqueness of the solution and the questions: in which cases do we obtain continuous solutions and in which cases do shocks appear?—have not progressed sufficiently in the last ten years.

In an attempt to obtain approximate but useful solutions of transonic flow problems, one replaces the differential equation for the disturbance potential by a system of difference equations. K. Friedrichs and his collaborators used this method; they put the problem into a computing machine. If the problems are properly formulated for the computing device, one can obtain fair approximations even for flows containing discontinuities (shocks) without an elaborate discussion concerning the existence or nonexistence of continuous solutions. Such formulations can also be used in the case of detached shocks in hypersonic flow around blunt bodies.

(VII) Hypersonic Flow

The hypersonic speed range is characterized by the fact that the sonic velocity c is small compared with the flight velocity U. The interest in this speed range was recently very much enhanced by the problems connected with missile design, especially with the design of re-entry vehicles and nose cones.

If we first consider the flow against an inclined surface, for example, the case of a wedge with small apex angle, the theory of inviscid fluids predicts attached and straight shock waves which slightly deflect the flow so that the streamlines practically become parallel to the wedge surfaces. Hence the flow picture is very similar to that assumed in the model treated by Isaac Newton. The essential difference is that according to Newton's model the fluid particles move in parallel straight lines until they hit the surface and then are deflected into a motion along the body surface, whereas according to the ideal-flow theory they are deflected at the shock surface which, however, lies very near to the body surface. Thus, for a small angle of inclination, both for the case of the two-dimensional wedge and that of the axisymmetrical cone, we obtain the result that the pressure acting on the surface element is given by

$$p = (\rho/2)U^2 \cdot 2\sin^2\beta$$

where ρ is the density in the undisturbed fluid, U the velocity of the same, and β the angle of inclination of the surface.

We may call a flow of this nature a Newtonian flow. The actual evidence is, of course, strongly modified by two factors. First, the presence of the solid surface produces viscous effects—i.e., a boundary layer; and second, no mathematically exact sharp edge exists, and, therefore, one always obtains a kind of detached shock with very large curvature near the front portion. The real picture of the flow therefore looks more like the one for the case of a body with a blunt edge, where the "equivalent body" corresponds in a broad sense to the domain occupied by the boundary layer. This description even applies to the flow observed in the case where the undisturbed flow is parallel to one surface of the unsymmetric wedge (see Fig. 7). Furthermore, the large curvature of the detached shock wave introduces vorticity in the inviscid domain of the flow between the shock and the boundary layer.

Nevertheless, the rules of Newtonian flow can be accepted as fair approximations for two- and three-dimensional flows. If the body surface is curved, the flow in the inviscid region is necessarily curved and a correction for the Newtonian law can be obtained by computing the effect of "centrifugal forces" between the shock and the body surface. Such a correction was suggested by A. Busemann at an early date (*Handbuch der Naturwissenschaften*, 1933) and recently further developed by H. R. Ivey and R. R. Morisette, and further by H. R. Ivey, E. B. Klunker, and E. N. Bowen.

If we consider a blunt body—for example, a cylindrical or spherical body exposed to a flow hitting the body normal to its surface—two considerations have to be introduced.

First, the value of the pressure at the stagnation point is, strictly speaking, unknown, since it is influenced by the thermodynamic process. This was unknown to Newton, as is evident if we consider that he computed the sound velocity, for example, assuming an isothermal compression process.

In fact, there are in addition changes in the distribution of the thermal energy between the several kinds of degrees of freedom in the gas molecules; at the high temperatures produced by the shock we certainly will encounter dissociation and recombination of atoms. Heat-transfer effects will modify the temperature and pressure distribution between the shock and the surface.

The second consideration, which further complicates the problem, is the fact that we have a mixed-flow prob-

* This idea has been developed further by J. R. Spreiter.

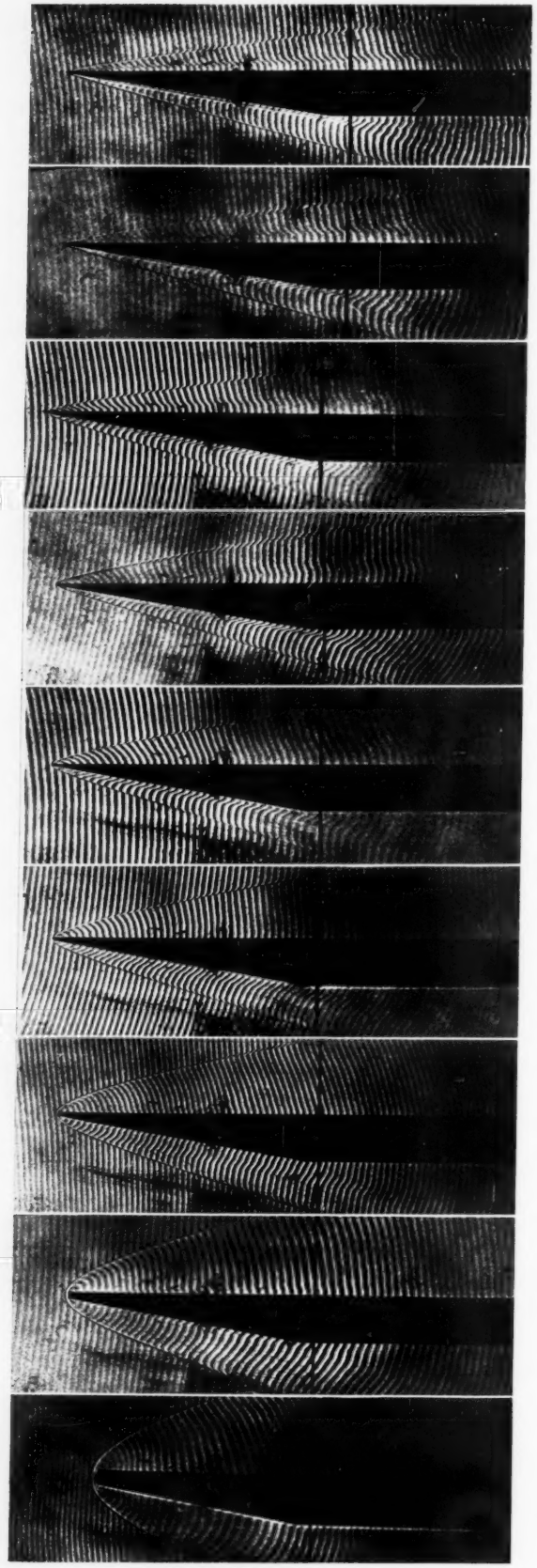

lem. Whereas, in the case of the sharp wedge or ogive, the flow in the inviscid region was supersonic on both sides of the shock wave, we now have downstream of the shock a subsonic region followed by a supersonic domain.

Nevertheless, if we consider the general type of flow shown schematically in Fig. 8, we can see that, at least in the neighborhood of the stagnation region, the fate of the individual gas particles is not very different from that assumed in Newton's model. The shock surface approximately follows the body surface and the individual streamlines show that the particles, broadly speaking, are deflected from their initial direction in the direction along the body surface. Correspondingly, we obtain a quasi-Newtonian pressure distribution in the sense that the local pressure coefficient C_p is given approximately by the formula

$$C_p = C_{p\ max} \sin^2 \beta$$

where $C_{p\ max}$ is the local pressure coefficient at the stagnation point and β is the local inclination of the surface relative to the flow direction.

Beyond this quasi-Newtonian pressure distribution, attempts to determine the exact flow conditions in the region between the shock wave and the blunt body were not too successful until recently. There are many uncertainties: first, the location of the shock wave is uncertain; second, the sonic line can be determined only by a kind of iteration process, so that the subsonic and supersonic flow regions really match. Even if we stick to ideal-gas laws, we cannot consider the flow as a potential flow because of the vorticity produced in the shock region. The best approximation is that of constant vorticity along streamlines in the two-dimensional case and constant-vorticity flow in the axially symmetric case. The computation usually requires the help of electronic computers. Among the iteration methods, one used by the Soviet mathematicians Dorodnitsyn and Belotserkovski is reported to be quite successful.

The flow beyond the sonic line can be calculated by the method of characteristics. Recent publications by H. M. Lieberstein and P. R. Garabedian, M. D. Van Dyke, and R. Vaglio-Laurin and A. Ferri deal with this problem. They consider the inverse case—to assume a shock shape and find the corresponding body shape.

Fig. 9 shows experimental pressure measurements for the case of a body consisting of a long circular cylinder with a hemispherical frontpiece. The measurements were made at $M = 7.7$.

Near the stagnation point the pressure distribution corresponds to the quasi-Newtonian rule; on the shoulder, where the curvature of the meridian section changes discontinuously, apparently the rate of the

FIG. 7 (*left*). Interferograms of flat plate model at various values of the Reynolds Number Re_t based on the leading-edge thickness. $M = 12.7$. Top to bottom: (a) $Re_t = 177$; (b) $Re_t = 578$; (c) $Re_t = 1{,}510$; (d) $Re_t = 2{,}480$; (e) $Re_t = 4{,}050$; (f) $Re_t = 7{,}480$; (g) $Re_t = 15{,}010$; (h) $Re_t = 35{,}200$; (i) $Re_t = 62{,}200$ (Princeton Univ. Dept. of Aero. Engineering, Report No. 326).

pressure drop can be described by the assumption of a Prandtl-Meyer expansion process. Then, however, one would expect that the pressure would rather quickly approach the final value (which because of the expansion in the wake is slightly below the value corresponding to the undisturbed flow). However, observation shows a very slow decrease; evidently this corresponds to an expanding shock-wave surface over the cylindrical portion of the body.

This process was made understandable by application of the analogy between an unsteady motion, in which the flow picture remains similar to itself, and a steady flow, in which the length coordinate in the flight direction replaces the time coordinate of the unsteady process A characteristic example of such unsteady solutions is the well known solution which G. I. Taylor obtained during World War II for the problem of a violent spherical explosion. The propagation of a weak explosion with sound velocity can be considered as one limiting case, namely the case where the energy introduced by the explosion is small relative to the enthalpy of the gas involved. Taylor's problem is the other extreme: he assumed that the energy introduced is very large in comparison with the enthalpy of the gas in which the explosion occurs. However, Taylor's unsteady solution is three-dimensional in space; thus it cannot be used immediately for the description of a steady flow (except perhaps in a four-dimensional space). Recently S. C. Lin solved the problem of a violent cylindrical explosion

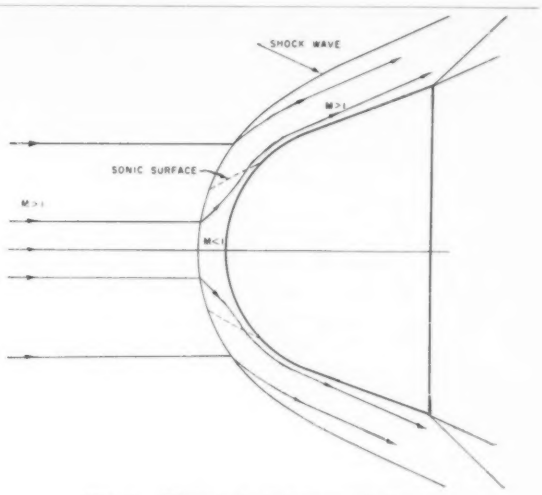

FIG. 8. Blunt body in hypersonic flow.

and this computation led to the "blast-wave theory" of hypersonic motion. Especially, the variable distance between the shock wave and the surface of a long body can be computed by this method, in that one builds up the flow picture in consecutive perpendicular planes of a sequence of solutions for the unsteady cylindrical explosion at various states of the propagation process. The location of the shock wave of the steady flow problem is identical with the location of the expanding wave at the corresponding time element. One assumes that

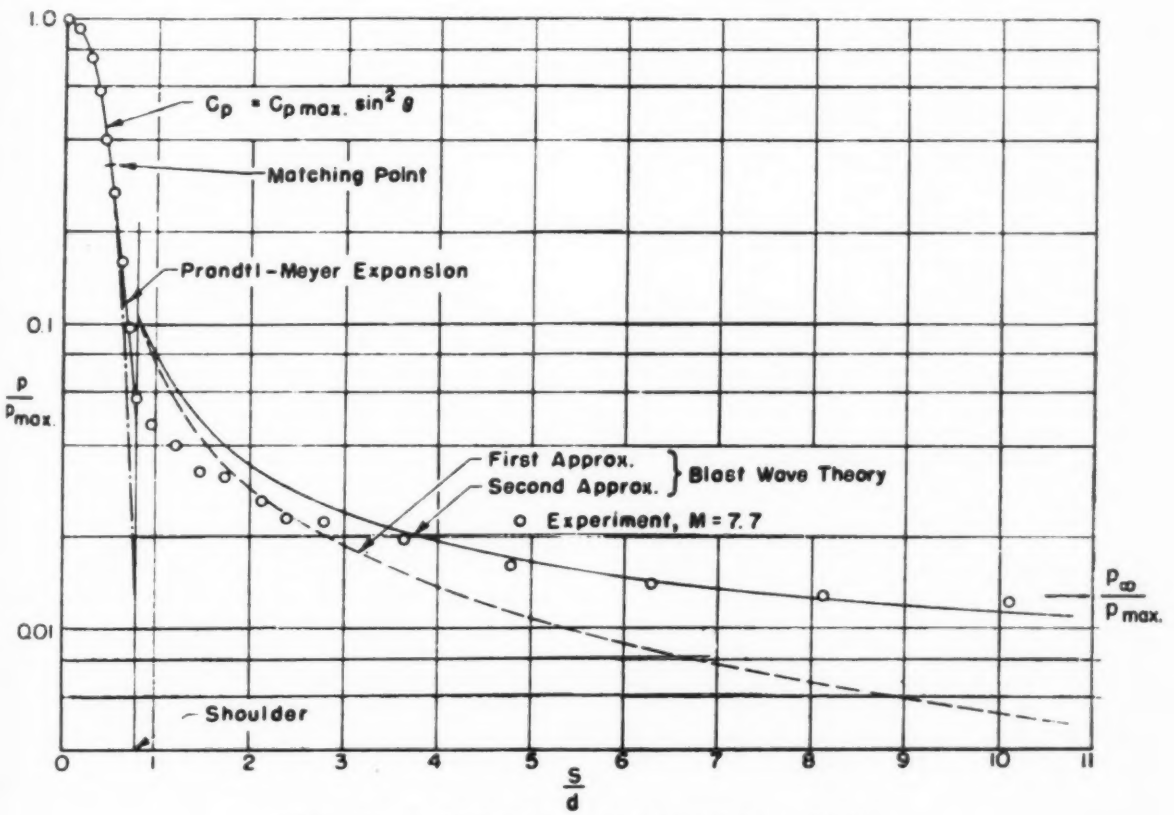

FIG. 9. Pressure distribution on a hemisphere-cylinder combination.

the explosion occurs at the cylindrical body surface and the energy introduced by the explosion corresponds to the energy introduced into the fluid by the resistance of the body; it is, in general, time-dependent. It is seen from Fig. 9 that the results of the blast-wave theory are in fair agreement with the observations. From the rather extensive literature on the subject, the contributions of A. Sakurai, S. C. Lin, L. Lees and T. Kubota, and also H. K. Cheng and A. J. Pallone can be mentioned. Independently, the theory was also developed in Russia, where the self-similar process was named an "auto-model." In particular, L. Sedov and his collaborators worked on the theory of strong explosions. Grodzovski, Chernyi, and Stanynkovich found and employed the analogy between the unsteady and the steady motion.

The true problem of the blunt body exposed to hypersonic flow involves aerothermochemistry, since the temperatures reached behind the shock are so high that the air dissociates. However, before discussing this problem, we want to consider some general questions related to boundary-layer theory.

(VIII) Boundary-Layer Theory

In 1954 we celebrated the fiftieth anniversary of the concept of the boundary layer, in view of the fact that Ludwig Prandtl presented the fundamentals of the boundary-layer theory in 1904 to the International Congress for Mathematics assembled in Heidelberg, Germany. For half a century the new concept proved to be one of the most fruitful ideas in fluid mechanics. The anniversary volume, entitled "Fifty Years of Boundary Layer Research," can give an approximate picture of the main aspect of this development. We also want to mention that, in 1947, Loitsianski published a review of the contributions of Soviet scientists to boundary-layer theory.

Most investigations of boundary-layer problems refer to plane or axisymmetric flows. We will mention later more general three-dimensional cases. At this point we only want to mention that Mangler succeeded, by means of a transformation, in reducing the axisymmetric case to a corresponding two-dimensional problem.

There are two different approaches which were used in the practical solution of boundary-layer problems, especially in the case of incompressible fluids. One is the so-called integral method suggested by me and first used by K. Pohlhausen. This method reduces the problem of finding a solution of a partial differential equation to that of a solution of an ordinary differential equation. Recently, an essential improvement of the method was achieved by I. Tani. The second approach consists also in a reduction of the partial differential equation to an ordinary differential equation by looking for special pressure distributions along the wall which allow similar solutions through the cross sections of the boundary layer. V. M. Falkner, S. W. Skan, D. R. Hartree, and B. Thwaites in the early thirties excelled in the development of such "similarity solutions."

As far as laminar compressible boundary-layer problems are concerned, some special cases were solved before 1946 by A. Busemann, myself, H. S. Tsien, W. Hantsche and H. Wendt, L. Crocco, and by H. W. Emmons and J. G. Brainerd. Special attention was given to the heat-transfer aspect of the problems.

The treatment of the compressible boundary layer in more general cases was greatly facilitated by a clever transformation of the independent variable across the boundary layer, which takes into account the variable density. Such a transformation apparently was first suggested by A. A. Dorodnitsyn and independently discovered by L. Howarth, K. Stewartson, and C. R. Illingworth.

Since this transformation essentially reduces the problem of the compressible boundary layer to the incompressible case, the methods mentioned above could be applied to a broad field of problems. Thus, the integral method could be used for the flow about airfoils and bodies of revolution in supersonic flight. We can mention the contributions of L. E. Kalikhman, H. Weil, P. A. Libby and M. Morduchow, I. E. Beckwith, D. N. Morris and J. W. Smith, and others.

Also, the method of similar solution was combined with the Stewartson-Illingworth transformation by L. Crocco and C. B. Cohen; they also extended the method of Thwaites by putting together sequence of similarity solutions. This procedure was further developed by C. B. Cohen and E. Reshotko. It appears that the work of S. Levy allows a great degree of generality in the formulation of the problem, viz., large temperature changes, including viscous heating and arbitrary values of the Prandtl Number. This nondimensional quantity was taken in many previous investigations to be equal to unity.

For a long time the theory of the laminar boundary layer was considered as having more academic than practical value. Recently, it was found that there are two reasons why the study of the laminar boundary layer is interesting also from the viewpoint of practical applications. First, there is the problem of re-entry of blunt bodies into the atmosphere. The highest value of heat transfer occurs at the stagnation point, and at the beginning the boundary layer probably has laminar structure. Second, the flight of missiles and vehicles at high altitude—i.e., in a medium of extremely low density—enhances the interest for conditions at small Reynolds Numbers.

As we mentioned before, the problem of the boundary layer behind a detached shock produced by hypersonic motion of a blunt body is complicated by changes in the physical and chemical nature of the gas at the high temperatures produced by the shock. The main changes to be expected are changes in the distribution of the thermal energy over the degrees of freedom of the gas molecule, dissociation, and, finally, ionization. The first phenomenon leads especially to a variation in the value of the specific heat and particularly of the ra-

tio between the specific heats; the dissociation may fundamentally change the mechanism of heat transfer by introducing the possibility of diffusion. It is found that ionization does not essentially influence the heat transfer; however, the fact that the gas becomes conductive raises the question of whether there is a practical way to change the structure of the boundary layer by artificially imposed electromagnetic-field effects. In addition, the behavior of an ionized gas against radar waves is of practical interest in view of problems of detection and communication in general.

Concerning the methods for theoretical investigation of the influence of variable physical and chemical characteristics, two limiting cases appear as relatively simple—equilibrium state and frozen state. For example, assume a high degree of dissociation immediately behind the shock and consider this degree of dissociation constant over the flow field; recombination in this case would be restricted to the immediate neighborhood of the body surface. Then, of course, an important question of great practical value arises: whether it is possible to prevent recombination at the surface by so-called noncatalytic surface coating. The application of such materials would essentially diminish heat transfer in the critical region and distribute the heat produced by the shock over a larger region.

The more exact investigation of variable concentration according to some rate law of dissociation and recombination is more complicated, but the calculation can be carried out numerically at least for the stagnation point. The most extensive investigation of stagnation-point conditions may be attributed to J. A. Fay and F. R. Riddell. The most complete discussion of the entire problem of the hypersonic boundary layer is by L. Lees. He found that two assumptions—equilibrium state and Lewis Number (ratio between thermal conductivity and diffusion coefficient) equal to unity—make the computation relatively simple. Thus, the possibility arises of carrying out an exact investigation for the stagnation-point region and of using the ratio between the heat transfer at various points furnished by a simplified theory for an estimate of the heat transfer at other points.

In general it seems that the various assumptions concerning the dissociation process do not change the heat-transfer values more than about 40 to 50 per cent.

Investigations of boundary-layer flow with mass transfer are important in view of the possibilities of cooling by injection of material and also absorption of heat by melting or evaporation of the surface, generally called "ablation."

A remarkable phenomenon was found by experiments on boundary layers in hypersonic flow over a flat plate parallel to the flow direction or inclined to the flow direction at a small angle (sharp wedge). It appears that in such cases the fundamental assumption of the usual theory—that the pressure in the boundary layer is equal to the pressure in the external flow—is quite wrong. One finds considerable pressure increase, apparently induced by the boundary layer itself. We

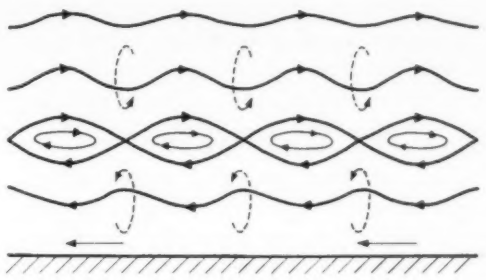

FIG. 10. Illustration to Görtler's theory of transition between laminar and turbulent boundary-layer flow.

mentioned that, probably due to the finite dimension of the leading edge, the flow picture corresponds to a detached shock caused by a kind of equivalent body corresponding to the domain occupied by the boundary layer. Then the motion inside this equivalent body has the general character of a flow through a pipe with increasing cross section, and this kind of motion produces the pressure increase. This phenomenon was called hypersonic boundary-layer - shock-wave interaction.

There is no satisfactory criterion that would permit the prediction of the transition from laminar flow in the boundary layer to turbulent flow—for example, in the case of a blunt body. It is found both theoretically and experimentally that cooling of the surface helps to keep the flow laminar. This point has great practical importance because the heat transfer through a turbulent boundary layer is, in any case, much greater than the transfer through a laminar layer.

Concerning the general problem of stability of the laminar boundary layer, the mathematical theory shows excellent agreement with experiment as far as the damping or the increasing of oscillations is concerned, especially after C. C. Lin corrected Schlichting's original numerical calculations. However, this does not mean that we really understand the mechanism of transition. Recently, Emmons suggested the following mechanism: turbulence is created at isolated spots, and these spots cause contamination of the downstream flow. According to Theodorsen the turbulence originates with the formation of horseshoe vortices which are formed near the walls and penetrate into the fluid. Pfenninger and Lachmann observed similar phenomena in their experiments to keep the boundary-layer flow laminar by means of suction. Görtler proposed the Schlichting-Tollmien waves, as a starting point for the understanding of the transition phenomena, but pointed out that the circulation around the curved streamlines plays a role in the transition, which according to him is an essentially three-dimensional phenomenon (Fig. 10). I. Tani and F. R. Hama have studied the influence of isolated roughnesses on the transition.

Most investigations mentioned above refer to two-dimensional planes of axisymmetrical flow. In recent years, there has been considerable effort devoted to the interesting problems of the boundary-layer behavior when three velocity components are involved. Such

flows arise in a variety of ways; of particular interest for aeronautical applications are the flows over swept wings, over axisymmetric bodies at angle of attack, and in rotating blade systems. Recently, F. K. Moore provided an excellent survey of developments in three-dimensional boundary-layer theory.

The boundary layer on swept wings influences the stalling and lateral control of the wing and has been the subject of considerable research. This problem is idealized by considering the wing to be infinite, so that changes in the spanwise direction are neglected. One can distinguish between a boundary layer normal to the leading edge and a spanwise boundary layer. This consideration leads for incompressible flows to the important "independence principle." According to this, the two boundary layers are independent; one calculates first the chordwise boundary layer in the usual way and then the spanwise boundary layer. The combination of the two boundary layers permits the streamlines within the boundary layer to be constructed. In general, these streamlines differ from those in the external flow so that secondary flows arise. Research on this problem was carried out by L. Prandtl, V. Struminsky, R. T. Jones, and W. R. Sears.

For the compressible case the density depends on both the chordwise and spanwise velocity components, so that the momentum equations in the two directions are "coupled" through the energy equation. The well-known Crocco integral applies in this case under certain restrictions. However, the most general case of chordwise pressure gradient and heat transfer requires simultaneous solution of the chordwise and spanwise momentum equations. Recently E. Reshotko and I. E. Beckwith provided a solution for the boundary-layer and heat-transfer characteristics in the neighborhood of the stagnation line, such as arise at the leading edge of a blunt-nosed, swept wing. This analysis shows that significant reductions in heat transfer can be achieved by sweeping the leading edge of a wing; thus, the concept of sweep is seen to be useful also for hypersonic flight.

(IX) Theory of Turbulence

The theory of turbulence has two separate aspects. Evidently there is some analogy between the random motion of molecules in laminar flow and the random motion of eddylike formations in turbulent flow. The random motion of molecules leads to definite laws of molecular viscosity, heat conduction, and diffusion. In a similar way, the random motion we observe, on a much larger scale, in the turbulent flow of rivers, canals, pipes, and boundary layers apparently also results in definite laws for momentum transfer, energy transfer, and the transfer of matter, which we call turbulent friction, heat transfer, and diffusion, respectively. This analogy between the molecular and the turbulent processes was recognized and treated at a rather early date by Osborne Reynolds. The great difference between the two concepts is the fact that in the case of the molecular random motion the elements are well defined, as molecules, whereas in the case of the turbulent motion they are not given a priori. Hence, whereas in the first case the Boltzmann theory shows the right way to a definite theoretical solution of the problem, in the case of turbulent motion new principles must be found.

Because of this situation, the turbulence theory developed in two essentially different directions. One school of thought endeavored to find half-empirical relations which would lead to definite rules for the prediction of the turbulent friction, heat transfer, and diffusion phenomena. On the other hand, very interesting ideas were proposed for building up a systematic statistical theory of turbulence.

As far as the first line of development is concerned, for the case of an incompressible fluid a satisfactory state of affairs was reached by the introduction of a concept of the mixing length—as a kind of generalization of the mean free path of the kinetic gas theory—due to L. Prandtl, and then, I believe, by the logarithmic law for the velocity distribution, which I found in 1930. Assuming the validity of the logarithmic law for the portion of the flow field which is mainly influenced by the wall, and the so-called "velocity decrement" law for the rest of the field, the turbulent flow in the boundary layer, in a circular pipe, and in a two-dimensional channel can be predicted for given Reynolds Numbers. The application of the integral method used by myself and Pohlhausen, also mentioned in connection with the laminar boundary layer, makes it also possible to calculate general boundary-layer problems. In this direction, F. Clauser recently proposed interesting new concepts and computing methods.

We have to mention that the concept of local similarity of the turbulent flow picture is an important factor as a lead for further development of the theory. When I first presented the idea in 1930, its practical formulation may have been somewhat over-simplified, but I believe—especially after the concept was clarified in some of my own publications together with C. C. Lin and in those of C. C. Lin and his collaborators—that it will have considerable influence on further development of the theory of turbulence.

The main need today is for a reliable prediction of the practically important quantities, especially skin friction and heat transfer for compressible fluids, particularly for supersonic boundary layers at higher Mach Numbers. Fig. 11 convincingly shows the discrepancies between the predictions derived from various proposed "theories."

The diagram, taken from NACA TN 3097 (1954), presents the ratio between the predicted value of the skin-friction coefficient in a compressible boundary layer and the well-known value of the same coefficient for incompressible flow. The experimental value for $M = 4$ is about 0.5. I notice that the value which goes with my name is closer to the experimental value than many others deduced by later elaborate theories. I considered my so-called theory which I proposed more than

twenty years ago as a "guestimate." I simply substituted for the density, in the formula for incompressible flow, the value corresponding to the stagnation temperature which develops at the wall. This procecedure naturally underestimates the skin friction, since to be correct some appropriately determined average temperature should be used. Unfortunately, the results of the theories of the Soviet scientists A. A. Dorodnitsyn and L. A. Kalikhman are not included in the comparison.

The systematic development of a statistical theory of turbulence was initiated by G. I. Taylor in 1935. He introduced the concept of isotropic turbulence, which was later modified and somewhat generalized by G. K. Batchelor to homogeneous turbulence. Batchelor's book, published by the Cambridge University Press in 1953, contains extremely valuable information on the developments of the statistical theory. Taylor proposed the average values of velocity correlations as a means of description of the turbulent flow. In 1938, L. Howarth and I gave a general analysis of the correlations and initiated the branch of the statistical theory which can be designated as the "dynamics of turbulence." We arrived at a differential equation for the prediction of the variations of the correlation values with time—i.e., the propagation of turbulence. G. I. Taylor himself introduced the representation of the turbulent fluctuations by spectral functions as an alternative for the correlation functions. J. Kampé de Feriet investigated the concept of the spectral tensor especially from the mathematical point of view. The spectral viewpoint was adopted by Obukoff and Heisenberg in their general investigations. Perhaps the most important result of these developments is a universal law for the spectral function—i.e., turbulent energy vs. wave number—which is valid for high frequencies and was found independently by A. N. Kolmogoroff and W. Heisenberg. S. Chandrasekhar made significant contributions in this direction of the development.

The theory of homogeneous turbulence—which covers the case of a turbulent fluctuation field without mean flow or the turbulent field superposed upon a uniform stream—is in relatively good shape. However, the more interesting and practically more important case, the theory on the mechanism of turbulent shear, is still in its initial phase. From a physical point of view, the main difficulty seems to be that for the momentum transfer the large eddies are mostly responsible, whereas the energy dissipation is performed by the small eddies. This causes a diffusion of energy from low to high frequencies which does not comply with Onsager's general energy-transfer scheme which provides the real basis for Kolmogoroff's and Heisenberg's theories.

From the mathematical point of view, one could expect that the dynamic equation first written up by me, jointly with L. Howarth, would apply also to the general case of nonisotropic turbulence. However, this equation essentially predicts the fate of the second-order and third-order correlations only if the higher correlations

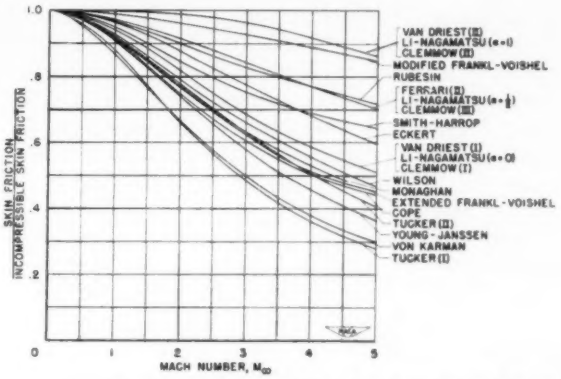

FIG. 11. Results of various analyses of turbulent skin friction for compressible flow over an insulated flat plate (NACA TN 3097).

are known. I believe real progress was made by the hypothesis that a so-called "quasi-normal joint-probability" (Gaussian probability) can be assumed for the velocity field. This assumption makes it possible to express the fourth-order correlations essentially by products of the second-order correlations. It was first suggested by M. Millionschikoff. Attempts were recently made to apply the hypothesis for the solution of the shear problem by J. Proudman, W. H. Reid, T. Talsumi, and A. Craya. Other approaches for the solution of the shear problem were made by S. Chandrasekhar, W. V. R. Malkus, J. M. Burgers, and M. Mitchner. All these theories are in an initial state. We are still far away from a theoretical deduction of the basic laws for shear and heat transfer which would give results in agreement with experimental evidence. I believe that the refinement of the similarity concept has to play a role in the establishment of a final theory.

The experimental evidence on turbulent boundary layer and turbulent shear was very much enriched by the excellent work of many experimenters such as L. Kovasznay, J. Laufer, A. A. Townsend, G. B. Schubauer, and others.

I mentioned before that "heavenly turbulence"—i.e., the turbulent phemonena observed in gaseous clouds of cosmic dimensions—fascinated the imagination of quite a number of mathematicians, astronomers, and aerodynamicists. It was one of the problems which contributed to the interest in the most recent branch of fluid mechanics: "magnetofluidmechanics."

I may close with the remark that it appears to me that even in this so-called nuclear or space age, aerodynamics is not a science to be shelved as an obsolescent branch of the physical sciences. Of course, we may have to study the methods and results of many sister sciences more than in the past; viz., in addition to mathematics, mechanics, and thermodynamics, also chemistry and electromagnetism. However, I hope that the future training of young aerodynamicists will enable them to cope with the problems of the future.

It is my agreeable duty to express my thanks and appreciation to my friends P. A. Libby and C. C. Lin for their assistance in collecting the material treated in

this lecture. Professor Libby collected the papers dealing with supersonic wing theory, slender aircraft, interference effects, higher approximations, hypersonic flow, and boundary-layer theory, and Professor Lin those dealing with the theory of turbulence. The choice of authors mentioned in the paper is somewhat arbitrary. I am also indebted to Prof. Wallace D. Hayes for letting me have the galley proofs of his book on hypersonic flow which he has written jointly with R. F. Probstein, and which will appear in the near future. Prof. I. Tani has prepared abstracts for me of important Japanese papers published in the last decade. The problems of flow in rarefied gases, sometimes referred to as problems of *superaerodynamics* are not treated here at all; the reader may find good summaries in the Preceedings of an International Conference held in Nice, France, in July, 1958. Also, the aeroelastic problems—e.g., flutter at high speed—are only briefly mentioned.

Bibliography

(I) *Wing Theory*

von Kármán, T., *Supersonic Aerodynamics. Principles and Applications*, Journal of the Aeronautical Sciences, Vol. 14, No. 7, pp. 373–409, 1947.

Sears, W. R. (Ed.), "High Speed Aerodynamics and Jet Propulsion," Jones, R. T., and Cohen, D., *Aerodynamics of Wings at High Speeds*, Section A, Volume VII, pp. 3–243, Princeton University Press, 1957.

von Kármán, T., and Moore, N. B., *The Resistance of Slender Bodies Moving with Supersonic Velocities with Special Reference to Projectiles*, Trans. ASME, Vol. 54, pp. 303–310, 1932.

Puckett, A. E., *Supersonic Wave Drag of Thin Airfoils*, Journal of the Aeronautical Sciences, Vol. 13, No. 9, pp. 475–484, September, 1946.

Evvard, J. C., *Use of Source Distributions for Evaluating Theoretical Aerodynamics of Thin Finite Wings at Supersonic Speeds*, NACA TR 951, 1950.

Krasilshchikova, E. A., Scientific Records of the Moscow State University, Vol. 154, Mechanics No. 4, 181–239 (1951), translated as NACA TM 1383, 1956.

Jones, R. T., *The Minimum Drag of Thin Wings in Frictionless Flow*, Journal of the Aeronautical Sciences, Vol. 18, No. 2, pp. 75–81, February, 1951.

Cohen, Doris, *The Warping of Triangular Wings for Minimum Drag at Supersonic Speeds*, Journal of the Aeronautical Sciences, Vol. 24, No. 1, pp. 67–68, January, 1957.

Anon., *Conical Camber*, Aviation Age, Vol. 24, No. 2, p. 62, August, 1957.

(II) *Slender Wings and Aircraft*

Tsien, H. S., *Supersonic Flow over an Inclined Body of Revolution*, Journal of the Aeronautical Sciences, Vol. 5, pp. 480–483, 1938.

Lighthill, M. J., *Supersonic Flow Past Bodies of Revolution*, ARC R&M 2003, 1945.

Broderick, J. B., *Supersonic Flow Round Pointed Bodies of Revolution*, Quart. J. Mech. & Appl. Math., Vol. 2, pp. 98–120, 1949.

Ward, G. N., *Linearized Theory of Steady High-Speed Flow*, Cambridge University Press, 1955.

Jones, R. T., *Properties of Low-Aspect-Ratio Pointed Wings at Speeds Below and Above the Speed of Sound*, NACA TR 835, 1946.

Allen, H. J., *Pressure Distribution and Some Effects of Viscosity on Slender Inclined Bodies of Revolution*, NACA TN 2004, 1950.

Flax, A. H., and Lawrence, H. R., *The Aerodynamics of Low-Aspect-Ratio Wings and Wing-Body Combinations*, Proceedings, Third Anglo-American Aeronautical Conference, pp. 363–398, 1951.

(III) *Interference Effects*

Ward, G. N., *Supersonic Flow Past Slender Pointed Bodies*, Quart. J. Mech. & Appl. Math., Vol. 2, Part 1, pp. 76–97, 1949.

Lawrence, H. R., and Flax, A. H., *Wing-Body Interference at Subsonic and Supersonic Speeds—Survey and New Developments*, Journal of the Aeronautical Sciences, Vol. 21, No. 5, pp. 289–324, May, 1954.

Adams, Mac C., and Sears, W. R., *Slender Body Theory—Review and Extension*, Journal of the Aeronautical Sciences, Vol. 20, No. 2, pp. 85–98, February, 1953.

Sears, W. R. (Ed.), "High Speed Aerodynamics and Jet Propulsion," Ferrari, C., *Interaction Problems*, Section C. Vol. VII, Princeton Univ. Press, Princeton, 1957.

Morikawa, G. K., *A Non-planar Boundary Problem for the Wave Equation*, Quart. Appl. Math., Vol. 10, No. 2, pp. 129–140, 1952.

Nielsen, J. N., and Pitts, W. C., *Wing-Body Interference at Supersonic Speeds with an Application to Combinations with Rectangular Wings*, NACA TN 2677, April, 1952.

Browne, S. H., Friedman, L., and Hodes, I., *A Wing-Body Problem in a Supersonic Conical Flow*, Journal of the Aeronautical Sciences, Vol. 15, No. 8, pp. 443–452, August, 1948.

Graham, E. W., Lagerstrom, P. A., Licher, R. M., and Beane, B. J., *A Theoretical Investigation of the Drag of Generalized Aircraft Configurations in Supersonic Flow*, Douglas Aircraft Co., Inc., Rep. SM-19181, July, 1955.

Cramer, R. H., *Wing-Body Interference at Supersonic Speeds—Recent Experimental Results and their Bearing on Advances in Theory*, Presented at Navy Bureau of Ordnance Symposium on Aeroballistics, May 13, 1952.

Morikawa, G. K., *Supersonic Wing-Body Lift*, Journal of the Aeronautical Sciences, Vol. 18, No. 4, pp. 217–228, April, 1951.

Sacks, A. H., *Vortex Interference Effects on the Aerodynamics of Slender Airplanes and Missiles*, Journal of the Aeronautical Sciences, Vol. 24, No. 6, pp. 393–402, June, 1957.

Busemann, A., *Aerodynamischer Auftrieb bei Uberschallgeschwindigkeit*, Fifth Volta Congress, Reale Academia D'Italia, 1935.

Ferrari, C., *Campi di Corrente Ipersonora Attorno a Solidi di Rivoluzione*, L'Aerotecnica, Vol. XVII, Fasc. 6, pp. 507–518, 1937.

Ferri, A., *Application of the Method of Characteristics to Supersonic Rotational Flow*, NACA TR 841, 1946.

Ferri, A., and Clarke, J. H., *On the Use of Interfering Flow Fields for the Reduction of Drag at Supersonic Speeds*, Journal of the Aeronautical Sciences, Vol. 24, No. 1, pp. 1–18, January, 1957.

Oswatitsch, K., *The Area Rule*, Applied Mechanics Reviews Vol. 10, No. 12, pp. 543–545, December, 1957.

Sears, W. R., *On Projectiles of Minimum Wave Drag*, Quart. Appl. Math., Vol. 14, pp 361–366, 1947.

Haack, W., *Geschossformen kleinsten Wellenwiderstandes*, Lilienthal-Gesellschaft, Bericht 139, pp. 14–21, 1941.

Hayes, W. D., *Linearized Supersonic Flow*, North American Aviation Report AL-222, June, 1947.

Ferri, A., *Recent Theoretical Work in Supersonic Aerodynamics at the Polytechnic Institute of Brooklyn*, Proceedings of the Conference on High-Speed Aeronautics, Polytechnic Institute of Brooklyn, January, 1955.

Ferri, A., Clarke, J. H., and Ting, L., *Favorable Interference in Lifting Systems in Supersonic Flow*, Journal of the Aeronautical Sciences, Vol. 24, No. 11, pp. 791–804, November, 1957.

Jones, R. T., *Minimum Wave Drag for Arbitrary Arrangements of Wings and Bodies*, NACA TN 3530, February, 1956.

Lomax, H., and Heaslet, M. A., *Recent Developments in the Theory of Wing-Body Wave Drag*, Journal of the Aeronautical Sciences, Vol. 23, No. 12, pp. 1061–1074, December, 1956.

(V) *Nonlinear Theories—Higher-Order Approximations*

Busemann, A., *Aerodynamischer Auftrieb bei Uberschallgeschwindigkeit*, Luftfahrtforschung 12, 210, 1935.

Friedrichs, K. O., *Formation and Decay of Shock Waves*, Communications on Pure and Applied Mathematics, 1, 211, 1948.

Sears, W. R. (Ed.), "High Speed Aerodynamics and Jet Propulsion," Lighthill, M. J., *Higher Approximations*, Section E, Vol. VI, pp. 345–489. Princeton Univ. Press, 1954.

Van Dyke, M. D., *First- and Second-Order Theory of Supersonic Flow Past Bodies of Revolution*, Journal of the Aeronautical Sciences, Vol. 18, No. 3, pp. 161–178, March, 1951.

Whitham, G. B., *The Flow Pattern of a Supersonic Projectile*, Communications on Pure and Applied Mathematics, Vol. 5, 301, 1952.

Lighthill, M. J., *A Technique for Rendering Approximate Solutions to Physical Problems Uniformly Valid*, Phil. Mag., Series 7 Vol. 40, pp. 1179–1201, 1950.

Lighthill, M. J., *The Shock Strength in Supersonic Conical Fields*, Phil. Mag., Series 7, Vol. 40, pp. 1202–1223, 1950.

Kuo, Y. H., *Viscous Flow Along a Flat Plate Moving at High Supersonic Speed*, Journal of the Aeronautical Sciences, Vol. 23, No. 2, pp. 125–136, February, 1956.

Dryden, Hugh L., and Sears, W. R. (Eds.), *Advances in Applied Mechanics*, Tsien, H. S., "The Poincaré-Lighthill-Kuo Method," pp. 281–348, Vol. IV, Academic Press, Inc., 1956.

Ferri, A., and Vaglio-Laurin, R., *On Conical Flows of Mixed Type*, PIBAL Report No. 306, April, 1956.

Kaplun, S., and Lagerstrom, P. A., *Asymptotic Expansion of Navier-Stokes Solution for Small Reynolds Numbers*, IX International Congress of Applied Mechanics, Vol. 3, pp. 177–186, 1957.

Kaplun, S., *The Role of Coordinate Systems in Boundary Layer Theory*, J. Appl. Math. & Phys , Vol. V, No. 2, pp. 111–135, 1954.

Ferri, A., *The Linearized Characteristics Method and its Application to Practical Nonlinear Supersonic Problems*, NACA TR 1102, 1952.

(VII) Hypersonic Flow

Lees, L., *Recent Developments in Hypersonic Flow*, Jet Propulsion, Vol. 27, No. 11, pp. 1162–1178, November, 1957.

Logan, J., *Relaxation Phenomena in Hypersonic Aerodynamics*, presented at the Aerodynamics—III Session, Twenty-Fifth Annual Meeting, IAS, New York, January, 1957.

Feldman, S., *The Chemical Kinetics of Air at High Temperatures: A Problem in Hypersonic Aerodynamics*, Heat Transfer and Fluid Mechanics Institute, California Institute of Technology, 1957.

Camac, M., Camm, J., Keck, J., and Petty, C., *Relaxation Phenomena in Air Between 3,000 and 8,000°K.*, AVCO Research Laboratory, Report No. 22, March 13, 1958.

Lighthill, M. J., *Dynamics of a Dissociating Gas. Part I—Equilibrium Flow*, Aeronautical Research Council 18,837. See also, J. Fluid Mech., Vol. 2, Part 1, pp. 1–32, January, 1957.

Freeman, N. C., *Dynamics of a Dissociating Gas. III—Non-equilibrium Theory*, AGARD Report 133, July, 1957.

Hammitt, A. G., Vas, I. E., and Bogdonoff, S. M., *Leading Edge Effects on the Flow over a Flat Plate at Hypersonic Speeds*, Princeton Univ. Dept. of Aero. Engineering, Report No. 326, September, 1955.

Hayes, W. D., *Some Aspects of Hypersonic Flow*, The Ramo-Wooldridge Corp., January 4, 1955.

Hayes, W. D., *Hypersonic Flow Fields at Small Density Ratio*, The Ramo-Wooldridge Corp., May 12, 1955.

Chester, W., *Supersonic Flow Past a Bluff Body with a Detached Shock. Part I—Two-Dimensional Body*, J. Fluid Mech., Vol. 1, Part 4, pp. 353–365, October, 1956.

Freeman, N. C., *On the Theory of Hypersonic Flow Past Plane and Axially Symmetric Bluff Bodies*, J. Fluid Mech., Vol. 1, Part 4, pp. 366–387, October, 1956.

Hida, K., *An Approximate Study on the Detached Shock Wave in Front of a Circular Cylinder and a Sphere*, J. Phys. Soc. of Japan, Vol. 8, No. 6, pp. 740–745, November-December, 1953.

Taylor, G. I., *The Formation of a Blast Wave by a Very Intense Explosion. Part I—Theoretical Discussion. Part II—The Atomic Explosion of 1945*, Proc. Roy. Soc. (A), Vol. 201, No. 1065, pp. 159–186, March, 1950.

Lin, S. C., *Cylindrical Shock Waves Produced by Instantaneous Energy Release*, J. of Appl. Phys., Vol. 25, No. 1, pp. 54–57, January, 1954.

Sakurai, A., *On the Propagation and Structure of the Blast Wave, Part I*, J. Phys. Soc. Japan, Vol. 8, No. 5, pp. 662–669, September-October, 1953. *Part II*, Vol. 9, pp. 256–266, April, 1954.

Cheng, H. K., and Pallone, A. J., *Inviscid Leading-Edge Effect in Hypersonic Flow*, Journal of the Aeronautical Sciences, Vol. 23, No. 7, pp. 700–702, July, 1956.

Lees, L. and Kubota, T., *Inviscid Hypersonic Flow Over Blunt-Nosed Slender Bodies*, Journal of the Aeronautical Sciences, Vol. 24, No. 3, pp. 195–202, March, 1957.

Garabedian, P. R., and Lieberstein, H. M., *On the Numerical Calculation of Detached Bow Shock Waves in Hypersonic Flow*, Journal of the Aeronautical Sciences, Vol. 25, No. 2, pp. 109–118, February, 1958.

Van Dyke, M. D., *The Supersonic Blunt-Body Problem—Review and Extension*, Institute of the Aeronautical Sciences, Preprint No. 801, January, 1958.

Vaglio-Laurin, R., and Ferri, A., *Theoretical Investigation of the Flow Field About Blunt-Nosed Bodies in Supersonic Flight*, Gruen Applied Science Laboratories, Inc., Technical Report No. 54, February, 1958.

(VIII) Boundary-Layer Theory

Chapman, D. R., and Rubesin, M. W., *Temperature and Velocity Profiles in the Compressible Laminar Boundary Layer with Arbitrary Distribution of Surface Temperature*, Journal of the Aeronautical Sciences, Vol. 16, No. 9, pp. 547–565, September, 1949.

Crown, C., *The Laminar Boundary Layer at Hypersonic Speeds*, NAVORD Report 2299, 1952.

Young, G. B. W., and Janssen, E., *The Compressible Boundary Layer*, Journal of the Aeronautical Sciences, Vol. 19, No. 4, pp. 229–236, 288, April, 1952.

Dorodnitsyn, A. A., *Laminar Boundary Layer in a Compressible Gas*, DAN, Vol. XXXIV, No. 8, 1942.

Howarth, L., *Concerning the Effect of Compressibility on Laminar Boundary Layers and their Separation*, Proc. Roy. Soc. London (A), 194, 16–42, 1948.

Stewartson, K., *Correlated Compressible and Incompressible Boundary Layers*, Proc. Roy. Soc. London (A), 200, 84, 1949.

Illingworth, C. R., *Steady Flow in the Laminar Boundary Layer of a Gas*, Proc. Roy. Soc. (A), 199, 533, 1949.

Kalikhman, L. E., *Heat Transmission in the Boundary Layer* NACA TM 1229, 1949.

Weil, H., *Effects of Pressure Gradient on Stability and Skin Friction in Laminar Boundary Layers in Compressible Fluids*, Journal of the Aeronautical Sciences, Vol. 18, No. 5, pp. 311–318, May, 1951.

Libby, P. A., and Morduchow, M., *Method for Calculation of Compressible Laminar Boundary Layer with Axial Pressure Gradient and Heat Transfer*, NACA TN 3157, January, 1954.

Beckwith, I. E., *Heat Transfer and Skin Friction by an Integral Method in the Compressible Laminar Boundary Layer with a Streamwise Pressure Gradient*, NACA TN 3005, September, 1953.

Morris, D. N., and Smith, J. W., *The Compressible Laminar Boundary Layer with Arbitrary Pressure and Surface Temperature Gradients*, Journal of the Aeronautical Sciences, Vol. 20, No. 12, pp. 805–818, December, 1953.

Crocco, L., and Cohen, C. B., *Compressible Laminar Boundary Layer with Heat Transfer and Pressure Gradient*, pp. 280–293, 50 Jahre Grenzschichtforschung, Friedr. Vieweg and Sohn Braunschweig, 1955.

Cohen, C. B., and Reshotko, E., *Similar Solutions for the Compressible Laminar Boundary Layer with Heat Transfer and Pressure Gradient*, NACA TN 3325, 1955.

Cohen, C. B., and Reshotko, E., *The Compressible Laminar Boundary Layer with Heat Transfer and Arbitrary Pressure Gradient*, NACA TN 3326, 1955.

Levy, S., *Effect of Large Temperature Changes (Including Viscous Heating) upon Laminar Boundary Layers with Variable*

Free-Stream Velocity, Journal of the Aeronautical Sciences, Vol. 21, No. 7, pp. 459–474, July, 1954.

Lees, L., *Laminar Heat Transfer over Blunt-Nosed Bodies at Hypersonic Flight Speeds*, Jet Propulsion, Vol. 26, pp. 259–269, April, 1956.

Fay, J. A., and Riddell, F. R., *Theory of Stagnation Point Heat Transfer in Dissociated Air*, Journal of the Aeronautical Sciences, Vol. 25, No. 2, pp. 73–85, February, 1958.

Rose, P. H., and Stark, W. I., *Stagnation Point Heat-Transfer Measurements in Dissociated Air*, Journal of the Aeronautical Sciences, Vol. 25, No. 2, pp. 86–97, February, 1958.

Hammitt, H. G., *A Preliminary Study of the Details of the Flow Field About a Flat Plate at Hypersonic Speeds*, Princeton University, Department of Aeronautical Engineering Report No. 327, November, 1955.

Shen, S. F., *An Estimate of Viscosity Effect in Hypersonic Flow over an Insulated Wedge*, J. Math. & Phys., Vol. 31, No. 3, pp. 192–205, October, 1952.

Li, T.-Y., and Nagamatsu, H., *Shock Wave Effects on the Laminar Skin Friction of an Insulated Flat Plate at Hypersonic Speeds*, Journal of the Aeronautical Sciences, Vol. 20, No. 5, pp. 345–355, May, 1953.

Lees, L., and Probstein, R. F., *Hypersonic Viscous Flow over a Flat Plate*, Princeton University, Department of Aeronautical Engineering Report No. 195, April, 1952.

Bertram, M. H., *An Approximate Method for Determining the Displacement Effects and Viscous Drag of Laminar Boundary Layers in Two-Dimensional Hypersonic Flow*, NACA TN 2773, September, 1952.

Kendall, J. M., Jr., *An Experimental Investigation of Leading-Edge Shock-Wave-Boundary-Layer Interaction at $M = 5.8$*, Journal of the Aeronautical Sciences, Vol. 24, No. 1, pp. 47–56, January, 1957.

Bertram, M. H., *Viscous and Leading-Edge Thickness Effects on the Pressures on the Surface of a Flat Plate in Hypersonic Flows*, Journal of the Aeronautical Sciences, Vol. 21, No. 5, pp. 430–431, June, 1954.

Bogdonoff, S. M., and Hammitt, A. G., *Fluid Dynamic Effects at Speeds from $M = 11$ to 15*, Journal of the Aeronautical Sciences, Vol. 23, No. 2, pp. 108–116, February, 1956.

Hammitt, A. G., and Bogdonoff, S. M., *Hypersonic Studies of the Leading Edge Effect on the Flow Over a Flat Plate*, J. ARS, Vol. 26, No. 4, pp. 241–246, April, 1956.

Dryden, Hugh L., and Sears, W. R. (Eds.), *Advances in Applied Mechanics*, Moore, F. K., "Three-Dimensional Boundary Layer Theory," pp. 159–228, Vol. IV, Academic Press, 1956.

Reshotko, E., and Beckwith, I. E., *Compressible Laminar Boundary Layer over a Yawed Infinite Cylinder with Heat Transfer and Arbitrary Prandtl Number*, NACA TN 3986, June, 1957.

Hayes, W. D., *The Three-Dimensional Boundary Layer*, NAVORD Report No. 1313, USNOTS, May, 1951.

Howarth, L., *The Boundary Layer in Three-Dimensional Flow*, Phil. Mag. (7) 42, pp. 239–243, 1951.

Moore, F. K., *Laminar Boundary Layer on Circular Cone in Supersonic Flow at Small Angle of Attack*, NACA TN 2521, 1951.

Mager, A., *Three-Dimensional Laminar Boundary Layer with Small Cross-Flow*, Journal of the Aeronautical Sciences, Vol. 21, No. 12, pp. 835–845, December, 1954.

Vaglio-Laurin, R., *Laminar Heat Transfer on Blunt-Nosed Bodies in Three-Dimensional Hypersonic Flow*, WADC TN 58-147, May, 1958.

Dryden, H. L., *Transition from Laminar to Turbulent Flow at Subsonic and Supersonic Speeds*, Proceedings of the Conference on High Speed Aeronautics, pp. 41–74, Polytechnic Institute of Brooklyn, January 20–22, 1955.

Lin, C. C., *On the Stability of Two-dimensional Parallel Flows*, Quart. Appl. Math., Vol. 4, *Part I, General Theory*, pp. 117–142, 1945; *Part II, Stability in an Inviscid Fluid*, pp. 218–234, 1945; *Part III, Stability in a Viscous Fluid*, pp. 277–301, 1946.

Lees, L., *The Stability of the Laminar Boundary Layer in a Compressible Fluid*, NACA TR 876, 1947.

Theodorsen, T., *Mechanism of Turbulence*, Proceedings of Second Midwestern Conference on Fluid Mechanics, pp. 1–16, 1952.

Emmons, H. W., *The Laminar-Turbulent Transition in a Boundary Layer*, Journal of the Aeronautical Sciences, Vol. 18, No. 7, pp. 490–498, July, 1951.

Dryden, H. L., and von Kármán, T. (Eds.), *Advances in Applied Mechanics*, Dryden, H. L., "Recent Advances in the Mechanics of Boundary Layer Flow," Vol. 1, pp. 1–40, Academic Press, Inc., 1948.

Clauser, F. H., *Turbulent Boundary Layer in Adverse Pressure Gradients*, Journal of the Aeronautical Sciences, Vol. 21, No. 2, pp. 91–108, February, 1954.

Dryden, H. L., and von Kármán, T. (Eds.), *Advances in Applied Mechanics*, Clauser, F. H., "The Turbulent Boundary Layer," Vol. IV, pp. 1–51, Academic Press, Inc., 1956.

Townsend, A. A., *The Structure of Turbulent Shear Flow*, Cambridge University Press, 1956.

Coles, D., *The Law of the Wake in the Turbulent Boundary Layer*, J. Fluid Mech., Vol. 1, Part 2, pp. 191–226, July, 1956.

Chapman, D. R., and Kester, R. H., *Turbulent Boundary-Layer and Skin-Friction Measurements in Axial Flow along Cylinders at Mach Numbers Between 0.5 and 3.6*, NACA TN 3097, 1954.

Eckert, E. R. G., *Engineering Relation for Friction and Heat Transfer to Surfaces in High Velocity Flow*, Journal of the Aeronautical Sciences, Vol. 22, No. 8, pp. 585–586, August, 1955.

Libby, P. A., and Cresci, R. J., *Evaluation of Several Hypersonic Turbulent Heat Transfer Analyses by Comparison with Experimental Data*, WADC TN 57-72, July, 1957.

Beckwith, I. E., and Gallagher, J. J., *Heat Transfer and Recovery Temperatures on a Sphere with Laminar, Transitional, and Turbulent Boundary Layers at Mach Numbers of 2.00 and 4.15*, NACA TN 4125, December, 1957.

Lees, L., *Convective Heat Transfer with Mass Addition and Chemical Reactions*, Third AGARD Combustion and Propulsion Panel Colloquium, Palermo, Sicily, March 17–21, 1958.

Scala, S., and Sutton, G. W., *The Two-Phase Hypersonic Laminar Boundary Layer*, 1958 Heat Transfer and Fluid Mechanics Institute, University of California at Berkeley, June, 1958.

(IX) Theory of Turbulence

Batchelor, G. K., *The Theory of Homogeneous Turbulence*, Cambridge University Press, 1953.

Batchelor, G. K., and Townsend, A. A., *Survey in Mechanics*, "Turbulent Diffusion," Cambridge University Press, 1956.

Burgers, J. M., and Mitchner, M., *On Homogeneous Non-Isotropic Turbulence Connected with a Mean Motion Having a Constant Velocity Gradient*, K. Neder. Akad. Wet,. Vol. 56, pp. 228–235, 343–354, 1953.

Chandrasekhar, S., *On Heisenberg's Elementary Theory of Turbulence*, Proc. Roy. Soc. Lond. (A) Vol. 200, p. 20, 1949.

Chandrasekhar, S., *A Theory of Turbulence*, Proc. Roy. Soc., London (A), Vol. 229, pp. 1–9, 1955.

Chandrasekhar, S., *Theory of Turbulence*, Phys. Rev., Vol. 102, p. 941, 1956.

Chandrasekhar, S., *Convective Instability*, Daedalus, Stockholm, 1957.

Clauser, F. H., *The Behavior of Nonlinear Systems*, Journal of the Aeronautical Sciences, Vol. 23, No. 5, pp. 411–434, May, 1956.

Craya, A., C. R. Acad. Sci. (Paris), Vol. 244, pp. 560, 847, 1448, 1969, 1957.

Dunn, D. W., and Reid, W. H., *Heat Transfer in Isotropic Turbulence During the Final Period of Decay*, NACA TN 4186, 1958.

Emmons, H. W., *The Laminar-Turbulent Transition in a Boundary Layer*, Journal of the Aeronautical Sciences, Vol. 18, No. 7, p. 490, July, 1951.

Heisenberg, W., *Zur Statistischen Theorie der Turbulenz*, Z. Phys., Vol. 124, p. 628, 1948.

(Continued on page 154)

Direct-Analog Method of Analysis of the Influence of Aerodynamic Heating on the Static Characteristics of Thin Wings

MICHAEL A. BASIN,* RICHARD H. MACNEAL,** AND JOHN H. SHIELDS***

Computer Engineering Associates

SUMMARY

Application of the direct-analog computer method to the analysis of thin wings subjected to the influence of aerodynamic heating is described. A general method of analysis of temperature effects on structures is presented. The method is then applied to the example of a square, cantilever, constant-depth wing box, which is symmetrically heated along the leading and trailing edges. The electric analog computer is used to calculate the thermal in-plane stresses and the lateral load influence coefficients. Results are compared for the heated and unheated wing.

SYMBOLS

x, y, w	= rectangular coordinates defined in Fig. 1
U_x, U_y, U_w	= linear deflections, defined positive in the positive coordinate direction
θ_x, θ_y	= angular rotations defined in Fig. 1
λ	= dimensionless deflection parameter, Eq. (29)
ϵ_x, ϵ_y	= axial strain
γ_{xy}	= shear strain
σ_x, σ_y	= axial stress
τ_{xy}	= shear stress
σ_{xT}, σ_{yT}	= equivalent axial stress produced by temperature distribution, Eq. (11)
q_{xT}, q_{yT}	= thermally induced load density, Eqs. (12) and (13)
α	= linear coefficient of temperature expansion
T	= temperature
E	= Young's modulus, voltage
G	= shear modulus, current generator
μ	= Poisson's ratio
D	= flexural rigidity of a plate
N_x, N_y	= normal force per unit length
N_{xy}	= shearing force per unit length
q	= externally applied lateral load density
$\bar{P}$	= equivalent lateral load density, Eq. (15)
P_1, P_2	= components of $\bar{P}$, Eqs. (17) and (18)
F_{w_1}, F_{w_2}	= total junction lateral loads corresponding to P_1 and P_2, Eqs. (19) and (20)
$\Delta x, \Delta y$	= finite difference cell dimensions
l	= structure span and chord
t	= skin thickness
h	= height, the distance from top skin centerline to bottom skin centerline
β	= dimensionless temperature parameter, Eq. (30)
L	= symmetric or antisymmetric unit load
F_x, F_y	= forces in axial load members
R	= resistance
F_x', F_y'	= equivalent thermal loads in axial load members
S_x, S_y	= horizontal panel shear loads
V	= vertical shear force in vertical shear web
P	= primary of a transformer
S	= secondary of a transformer

Received March 4, 1958. Revised and received August 13, 1958.

* Formerly, Engineering Service Division Manager, CEA. Now, Member of Technical Staff, Hughes Aircraft, Fullerton, Calif.

** Preliminary Analysis Department Manager.

*** Project Engineer.

INTRODUCTION

DURING THE PAST DECADE, direct analogy computer techniques have been applied to a wide spectrum of physical problems. In particular, such techniques have been extensively used in the areas of aircraft static, dynamic, and temperature distribution analysis.[1-4] This paper describes a recent application of the direct-analog method to the static analysis of structures in which thermal stresses are significant.

The direct-analog computer consists of a large number of discrete lumped-parameter, passive, electrical elements (resistors, capacitors, inductors, transformers), a number of electronic devices such as operational amplifiers and arbitrary function generators, and control circuitry. The basic underlying principle of operation of this computing system is the direct behavioral correspondence between electrical circuit elements and discrete mechanical "building blocks" such as levers, masses, and springs. The computer can be thought of as a large "tinker toy" which can be used to simulate numerous types of physical systems.

There are essentially two basic methods for deriving electrical analogies for physical systems. The first method makes use of the correspondence between a set of simultaneous differential equations (or their finite difference equivalents) representing a physical system and a set of equations describing an electrical circuit. Individual coefficients in the system equations are then identified with the coefficients of the electrical circuit equations. The second method, which is used for the analysis presented in this paper, makes use of the topological similarity of electrical and mechanical systems. In this method, the continuous mechanical system is first idealized into a prototype model consisting of discrete "building blocks." Analogies are then derived for each component and are interconnected on the computer in such a way as to satisfy the interconnection equations at all junctions and boundaries.

This paper considers the application of the direct analogy method to the general thermal stress problem of thin wings. In particular, a square, cantilever, constant-depth wing box subjected to aerodynamic heating is analyzed by means of the direct-analog com-

puter, and results are presented and compared with those obtained for an unheated wing.

Effect of Temperature Distribution on Structures

It is well known that the application of a temperature distribution to a structure produces several significant effects. First, stresses are generated in the structure by the thermally induced strains. Second, the response of the structure to externally applied loads is altered due to the presence of these induced stresses.[5] Numerous authors have analyzed the effect of thermal stresses on the torsional properties of beams. Vosteen and Fuller[6] present experimental results substantiating this phenomenon for a rectangular plate subjected to rapid heating conditions. The approach presented in this paper is to treat the temperature effects in light of the general equations of elasticity, and to arrive at a lumped prototype of the mechanical structure. The advantage of this method is its generality and its applicability to the analysis of highly redundant and geometrically complex structures.

The In-Plane Problem for Plates

The equations representing the plane stress problem which include the effects of an externally applied temperature distribution are presented below.

Strain Relationships:

$$\epsilon_x = \partial U_x/\partial x \tag{1}$$

$$\epsilon_y = \partial U_y/\partial y \tag{2}$$

$$\gamma_{xy} = (\partial U_x/\partial y) + (\partial U_y/\partial x) \tag{3}$$

Stress-Strain Relationships:

$$\epsilon_x = (1/E)\,(\sigma_x - \mu\sigma_y) + \alpha T \tag{4}$$

$$\epsilon_y = (1/E)\,(\sigma_y - \mu\sigma_x) + \alpha T \tag{5}$$

$$\gamma_{xy} = (1/G)\tau_{xy} \tag{6}$$

Equilibrium Relationships:

$$(\partial\sigma_x/\partial x) + (\partial\tau_{xy}/\partial y) = 0 \tag{7}$$

$$(\partial\sigma_y/\partial y) + (\partial\tau_{xy}/\partial x) = 0 \tag{8}$$

The temperature effects can be interpreted in either of two ways. One way, as shown by Eqs. (4) and (5), is to add a strain, αT, to both ϵ_x and ϵ_y. The alternate approach is to rewrite Eqs. (4) and (5) as

$$\epsilon_x = (1/E)\,[(\sigma_x + \sigma_{xT}) - \mu(\sigma_y + \sigma_{yT})] \tag{9}$$

$$\epsilon_y = (1/E)\,[(\sigma_y + \sigma_{yT}) - \mu(\sigma_x + \sigma_{xT})] \tag{10}$$

where $$\sigma_{xT} = \sigma_{yT} \equiv \alpha TE/(1 - \mu) \tag{11}$$

The load densities per unit volume that must be applied at interior points of the "cold" structure to produce the thermally induced stresses are

$$q_{xT} = -(\partial\sigma_{xT}/\partial x) \tag{12}$$

$$q_{yT} = -(\partial\sigma_{yT}/\partial y) \tag{13}$$

Normal stresses equal to $\alpha TE/(1 - \mu)$ must be applied at the free edges of the structure.

The suggested procedure for analyzing a plane stress problem including the effects of temperature is

(1) Construct a lumped model or prototype which satisfies the above equations with temperature set equal to zero. Such a prototype will be composed of axial load carrying members (including Poisson's ratio effect) and of idealized shear panels.

(2) Subject the prototype to a loading distribution calculated to satisfy Eqs. (11), (12), and (13).

(3) Measure or calculate the apparent internal stresses $\sigma_x + \sigma_{xT}$, $\sigma_y + \sigma_{yT}$, and τ_{xy}.

(4) Subtract σ_{xT} and σ_{yT} from the apparent internal direct stresses to obtain the true direct stresses.

The Lateral Load Problem

It has already been noted that the in-plane thermally induced stresses alter the response of a plate-like structure when it is subjected to lateral loads. This effect can best be studied by an examination of the plate equation,[7]

$$(\partial^4 U_w/\partial x^4) + (2\partial^4 U_w/\partial x^2\partial y^2) + (\partial^4 U_w/\partial y^4) = (1/D)\,[q + N_x(\partial^2 U_w/\partial x^2) + N_y(\partial^2 U_w/\partial y^2) + 2N_{xy}(\partial^2 U_w/\partial x\partial y)] \tag{14}$$

where the positive coordinate system for displacements and internal loads is illustrated in Fig. 1. N_x, N_y, and N_{xy} are in-plane loads while q is the externally applied lateral load distribution.

Examination of the right-hand side of Eq. (14) shows that the planar stresses in the skin effectively add "kick" load contributions to the applied distribution q. The effective lateral load distribution can then be defined as

$$\bar{P} = q + N_x(\partial^2 U_w/\partial x^2) + N_y(\partial^2 U_w/\partial y^2) + 2N_{xy}(\partial^2 U_w/\partial x\partial y) \tag{15}$$

The load distribution of Eq. (15) can be divided into two parts. Making use of the definitions of θ_x and θ_y (see Fig. 1),

$$\bar{P} = P_1 + P_2 \tag{16}$$

where

$$P_1 = q + N_x(\partial\theta_x/\partial x) + N_y(\partial\theta_y/\partial y) \tag{17}$$

$$P_2 = N_{xy}[(\partial\theta_y/\partial x) + (\partial\theta_x/\partial y)] \tag{18}$$

The lateral problem can thus be solved by setting up a lumped prototype for the "cold" mechanical system and then subjecting it to the load density prescribed by Eqs. (17) and (18).

Many methods of analysis such as the one presented by Benscoter and MacNeal[8] make use of finite difference techniques. Fig. 2 presents the points of definition of the lateral deflection U_w, and of the two orthogonal slopes θ_x and θ_y for a finite difference derived prototype. Since such a model can only be loaded at defined points, all lateral loads must be introduced at rib-spar intersections. The total junction

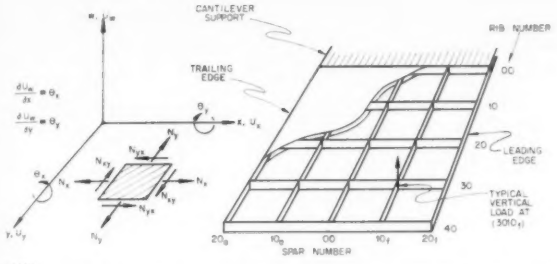
CANTILEVER SUPPORT
RIB NUMBER
TRAILING EDGE
LEADING EDGE
TYPICAL VERTICAL LOAD AT (3010+1)
SPAR NUMBER
NOTES:
1. TOP AND BOTTOM SKIN, EACH OF UNIFORM THICKNESS "t," IS REMOVED IN ORDER TO SHOW WEB DETAIL.
2. "h" IS THE TOTAL HEIGHT FROM TOP SKIN CENTERLINE TO BOTTOM SKIN CENTERLINE.
3. THE STRUCTURE IS SQUARE WITH CHORD = SPAN = "ℓ."

FIG. 1. Mechanical system.

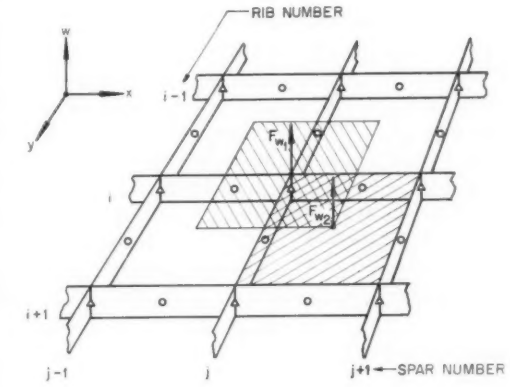

SYMBOLS: F_{w_1} FORCE AT RIB-SPAR INTERSECTION
F_{w_2} FORCE AT PANEL CENTER
o DENOTES POINT OF DEFINITION OF θ_x OR θ_y IN ANALOG MODEL
Δ DENOTES POINT OF DEFINITION OF U_w IN ANALOG MODEL

FIG. 2. Typical rib web-spar web intersection.

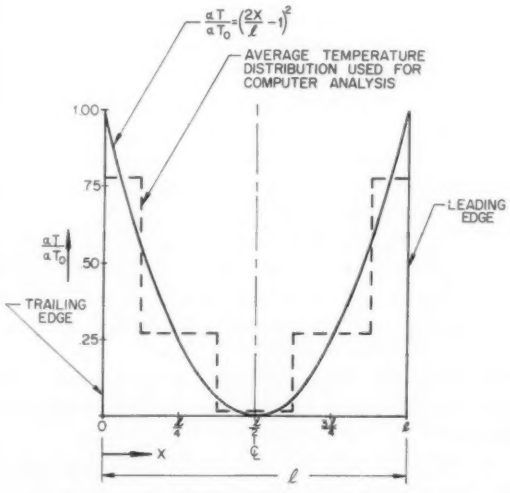

FIG. 3. Applied temperature distribution.

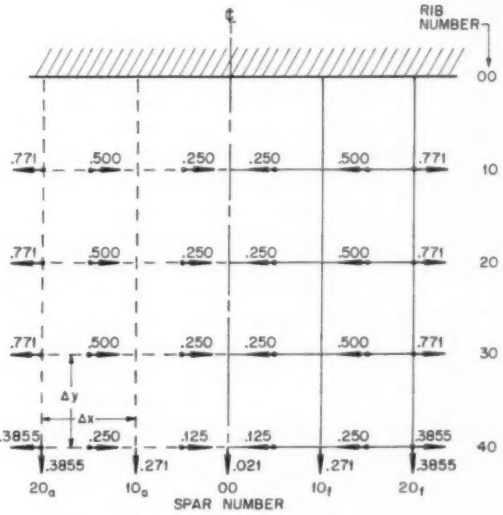
RIB NUMBER
SPAR NUMBER
NOTES:
1. EQUIVALENT LOADS ARE CALCULATED WITH THE AID OF EQS. (11), (12), AND (13).
2. THE NUMBERS SHOWN ABOVE ARE:
AND

FIG. 4. In-plane problem applied thermal loads.

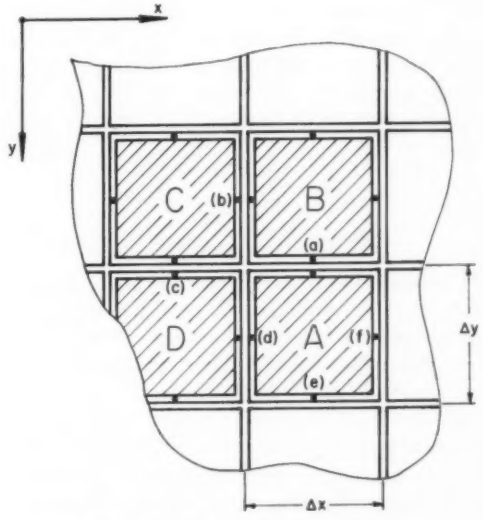

FIG. 5. Lumped model of a plane sheet.

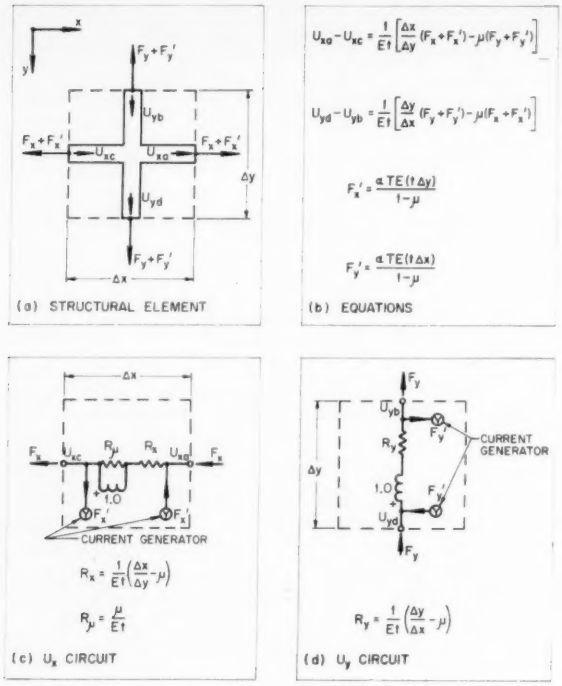

FIG. 6. Electrical analogy for axial load carrying elements, including Poisson's ratio effect.

load component corresponding to Eq. (17) can thus be written as

$$F_{w_1} \equiv P_1 \Delta x\, \Delta y = q_{i,j}\, \Delta x\, \Delta y + N_{x_{i,j}} \Delta y(\theta_{x_{i,j+(1/2)}} - \theta_{x_{i,j-(1/2)}}) + N_{y_{i,j}} \Delta x(\theta_{y_{i+(1/2),j}} - \theta_{y_{i-(1/2),j}}) \quad (19)$$

In order to calculate the load component described by Eq. (18), it should be noted that N_{xy} is defined at panel centers and not at rib spar intersections. Consider the finite difference expansion of Eq. (18) about panel center $[i + (1/2), j + (1/2)]$:

$$F_{w_2} \equiv P_2 \Delta x\, \Delta y = N_{xy_{i+(1/2),j+(1/2)}} \times [\Delta x(\theta_{x_{i+1,j+(1/2)}} - \theta_{x_{i,j+(1/2)}}) + \Delta y(\theta_{y_{i+(1/2),j+1}} - \theta_{y_{i+(1/2),j}})] \quad (20)$$

The equivalent load F_{w_2} can now be calculated at each panel center and then be prorated equally to the four adjacent rib-spar intersections. These prorated contributions can be added directly to the F_{w_1} contributions.

Since the total equivalent lateral load distribution as given by Eqs. (19) and (20) is a function of measured slopes, the procedure for calculating or measuring the solution to the problem of a laterally loaded heated structure is as follows:

(1) Apply load distribution, q, to the cold structure and measure appropriate slope differences for use in Eqs. (19) and (20).

(2) Calculate the new value of the equivalent lateral load distribution by means of Eqs. (19) and (20).

(3) Apply the new lateral load distribution to the structure.

(4) Repeat the above iteration procedure until the solution converges. For problems where the effects of thermal stresses are reasonably small, one or two iterations should be satisfactory. The iterative process will fail to converge if the structure buckles under the action of thermal stresses.

An Illustrative Example

In order to demonstrate the above techniques, a simple problem will be formulated and analyzed by means of the direct analogy analog computer. The system to be studied (Fig. 1) is a square, cantilever, constant-depth wing box covered with a constant thickness skin on both top and bottom sides. The wing box contains four equally spaced rib webs intersected orthogonally by five equally spaced spar webs. The temperature distribution for the structure, which is assumed to be the same at all spanwise stations, is shown in Fig. 3. The equivalent external loads to be applied to the in-plane structure, which are produced by the average temperature distribution of Fig. 3, are calculated with the aid of Eqs. (11), (12), and (13) and are presented in Fig. 4. The thermal stresses induced by this temperature distribution will be calculated first. The deflection influence coefficients for lateral loads will then be calculated, first in the absence of thermal stresses ("cold" wing), and then for two cases corresponding to different temperature levels ("hot" wing cases).

The Construction of the Lumped Prototype

In order to analyze a distributed mechanical system, a prototype model composed of lumped "building blocks" must first be constructed. In the construction of this finite difference model, numerous approximations and assumptions are made. For the purposes of the sample problem presented in this paper, simplifying assumptions are used which may not be generally valid, but their use should not be considered as a restriction on the general method. The following assumptions and representations are embodied in the lumped model:

(1) The structure is assumed to possess symmetry about the horizontal wing center plane and about the vertical plane passing through spar (00) (see Fig. 1).

(2) The rib and spar webs are assumed to remain unstressed when the temperature distribution is applied to the wing. This is a valid assumption if the webs are assumed to be constructed in such a manner as to relieve thermal stresses completely.

(3) Although the rib and spar webs are allowed to carry vertical shear, the strain energy in these webs is neglected.

(4) All axial loads are carried by the skin—i.e., the spar and rib cap areas are assumed negligibly small in comparison to the equivalent cover skin axial load carrying areas.

(5) The state of stress in the skin is considered separable. The cover skin is thus represented by idealized axial load carrying members and by idealized skin shear panels which are in equilibrium under shear loads.

(6) The Poisson's ratio effect between normal stresses in the cover skins is included in the analysis.

(7) In order to emphasize the effects of thermally induced stresses on the static behavior of the wing subjected to lateral loads, the values of the elastic constants E and G are assumed to be invariant with respect to temperature.

Symmetry Considerations

In constructing prototypes of mechanical systems such as the one under consideration, full use may be made of structural and load symmetry. In addition to a horizontal plane of symmetry which is used to separate the in-plane and lateral problems, the structure of Fig. 1 has a vertical plane of symmetry about spar (00). Making use of this fact, only half of the prototype need be constructed. Then, by proper application of boundary conditions at this plane of symmetry, the response of the system to symmetrical and antisymmetrical loading conditions can be obtained. All that is required is to decompose the applied load distribution into its symmetric and antisymmetric components.

It should be noted that, for the in-plane problem, the assumed thermal loading distribution is symmetrical with respect to the center spar; hence, only one set of boundary conditions along spar (00) is required for the in-plane problem. The loading in the lateral load problem is, however, unsymmetrical. The lateral problem is analyzed by applying unit symmetric and antisymmetric lateral loads to the structure. Results are presented in terms of symmetric and antisymmetric influence coefficient matrices.

Derivation of the Electrical Circuits

A direct-analog computer is essentially a large "tinker toy" containing electrical elements which can be made to possess behavioral correspondence to levers, masses, springs, dashpots, and forcing functions. Electrical measuring instruments are used to record the response of the electrical (analog) system. Since the problem being analyzed is a static one, the analog model can be constructed from levers, springs, and forcing functions only. The analogous quantities given in Table 1 are used.

Scale factors are normally used in the relationships between electrical quantities physically present in a computer and their analogs. The selection of scale factors is an important practical consideration that will not be discussed here because it is not essential. The reader is referred to reference 1 for details on scale factors.

Table 1

Mechanical Quantity	Electrical Quantity
Displacement, U	Voltage
Rotation or Slope, θ	Voltage
Force, F	Current
Moment, M	Current
Spring Constant, K	(Resistance)$^{-1}$
Leverage, and other similar effects	Transformer

The method that will be used for deriving the electrical analogy starts with the observation that the lumped mechanical prototype consists of a (large) number of simple structural elements which can be grouped into two or three basic types. The basic types of elements considered here are axial load carrying members, horizontal shear panels, and vertical shear webs. The derivation of the electrical analogy for the complete structure is accomplished in two steps. In the first step, electrical analogies are derived for the basic types of simple structural elements. In the second step, the electrical analogies for the elements are connected together so that the equilibrium relationships and displacement compatibility relationships existing at the intersections of the structural elements are satisfied.

Derivation of Electrical Circuit for the In-Plane Problem

Consider the lumped model of a plane sheet shown in Fig. 5. In this model each shear panel is connected to adjacent axial load members at *one* point on each side of the panel. Hence the pair of axial load members that cross at the intersection of panels A, B, C, and D are unloaded except at their ends and may, consequently, be removed from the structure and analyzed. These members and their electrical analogy are shown in Fig. 6. The equations satisfied by the members, as derived from Eqs. (9) and (10) by making finite difference approximations, are

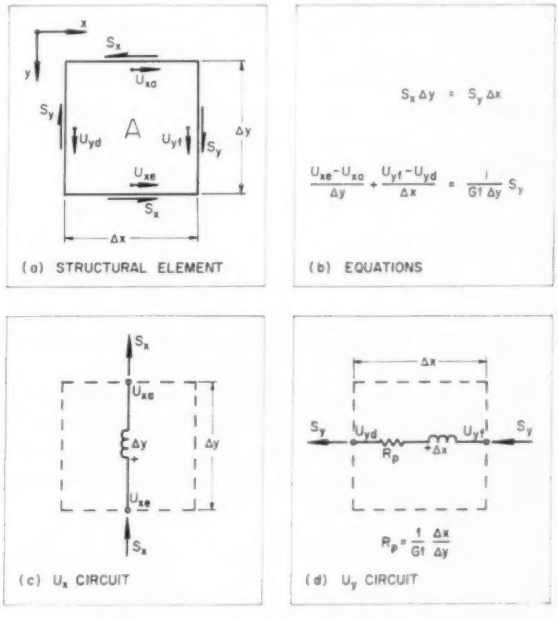

Fig. 7 Electrical analogy for a shear panel.

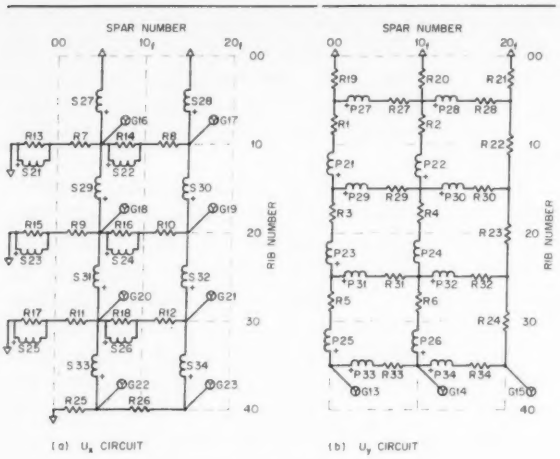

FIG. 8. Circuit for in-plane problem.

$$U_{xa} - U_{xc} = (1/Et)\,[(\Delta x/\Delta y)\,(F_x + F_x') - \mu(F_y + F_y')] \quad (21)$$

$$U_{yd} - U_{yb} = (1/Et)\,[(\Delta y/\Delta x)\,(F_y + F_y') - \mu\,(F_x + F_x')] \quad (22)$$

where

$$F_x = \sigma_x(t\Delta y), \quad F_y = \sigma_y(t\Delta x)$$

$$F_x' = \alpha TE(t\Delta y)/(1 - \mu)$$

$$F_y' = \alpha TE(t\Delta x)/(1 - \mu)$$

In the analogous electrical circuit, Fig. 6(c) and (d), currents are represented by force symbols and voltages are represented by displacement symbols. Voltages at nodes are the electric potentials with respect to a common reference (ground). Eqs. (21) and (22) can be interpreted as the expressions for the voltage drops in the U_x and U_y circuits, respectively. The current flowing in R_x is $F_x + F_x'$ and the current flowing in R_y is $F_y + F_y'$. Because of the presence of the unity turns ratio transformer, the current flowing in R_μ is $(F_x + F_x') - (F_y + F_y')$. Summing the voltage drops across R_x and R_μ, one obtains

$$U_{xa} - U_{xc} = R_x(F_x + F_x') + R_\mu[(F_x + F_x') - (F_y + F_y')] \quad (23)$$

If R_x is made equal to $[(\Delta x/\Delta y) - \mu]/Et$ and R_μ is made equal to μ/Et, Eq. (21) is obtained. The satisfaction of Eq. (22) by the circuit can be demonstrated in similar fashion.

Shear panel A in Fig. 5 and its electrical analogy are shown in Fig. 7. The equations satisfied by the forces and displacements at the edges of the panel, as derived from Eqs. (3) and (6) by making finite difference approximations, are

$$S_x\Delta y = S_y\Delta x \quad (24)$$

$$[(U_{xe} - U_{xa})/\Delta y] + [(U_{yf} - U_{yd})/\Delta x] = (1/Gt\Delta y)S_y \quad (25)$$

where $S_x = \tau_{xy}(t\Delta x)$, $S_y = \tau_{xy}(t\Delta y)$

These equations are satisfied by the analogous electrical circuit shown in Fig. 7(c) and (d) where, as in the case of the axial load members, force symbols are used for currents and displacement symbols are used for voltage. The turns ratio of the ideal transformer coupling the U_x and U_y circuits is equal to $\Delta x/\Delta y$. Eq. (24) is, consequently, a statement of the relationship between the currents in the two windings of this transformer. The voltage across resistor R_p is

$$E_{R_p} = U_{yf} - U_{yd} + (\Delta x/\Delta y)\,(U_{xe} - U_{xa}) = S_yR_p \quad (26)$$

If R_p is made equal to $\Delta x/Gt\Delta y$, Eq. (26) becomes identical to Eq. (25).

With the electrical circuits for the axial load members and the shear panel derived above, the stage is set for the second major step, which is to interconnect a number of these circuits to form an analogy for the complete structure. It will be noted in Fig. 5 that, at point (a), two shear panels and two axial load members are joined together. The displacement compatibility condition is simply that U_{xa} is the common x displacement for these four members. The equilibrium condition at point (a) is that the sum of the forces exerted on point (a) by the four adjacent members is zero. This condition is derivable from the displacement compatibility condition and the statement that the forces acting on point (a) do no work. In the electrical analogy, the displacement compatibility condition is satisfied by joining the terminals of the four circuits together so that their voltages are equal. Satisfaction of the no-work condition and, hence, of the equilibrium condition is assured since a solid connection consumes no power (the analogy of strain energy). In general, it is necessary to demonstrate either the displacement compatibility condition or the equilibrium condition, but not both, in deriving the electrical analogy of a built-up structure.

In a similar manner, the U_y circuits of two shear

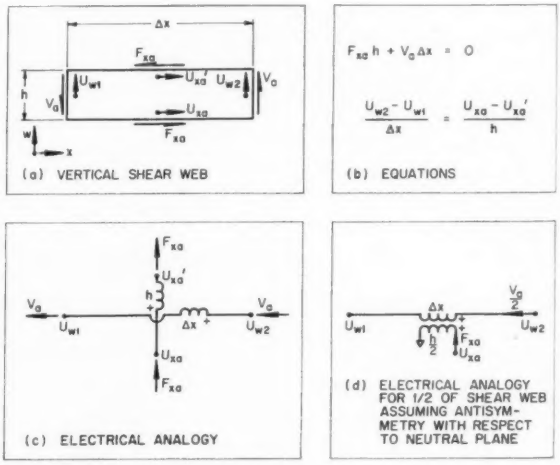
(a) VERTICAL SHEAR WEB
(b) EQUATIONS
(c) ELECTRICAL ANALOGY
(d) ELECTRICAL ANALOGY FOR 1/2 OF SHEAR WEB ASSUMING ANTISYMMETRY WITH RESPECT TO NEUTRAL PLANE

FIG. 9. Electrical analogy for a vertical shear web.

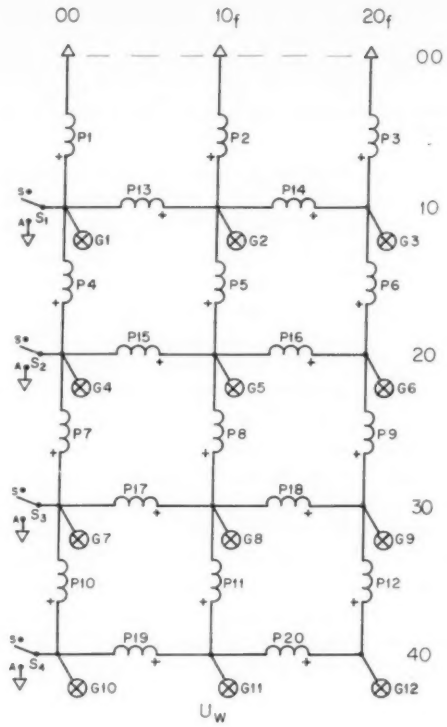

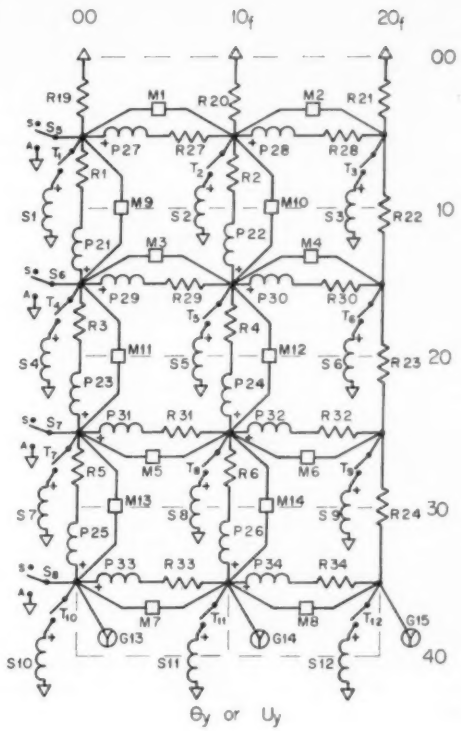

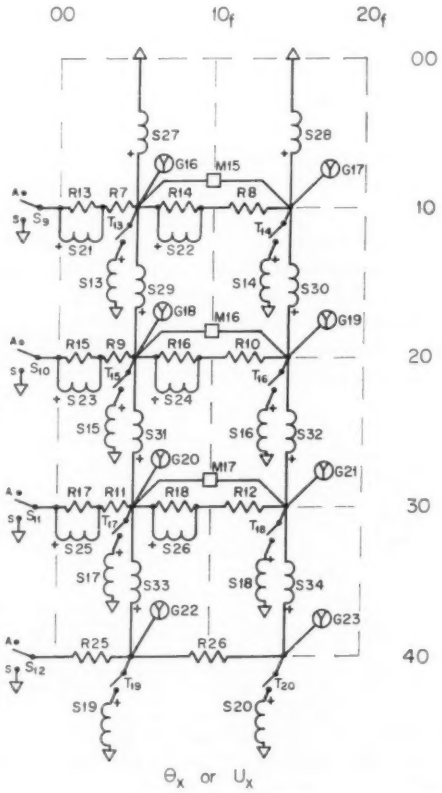

NOTES:

1. FOR IN-PLANE PROBLEM, OPEN ALL SWITCHES (T), AND CONNECT ALL SYMMETRY SWITCHES TO S TERMINALS; THE CIRCUIT THEN REPRESENTS U_x AND U_y. THE U_w CIRCUIT IS NOT USED.
2. FOR THE LATERAL LOAD ANALYSIS, CLOSE ALL SWITCHES (T). CONNECT SYMMETRY SWITCHES ACCORDING TO TYPE OF LOAD. (SYMMETRY IS DEFINED WITH RESPECT TO THE VERTICAL PLANE PASSING THROUGH SPAR 00.)
3. —□— SYMBOL REPRESENTS METERING POINT FOR VOLTAGES NECCESSARY FOR ITERATION PROCEDURE.
4. —Ⓨ— SYMBOL REPRESENTS CURRENT GENERATORS TO BE SET FOR IN-PLANE PROBLEM.
5. —⊗— SYMBOL REPRESENTS CURRENT GENERATORS TO BE SET FOR LATERAL PROBLEM.

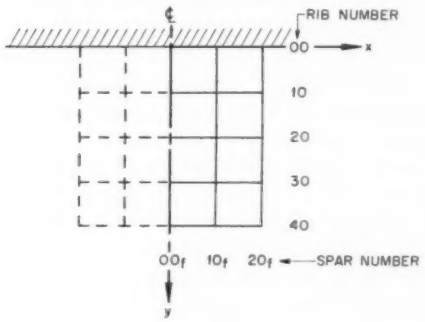

FIG. 10. Circuit diagram.

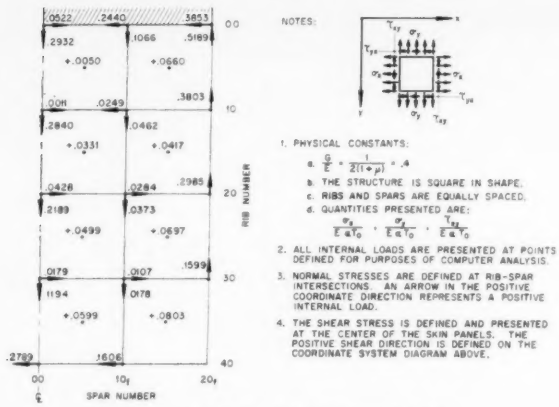

FIG. 11. In-plane problem computer data.

panels and of two axial load members are joined together at point (b) in Fig. 5.

The complete electrical analogy for the in-plane thermal stress problem is shown in Fig. 8.

Note that although there is no direct electrical connection between the U_x and U_y circuits, these circuits are magnetically coupled by transformers.

Boundary conditions are treated in a natural manner. Along a clamped edge, voltages are constrained to be zero. A free edge is characterized by an absence of electrical constraints. At the plane of symmetry along spar (00), voltages corresponding to x displacements are constrained to be zero and voltages corresponding to y displacements are unconstrained.

The circuits for axial force members can be simplified at points along the free edges because the force normal to the edge is zero. For example, along spar (20f) in Fig. 8, F_x is zero, so that Eq. (22) becomes

$$\left.\begin{aligned} U_{yd} - U_{yb} &= (1/Et)\,\{(\Delta y/\Delta x)F_y + \\ &\qquad [(\Delta y/\Delta x)F_y' - \mu F_x']\} \\ U_{yd} - U_{yb} &= (1/Et)\,(\Delta y/\Delta x) \times \\ &\qquad [F_y + (1-\mu)F_y'] \end{aligned}\right\} \quad (27)$$

Hence, an axial force member along spar (20f) is represented by a simple resistor with a constant current generator at each end.

It may be seen from Fig. 6(c) and (d) that two constant current generators occur at the junction of axial force members, but since one generator inserts current into the node and the other withdraws current, the net effect can be represented by a single generator inserting a current proportional to the difference in F_x' (or F_y') at adjacent rib-spar intersections. Furthermore, since the temperature and the physical properties of the structure are uniform in the y direction, generators for the U_y circuit are required at the outboard end only.

A simplification of the circuit also occurs at the clamped edge since it is assumed that the strain parallel to the clamped edge is zero. Hence, along rib (00) in Fig. 8, it is found that, by setting $U_{xa} - U_{xc}$ equal to zero in Eq. (21),

$$U_{yd} - U_{yb} = [(1-\mu^2)/Et]\,(\Delta y/\Delta x)\,(F_y + F_y') \quad (28)$$

An axial force member normal to the clamped edge is, consequently, represented by a simple resistor whose value is $(1-\mu^2)\Delta y/Et\Delta x$. Δy is, in this expression, equal to one half of the rib spacing.

Derivation of Electrical Circuits for the Lateral Load Problem

An electrical analogy for the bending of flat plates is described in reference 9; it is shown in reference 8 that the electrical analogy for the bending of thin multicell shells with orthogonal ribs and spars has an identical form. Hence the circuits described in references 8 and 9 are directly applicable to the lateral load problem.

The electrical analogy for the lateral load problem can also be obtained by an extension of the analogy used in the in-plane problem. In the lateral load problem the cover sheets are still in a condition of plane stress, but they are fastened to an internal system of vertical shear webs. In the lumped model it is assumed that the vertical shear webs are connected to the cover sheets at points midway between ribs and spars [points (a), (b), (c), and (d) in Fig. 5], and that they are connected to each other at rib-spar intersections. The electrical analogy for a vertical shear web in which shear strain is neglected is shown in Fig. 9. Since the structure is symmetrical with respect to a plane midway between the cover sheets and the loading is antisymmetrical with respect to the same plane, U_{za}' is equal to $-U_{za}$ in Fig. 9(a). This condition implies that the voltage at the center point of the vertical transformer winding in Fig. 9(c) is zero, and then, consequently, an analogy that represents only the lower one-half of the shear web can be formed, as shown in Fig. 9(d).

The complete analogy for the lateral load structure is constructed by adding electrical elements representing vertical shear webs to the circuit previously derived for the in-plane problem. The complete circuit shown in Fig. 10 is used for both the lateral and the in-plane load problems, with the transformers that represent vertical shear webs being removed for the in-plane problem. The constant current generators appearing at rib-spar intersections in the U_w circuit simulate one-

	1000	2000	3000	4000	1010f	2010f	3010f	4010f	1020f	2020f	3020f	4020f
1000	.045	.072	.100	.131	.031	.064	.096	.128	.021	.054	.090	.123
2000	.072	.206	.322	.442	.064	.185	.309	.434	.050	.164	.290	.418
3000	.100	.322	.602	.890	.094	.306	.576	.872	.078	.279	.542	.832
4000	.131	.442	.890	1.400	.125	.428	.868	1.340	.101	.388	.812	1.280
1010f	.031	.064	.094	.125	.035	.064	.094	.124	.028	.059	.092	.123
2010f	.064	.185	.306	.428	.064	.188	.308	.426	.056	.176	.299	.420
3010f	.096	.309	.576	.868	.094	.308	.578	.864	.082	.290	.558	.848
4010f	.128	.434	.872	1.340	.124	.426	.864	1.340	.105	.399	.832	1.300
1020f	.021	.050	.078	.101	.028	.056	.082	.105	.050	.073	.093	.114
2020f	.054	.164	.279	.388	.059	.176	.290	.399	.073	.210	.318	.421
3020f	.090	.290	.542	.812	.092	.299	.558	.832	.093	.318	.602	.872
4020f	.123	.418	.832	1.280	.123	.420	.848	1.300	.114	.421	.872	1.360

$\beta = 0$

FIG. 12. "Cold" structure symmetric deflection influence coefficients (all data presented in units of the dimensionless parameter λ).

half of the lateral loads given by Eqs. (19) and (20). The increments in slopes appearing in these equations are obtained from measurements of voltage increments in the cover sheet circuits. The slopes are, of course, equal to the displacements in the lower cover sheet divided by the semidepth of the wing.

Identification of Elements in the Complete Circuit Diagram

The electrical circuit diagram which represents both the in-plane and the lateral problems is presented in Fig. 10.

The functions of the elements in Fig. 10 are as follows:

P and S 1 to 20:	Vertical web (lateral problem only)
P and S 21 to 26:	Poisson ratio (both problems)
P and S 27 to 34:	Horizontal shear panel (both problems)
R1 to R6:	R_y for regions with Poisson ratio (both problems)
R7 to R12:	R_x for regions with Poisson ratio (both problems)
R13 to R18:	R_μ for regions with Poisson ratio (both problems)
R19 to R24:	R_y for regions without Poisson ratio (both problems)
R25 to R26:	R_x for regions without Poisson ratio (both problems)
R27 to R34:	R_p — Horizontal shear panel flexibility (both problems)
M1 to M17:	Metering dummies for purposes of measuring slope differences needed to calculate iteration currents in lateral load problem
T_1 to T_{20}:	Switches to disconnect web transformers in order to convert circuit to in-plane problem
S_1 to S_{12}:	Boundary condition symmetry switches
G1 to G_{12}:	Current generators used to introduce lateral loads
G17 to G23:	Current generators used to introduce effects of thermal strain for the in-plane problem

The Computer Solution

The In-Plane Problem

The self-equilibrating internal loads calculated by making appropriate measurements on the circuit of Fig. 10 are presented in dimensionless form in Fig. 11. It can be noted that the regions in the vicinity of the leading and trailing edges are in compression while the central region of the wing is in tension as expected. These data are then used in conjunction with Eqs. (19) and (20) and the lateral problem circuit to calculate the lateral influence coefficients.

The Lateral Problem

By proper switch connections, the circuit of Fig. 10 can now be used to calculate the lateral deflection influence coefficients for both the "hot" and "cold" structures. Data are presented in the form of deflection influence coefficient matrices for symmetric and antisymmetric unit loads. The results are presented in terms of a dimensionless deflection parameter λ, where

	1000	2000	3000	4000	1010$_f$	2010$_f$	3010$_f$	4010$_f$	1020$_f$	2020$_f$	3020$_f$	4020$_f$
1000	0	0	0	0	0	0	0	0	0	0	0	0
2000	0	0	0	0	0	0	0	0	0	0	0	0
3000	0	0	0	0	0	0	0	0	0	0	0	0
4000	0	0	0	0	0	0	0	0	0	0	0	0
1010$_f$	0	0	0	0	.0180	.0189	.0189	.0192	.0200	.0302	.0345	.0362
2010$_f$	0	0	0	0	.0189	.0461	.0510	.0544	.0306	.0716	.0912	.1000
3010$_f$	0	0	0	0	.0189	.0510	.0858	.1000	.0352	.0919	.1450	.1750
4010$_f$	0	0	0	0	.0192	.0544	.1000	.1590	.0374	.1020	.1780	.2520
1020$_f$	0	0	0	0	.0200	.0306	.0352	.0374	.0519	.0655	.0716	.0754
2020$_f$	0	0	0	0	.0302	.0716	.0919	.1020	.0655	.1580	.1880	.2050
3020$_f$	0	0	0	0	.0345	.0912	.1450	.1780	.0716	.1880	.3040	.3520
4020$_f$	0	0	0	0	.0362	.1000	.1750	.2520	.0754	.2050	.3520	.5090

$\beta = 0$

FIG. 13. "Cold" structure antisymmetric deflection influence coefficients (all data presented in units of the dimensionless parameter λ).

	1000	2000	3000	4000	1010$_f$	2010$_f$	3010$_f$	4010$_f$	1020$_f$	2020$_f$	3020$_f$	4020$_f$
1000	0	0	0	0	0	0	0	0	0	0	0	0
2000	0	0	0	0	0	0	0	0	0	0	0	0
3000	0	0	0	0	0	0	0	0	0	0	0	0
4000	0	0	0	0	0	0	0	0	0	0	0	0
1010$_f$	0	0	0	0	.0007	.0015	.0020	.0024	.0016	.0031	.0041	.0046
2010$_f$	0	0	0	0	.0015	.0037	.0054	.0066	.0028	.0075	.0107	.0125
3010$_f$	0	0	0	0	.0020	.0054	.0084	.0109	.0035	.0101	.0150	.0200
4010$_f$	0	0	0	0	.0024	.0066	.0109	.0150	.0038	.0116	.0198	.0260
1020$_f$	0	0	0	0	.0016	.0028	.0035	.0038	.0036	.0058	.0070	.0076
2020$_f$	0	0	0	0	.0031	.0075	.0101	.0116	.0058	.0150	.0201	.0229
3020$_f$	0	0	0	0	.0041	.0107	.0150	.0198	.0070	.0201	.0314	.0376
4020$_f$	0	0	0	0	.0046	.0125	.0200	.0260	.0076	.0229	.0376	.0481

$\beta = 3.192$

FIG. 14. Antisymmetric difference deflection influence coefficient matrix, $\beta = 3.192$ (all data presented in units of the dimensionless parameter λ).

	1000	2000	3000	4000	1010$_f$	2010$_f$	3010$_f$	4010$_f$	1020$_f$	2020$_f$	3020$_f$	4020$_f$
1000	0	0	0	0	0	0	0	0	0	0	0	0
2000	0	0	0	0	0	0	0	0	0	0	0	0
3000	0	0	0	0	0	0	0	0	0	0	0	0
4000	0	0	0	0	0	0	0	0	0	0	0	0
1010$_f$	0	0	0	0	.0015	.0032	.0044	.0052	.0034	.0068	.0089	.0102
2010$_f$	0	0	0	0	.0032	.0080	.0118	.0142	.0061	.0162	.0234	.0279
3010$_f$	0	0	0	0	.0044	.0118	.0185	.0238	.0076	.0221	.0356	.0445
4010$_f$	0	0	0	0	.0052	.0142	.0238	.0325	.0084	.0256	.0432	.0574
1020$_f$	0	0	0	0	.0034	.0061	.0076	.0084	.0078	.0128	.0152	.0168
2020$_f$	0	0	0	0	.0068	.0162	.0221	.0256	.0128	.0334	.0442	.0508
3020$_f$	0	0	0	0	.0089	.0234	.0356	.0432	.0152	.0442	.0689	.0838
4020$_f$	0	0	0	0	.0102	.0279	.0445	.0574	.0168	.0508	.0838	.1070

$\beta = 6.384$

FIG. 15. Antisymmetric difference deflection influence coefficient matrix, $\beta = 6.384$ (all data presented in units of the dimensionless parameter λ).

$$\lambda = U_w t h^2 E / l^2 L \tag{29}$$

and L is defined as the total load applied to *one half* of the structure. For symmetric boundary conditions, the total load applied to the complete structure is $2L$. For antisymmetric boundary conditions, the total load is an up load, L, at the point of application (forward part of structure) and a down load, L, at the corresponding point on the aft part of the structure.

Data are presented in Figs. 12, 13, 14, and 15 for three values of the dimensionless temperature parameter β, where

$$\beta = (l/h)^2 \alpha T_0 \tag{30}$$

In Figs. 14 and 15, for which β is not equal to zero, only the antisymmetric difference deflection influence coefficient matrices are presented. The difference matrix is defined as the difference between the "hot" influence coefficients and the "cold" influence coefficients. Symmetric difference influence coefficients were measured but are not presented since the applied temperature distribution does not significantly effect the symmetric results. The maximum effects in symmetric cases are approximately one tenth of the maximum effects in antisymmetric cases.

It may be worthy of mention that the results of the analysis are consistent with conclusions based on elementary beam theory that (1) self-equilibrating stresses have no (or little) influence on the effective bending stiffness, and (2) self-equilibrating stresses of the type produced by aerodynamic heating produce a decrease in the effective torsional rigidity of the structure.

References

[1] MacNeal, R. H., McCann, G. D., and Wilts, C. H., *The Solution of Aeroelastic Problems by Means of Electrical Analogies*, Journal of the Aeronautical Sciences, Vol. 18, No. 12, pp. 777–789, December, 1951.

[2] Mazelsky, B., and O'Connell, R. F., *The Integrated Use of Analog and Digital Computing Machines for Aircraft Dynamic Load Problems*, Journal of the Aeronautical Sciences, Vol. 23, No. 8, pp. 721–740, August, 1956.

[3] Paschkis, V., and Baker, H. D., *A Method for Determining Unsteady State Heat Transfer by Means of an Electrical Analogy*, Trans. ASME, Vol. 64, p. 105, 1942.

[4] MacNeal, R. H., *An Asymmetrical Finite Difference Network*, Quart. Appl. Math., Vol. XI, No. 3, October, 1953.

[5] Budianski, B., and Mayers, J., *Influence of Aerodynamic Heating on the Effective Torsional Stiffness of Thin Wings*, Journal of the Aeronautical Sciences, Vol. 23, No. 12, pp. 1081–1093, December, 1956.

[6] Vosteen, L. F., and Fuller, K. E., *Behavior of a Cantilevered Plate Under Rapid Heating Conditions*, NACA RM L55E20C, July, 1955.

[7] Timoshenko, S., *Theory of Plates and Shells*, 1st Ed., p. 301, McGraw-Hill Publishing Co., New York, 1940.

[8] Benscoter, S. U., and MacNeal, R. H., *Equivalent Plate Theory for a Straight Multicell Wing*, NACA TN 2786, September, 1952.

[9] MacNeal R. H., *The Solution of Elastic Plate Problems by Electrical Analogies*, J. Appl. Mech. March, 1951.

Significant Developments in Aerodynamics (*Continued from page 144*)

Kampé de Fériet, J., C. R. Acad. Sci., Paris, Vol. 227, p. 760, 1948.

von Kármán, T., and Howarth, L., *On the Statistical Theory of Isotropic Turbulence*, Proc. Roy. Soc. London (A), Vol. 164, p. 192, 1938.

von Kármán, T., and Lin, C. C., *On the Concept of Similarity in the Theory of Isotropic Turbulence*, Adv. Appl. Mech. Vol. 2, p. 1, 1951.

Kolmogoroff, A. N., C. R. Acad. Sci., URSS, Vol. 31, p. 538; Vol. 32, p. 16, 1941.

Kraichnan, Robert H., *Relation of Fourth to Second Moments in Stationary Isotropic Turbulence*, Phys. Rev., Vol. 107, pp. 1485–1490, 1957.

Kraichnan, Robert H., *Irreversible Statistical Mechanics of Incompressible Hydromagnetic Turbulence*, Phys. Rev., Vol. 109, 1407–1422, 1958.

Langer, R. E., *The Asymptotic Solutions of a Class of Ordinary Differential Equations of the Fourth Order, With Special Reference to an Equation of Hydrodynamics*, Trans. Amer. Math. Soc., Vol. 84, pp. 144–191, 1957.

Lin, C. C., *The Theory of Hydrodynamic Stability*, Cambridge University Press, 1955.

Lin, C. C., *On the Instability of Laminar Flow and Its Transition to Turbulence*, presented at the Symposium on Boundary Layer Theory, Freiburg, Germany, 1957 (to appear in Proceedings).

Laufer, J., *On the Oscillations in the Supersonic Boundary Layer*, Presented at the 9th International Congress of Applied Mechanics, 1956 (to appear in the Proceedings).

Malkus, W. V. R., *Outline of a Theory of Turbulent Shear Flow*, J. Fluid Mech. Vol. 1, pp. 521–539, 1956.

Meksyn, D., and Stuart, J. T., *Stability of Viscous Motion Between Parallel Planes for Finite Disturbances*, Proc. Roy. Soc. (A), Vol. 208, p. 517, 1951.

Millionshchikov, M., C. R. Acad. Sci. URSS, Vol. 22, pp. 231, 235, 1939; Vol. 32, pp. 615, 619, 1941.

Obukhoff, A. M., C. R. Acad. Sci., URSS, Vol. 32, p. 19, 1941.

Onsager, L., *The Distribution of Energy in Turbulence* (abstract only), Phys. Rev., 68, p. 286, 1945.

Proudman, I., and Reid, W. H., *On the Decay of a Normally Distributed and Homogeneous Turbulence Field*, Phil. Trans. Roy. Soc. London (A), 247, p. 163, 1954.

Reis, F. B., *Studies of Correlation and Spectra in Homogeneous Turbulence*, Ph.D. Thesis, M.I.T., 1952.

Schubauer, G. B., *Boundary Layer Transition*, Paper presented at the Freiburg Symposium, 1957.

Schubauer, G. B., and Klebenoff, P. S., *Contributions to the Mechanics of Boundary Layer Transition*, NACA TN 3489, 1955.

Stuart, J. T., *On the Nonlinear Theory of Hydrodynamic Stability*, J. Fluid Mech., May, 1958.

Tatsumi, T., *The Theory of Decay Process of Incompressible Isotropic Turbulence*, Proc. Roy. Soc. (A), Vol. 239, pp. 16–45, 1957.

Taylor, Sir Geoffrey, *Statistical Theory of Turbulence*, Proc. Roy. Soc. Vol. 181, p. 421, 1935.

Taylor, Sir Geoffrey, Proc. Roy. Soc. (A), Vol. 164, p. 476, 1938.

Townsend, A. A., *The Structure of Turbulent Shear Flow*, Cambridge University Press, 1956.

Wasow, W., *Asymptotic Solution of the Differential Equation of Hydrodynamic Stability in a Domain Containing a Transition Point*, Ann. Math., Vol. 58, pp. 222–252, 1953.

von Weiszäcker, C. F., *Das Spektrum der Turbulenz bei grossen Reynoldsschen Zahlen*, Z. Physik, Vol. 124, p. 614, 1948.

Investigation of Normal Force Distributions and Wake Vortex Characteristics of Bodies of Revolution at Supersonic Speeds†

J. F. MELLO*

McDonnell Aircraft Corporation

Summary

The supersonic aerodynamic characteristics of inclined bodies of revolution at high angles of attack have been investigated in order to provide a more basic understanding of the body vortex wake flow and its relation to the problem of body-wing interference. The results of wind-tunnel tests, whereby the normal force, pitching moment, normal force distributions, and the local flow properties in the vicinity of the body were determined, are discussed and analyzed.

Comparisons of experimental normal force coefficient and center of pressure data with values calculated in accordance with theories which include methods for estimating the effects of viscosity show that the accuracy of these estimates is strongly dependent on the body fineness ratio and the angle of attack. Further comparisons of the distributions of theoretical and experimentally derived cross-flow drag coefficients clearly show that, in general, the disagreement between experiment and existing theories is due to the inadequate prediction of the magnitude and distribution of the forces resulting from flow separation.

The circulation strengths of the concentrated vortices and the circulation strengths of the vortex feeding sheets in the body vortex wake are determined by closed-contour velocity-perimeter integrations for paths enclosing the vortex or the feeding sheet. The values of vortex strength calculated in this manner are in close agreement with the values predicted by vortex strength formulas written for a simple theoretical model for which it is assumed that the cross-flow in any plane along the cylindrical portion of the body is represented by the steady incompressible potential flow about a cylinder, two symmetrical vortices of equal strength, and the attendant image vortices. However, in computing these strengths it is necessary to use the vortex locations and the viscous normal force distributions determined from experiment.

The experimentally determined values of vortex strength are, in turn, used to calculate—by means of the aforementioned incompressible cross-flow potential—the local flow inclination angles which are in good agreement with the measured values, except in the vortex core, in the vicinity of the feeding sheet, and in regions for which transonic cross-flow velocities are expected. A consideration of these various regions with simple methods which account for the observed phenomena leads to substantial improvement in the agreement between theory and experiment.

It is indicated that the complete vortex wake flow may be adequately predicted for a body of revolution (for conditions represented by the theoretical flow model), provided that the distribution of the viscous normal force and the vortex locations are accurately known.

Received May 5, 1958. Revised and received September 26, 1958.

† This research was supported by the Bureau of Ordnance, U.S. Navy, under Contract NOrd 12826 and is part of a comprehensive aerodynamic research program administered under the Bumblebee Project by the Applied Physics Laboratory, The Johns Hopkins University, Baltimore, Md.

* Project Group Engineer, Aerodynamics, Missile Engineering Division.

Symbols

a	= body radius of the cylindrical section
c_{d_c}	= local cross-flow drag coefficient based on diameter
c'_{d_c}	= cross-flow drag coefficient of an infinite circular cylinder, per unit length, for steady-state flow, based on diameter
C_n	= local normal force coefficient per unit length $-(2a/S)\int_{-\pi/2}^{\pi/2} C_p \sin\theta d\theta$
C_N	= total normal force coefficient, $\int_0^l C_n\, dz = N/q_0 S$
C_p	= pressure coefficient, $p - p_0/q_0$
d	= body diameter, cylindrical section
i	= imaginary number, $\sqrt{-1}$
l	= overall body length
M_l	= local Mach Number
M_∞	= free-stream Mach Number
M_c	= cross-flow Mach Number
n	= local normal force per unit length, $n = dN/dz$
N	= resultant normal force
p	= local static pressure
p_0	= free-stream static pressure
p_{t_l}	= local total pressure, corrected for shock losses and losses due to local flow inclination
p_{t_0}	= free-stream total pressure
q_0	= free-stream dynamic pressure, $\rho_0 U_0^2/2$
s	= complex notation of a point in the cross-flow plane, $s = x + iy = re^{i\theta}$
S	= reference area, πa^2
t	= time
U_0	= free-stream velocity
U_l	= total local velocity, $U_l^2 = (U_0 \cos\alpha_B + w)^2 + u^2 + v^2$
u, v	= cross-flow velocity components in x and y directions, respectively
v_r, v_θ	= radial and tangential velocities in the cross-flow plane, respectively
V	= total local cross-flow velocity, $\sqrt{u^2 + v^2} = \sqrt{v_r^2 + v_\theta^2}$
V_0	= free-stream cross-flow velocity, $U_0 \sin\alpha_B$
w	= axial perturbation velocity
x, y, z	= model Cartesian coordinates, origin at vertex, z positive downstream along body axis
r, θ, z	= model cylindrical coordinates, $\theta = 0°$ in horizontal plane of model on right-hand side, looking upstream, while $\theta = 90°$ denotes the top location
α_B	= angle of attack of body
α	= tangential component of the local flow inclination angle, $\tan\alpha = v_\theta/U_0 \cos\alpha_B$
β	= radial component of the local flow inclination angle, $\tan\beta = v_r/U_0 \cos\alpha_B$
ϵ	= total local flow inclination angle, $\tan\epsilon = V/U_0 \cos\alpha_B$
$\Gamma/2\pi U_0 a$	= nondimensionalized circulation strength

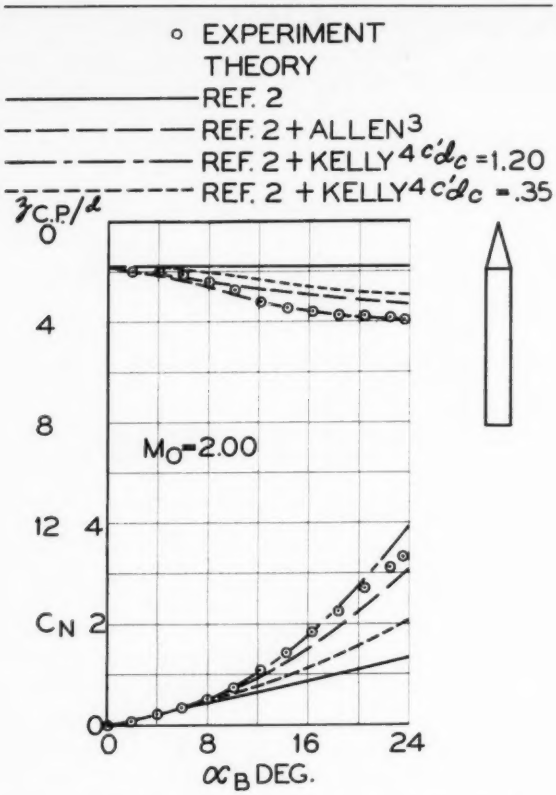

FIG. 1(a). The normal force and center of pressure characteristics of a 30° cone-cylinder configuration (l/d = 8.03).

σ	= position of vortex center in the cross-flow plane, $\xi + i\eta$ (right-hand side)
$-\bar{\sigma}$	= position of symmetrically located vortex in the cross-flow plane, $-\xi + i\eta$
$-a^2/\sigma$, $a^2/\bar{\sigma}$	= image vortex location, $\xi_i + i\eta_i$ and $-\xi_i + i\eta_i$, respectively
ξ, η	= Cartesian coordinates of right-hand real vortex
ξ_i, η_i	= Cartesian coordinates of right-hand image vortex
ρ_0	= free-stream air density
W	= complex potential, $\Phi + i\Psi$
Φ	= potential function in the cross-flow plane
Ψ	= stream function in the cross-flow plane
γ	= ratio of specific heats (γ = 1.40 for air)
ln	= natural logarithm
Rl	= real part of complex function

Subscripts

p = potential contribution
v = viscous contribution
i = image
z = conditions at axial station z from nose

(1) Introduction

The interaction of the vortex wake, which has been observed on the leeward side of bodies of revolution at moderate angles of attack in a supersonic stream, with any attached lifting surfaces is an important aspect of the total problem of wing-body interference. It has been shown that this vortex wake at high angles of attack can have a large effect upon the forces and the distribution of forces developed on wings or tails immersed in this flow. Since methods[1] are available for the calculation of lifting surface loads and load distributions for nonuniform supersonic flows, the immediate problem is that of predicting the properties of the flow in the vicinity of the lifting surface.

This paper presents the results of an experimental investigation of the aerodynamic characteristics of an inclined body of revolution and assesses the adequacy of available methods for estimating these characteristics. A 30° cone-cylinder configuration has been used to obtain normal force and pitching-moment data, normal force distributions, and local flow properties for these purposes. Comparisons of experimental and theoretical results are presented for a wide variety of conditions for which experimental data were obtained.

(2) Force and Moment Characteristics

The normal force and pitching-moment characteristics of inclined bodies of revolution at supersonic speeds have been treated by several authors. Theories are available for the prediction of these characteristics in both the low angle of attack and high angle of attack regimes. The high angle of attack theories are semi-empirical in nature and consist of the addition of a viscous contribution to a potential solution which is usually taken to be linear with the angle of attack.

In the present studies, the high angle of attack characteristics were of more immediate concern. Therefore, the potential solutions for the configurations discussed herein were calculated using the hybrid theory of Van Dyke,[2] and comparisons with other theories were not made. The viscous contributions to the

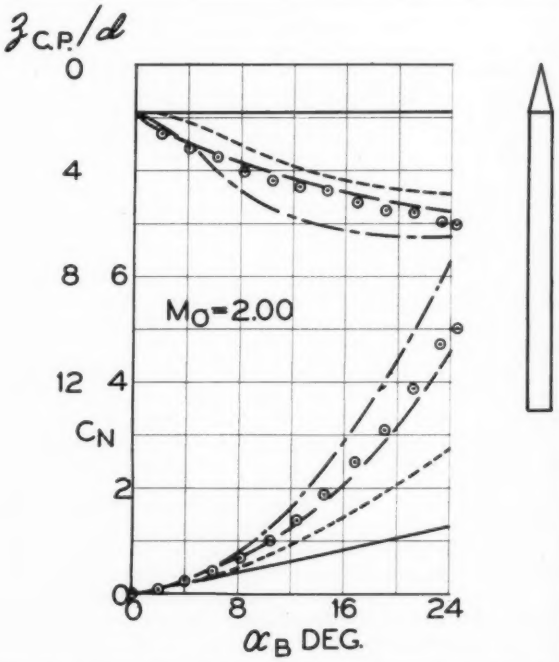

FIG. 1(b). The normal force and center of pressure characteristics of a 30° cone-cylinder configuration (l/d = 13.14).

body normal force magnitudes and distributions in all of the cases discussed were calculated by the method suggested by Allen,[3] and, for comparison purposes, by Kelly's method[4] as well.

The variation normal force coefficient and center of pressure with angle of attack at Mach Number 2 for two of several 30° cone-cylinder bodies of varying fineness ratio which were tested are presented in Fig. 1. Also shown are the predicted values using the hybrid theory of Van Dyke to which has been added the viscous contribution obtained by the methods of Allen and Kelly. The results shown for Kelly's method with $c'_{d_c} = 0.35$ and $c'_{d_c} = 1.20$ are for the case of a turbulent boundary layer and for the case of a laminar boundary layer, respectively.

These data illustrate how the methods of Allen or Kelly closely estimate the measured coefficients in certain cases but, nevertheless, indicate that neither method is satisfactory in all cases. In particular, it is noted that the accuracy of both methods depends on the fineness ratio of the body and on the angle of attack.

Because of the generally poorer agreement (except at very low angles of attack) shown for Kelly's method with $c'_{d_c} = 0.35$, subsequent calculations in this report are made with $c'_{d_c} = 1.20$ only. Furthermore, sufficient evidence is available to indicate that the form drag characteristics of a laminar-flow type separation are preserved (superficially, at least) for supersonic axial flow conditions, even though the boundary layer itself is turbulent. The reason for this is the low critical Mach Number (≈ 0.4) of a cylinder and the presence of lambda or shoulder shocks at the side of the body ($\theta = 0°$) at low angles of attack.

(3) Normal Force Distributions

Static-pressure data were obtained for the 30° cone-cylinder configuration at $M_0 = 2$ for angles of attack of 0°, 4°, 8°, 12°, 16°, 20°, and 23°. The data are reduced to coefficient form, and local normal force coefficients per degree of angle of attack are calculated at each station for all conditions tested. These data are presented in Fig. 2 in comparison with the Van Dyke solution. The inadequacy of linear potential-flow theories to predict the normal force distributions at all but very low angles of attack is shown very clearly in this figure.

As previously mentioned, there are two approximate methods (Allen's and Kelly's) which yield satisfactory results in some instances. However, the accuracy of these methods, to a great extent, is dependent upon the fineness ratio and the angle of attack range. In order to understand these anomalies, the potential normal-force-per-degree distribution is first obtained from the data shown in Fig. 2. Since the local normal force coefficient slope, shown in Fig. 2 for $\alpha_B = 4°$, begins to rise from zero approximately 8.5 body diameters aft of the nose, it may be assumed that this is a viscous lift and that no viscous lift is obtained ahead

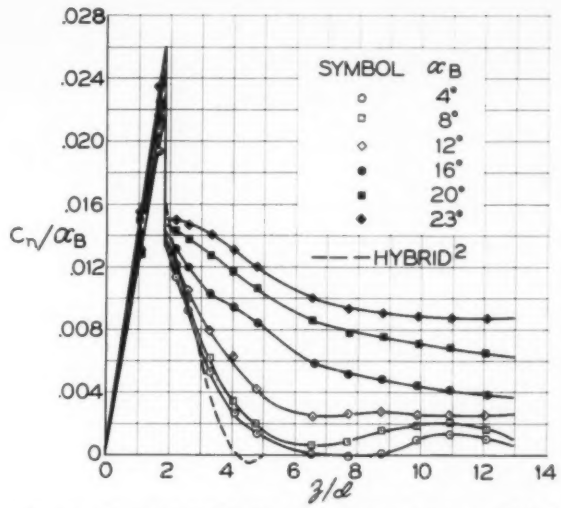

FIG. 2. The axial distribution of local normal force coefficient per degree of angle of attack for a 30° cone-cylinder configuration ($M_0 = 2.00$).

of this point at this angle of attack. Therefore, the total distribution shown for $\alpha_B = 4°$ ahead of this point is representative of the potential distribution.

The viscous normal force coefficients are then obtained as the difference between the experimentally derived potential distribution and the measured total local normal force coefficients. These viscous components are, in turn, used to calculate the axial distribution of cross-flow drag coefficient, c_{d_c}. These coefficients are presented in Fig. 3 for $\alpha_B = 8°$, 16°, and 23°. Also shown are the cross-flow drag coefficients calculated by the methods of Kelly and of Allen. The difference between the value shown for the infinite cylinder[5] and that obtained by Allen's method is due to the correction for finite body length. The correction applied is that estimated for the body of fineness ratio 13.14. It may be seen that, in general, Kelly's method is in good agreement with the data for the first four diameters only and thereafter diverges considerably from the measured results. On the other hand, it is clearly evident that Allen's method at best provides a cross-flow drag coefficient which is close to the average for bodies of high fineness ratio at high angles of attack but would, in general, fail to predict accurately the distribution of the viscous normal force. These results confirm the conclusions reached from analysis of the resultant force data that the accuracy of both methods is dependent upon the body fineness ratio and the angle of attack.

In the absence of a rigorous theory for the prediction of viscous forces and moments, it appears that more accurate predictions than provided by the two methods now available may have to depend on the use of correlated experimental results. The similarity noted in the data presented in Fig. 3 at higher angles of attack suggests that the data might be correlated by dividing the experimental results by the steady-state two-dimensional cross-flow drag coefficient for a circular cylinder, c'_{d_c}.[5]

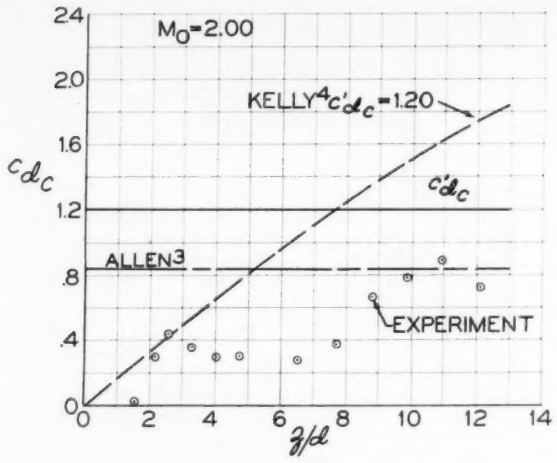

FIG. 3 (a). The axial distribution of cross-flow drag coefficient on a 30° cone-cylinder configuration (α_B = 8°).

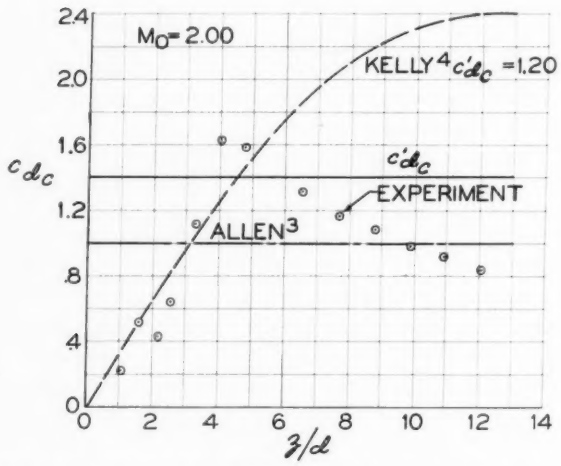

FIG. 3 (b). The axial distribution of cross-flow drag coefficient on a 30° cone-cylinder configuration (α_B = 16°).

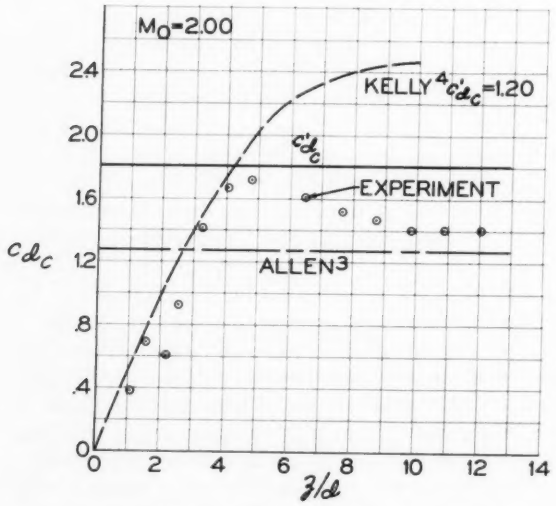

FIG. 3 (c). The axial distribution of cross-flow drag coefficient on a 30° cone-cylinder configuration (α_B = 23°).

These data, in the form c_{d_c}/c'_{d_c}, are presented in Fig. 4 for all conditions for which data were obtained. It is evident that good correlation is achieved for the higher angle of attack range.

These data also show that the viscous lift is first developed near the base of the body and moves forward and increases in magnitude with increasing the angle of attack. It is evident, therefore, that, in order to predict accurately the viscous lift and the center of pressure of viscous lift at all angles of attack, methods are required which are considerably more refined than any predicting a viscous contribution over the entire extent of the body, starting from zero angle of attack. In particular, it is indicated that the use of any existing method which is found to be successful at high angles of attack would tend to overestimate the lift-to-drag ratio for body alone configurations near the angle of attack for maximum lift-to-drag ratio. It is felt that additional data and an increase in the knowledge pertaining to viscous flow separation may provide theoretical or semiempirical methods which would account for all of the observed phenomena. It may be noted that the rise in cross-flow drag coefficient at the lower angles of attack appears to be associated with the station at which the body vortex system first becomes fully developed. The mechanism for the genesis of the lift is discussed in a later paragraph on vortex origins.

The correlated data, as represented by the solid curve in Fig. 4, were used to calculate the viscous normal force and the center of pressure as a function of angle of attack for the configurations tested, which had the same nose shape as the static-pressure model. These results are presented in Fig. 5. The normal force coefficient data presented in this figure are consistently slightly higher than the values predicted by the correlation curve. Further analysis revealed that at least half of the difference shown was directly attributable to the difference between the force data and the values obtained by integration of the surface pressure; the contribution to the cross-flow lift arising from the viscous shear is neglected when relying solely on the integration of the pressures. The remaining difference is within the accuracy to be expected. In any event, it is seen from the comparisons shown that the correlation curve used is by far preferable to the two existing methods (see Fig. 3) for the purpose of predicting the viscous phenomena for the range of the body fineness ratios tested.

In order to obtain some idea of the range of Mach Numbers, nose shape variations, and nose fineness ratios for which such correlation curves could be used for the estimation of the viscous characteristics, several other configurations were investigated. The results obtained for three typical cases are presented in Figs. 6 and 7. The selected cases are: (a) the test configuration at M_0 = 1.50; (b) a configuration of the same nose fineness ratio as the test configuration but having a tangent-ogive nose shape, and (c) a configuration with a tangent-ogive nose of double the fineness ratio of the test configuration.

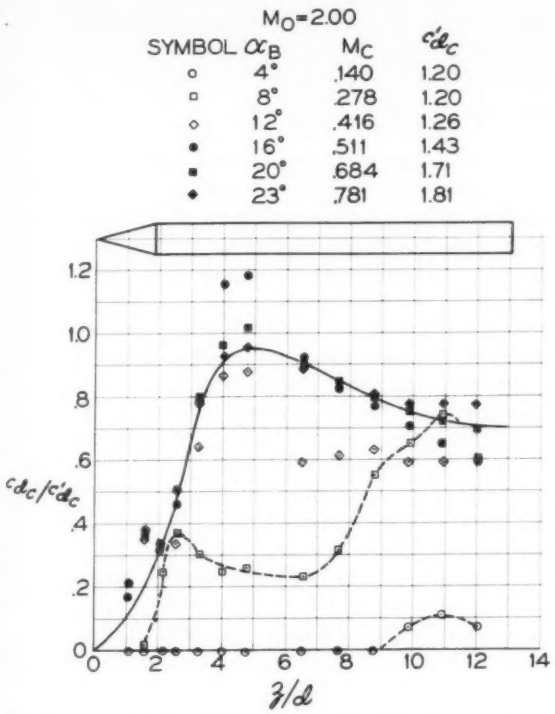

FIG. 4. The axial distribution of cross-flow drag coefficient ratio ($M_0 = 2.00$).

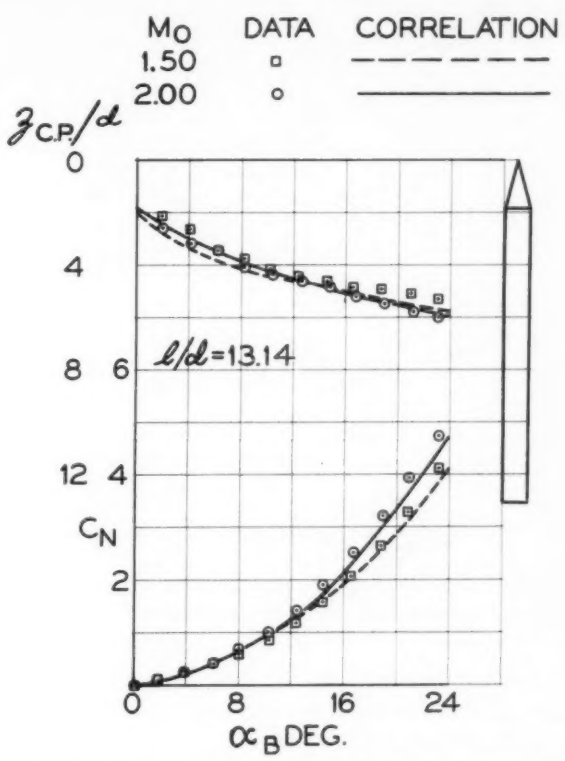

FIG. 6. The effect of Mach Number on the normal force and center of pressure characteristics of 30° cone-cylinder configuration ($l/d = 13.14$).

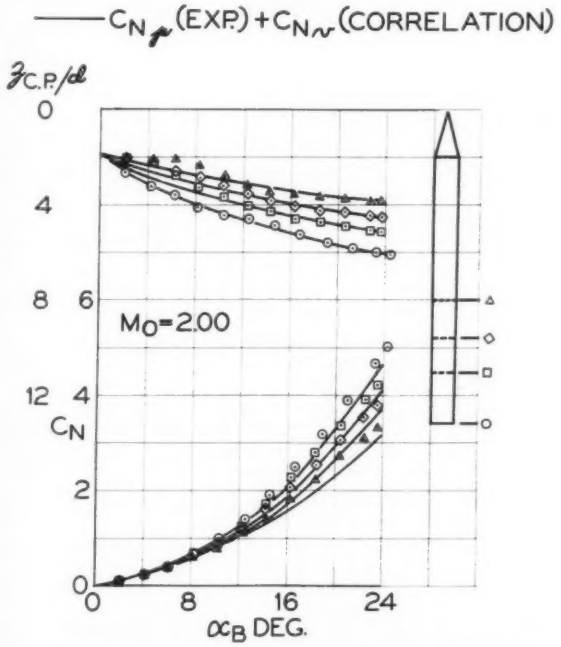

FIG. 5. The normal force and center of pressure characteristics of 30° cone-cylinder configurations of various fineness ratio.

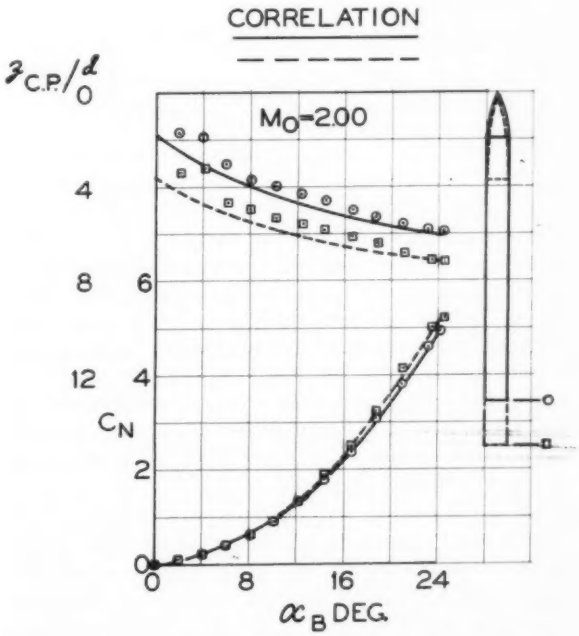

FIG. 7. The normal force and center of pressure characteristics of two ogive-cylinder configurations ($M_0 = 2.00$).

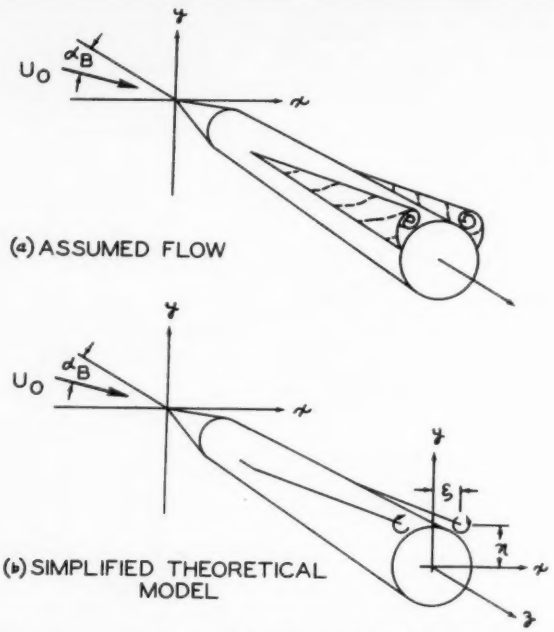

FIG. 8. Assumed body wake flow and simplified theoretical model.

Briefly, these comparisons indicate that the correlation curve presented herein is affected only slightly by the free-stream Mach Number and the nose fineness ratio, at least for the range of variables for which data were obtained. The data presented by Perkins and Jorgensen,[6] wherein a similar analysis was made, showed an effect of nose fineness ratio on the viscous lift distribution. This effect was observed, however, for a body having a nose fineness ratio more than three times that of the body tested in the present investigation.

(4) Body Flow Characteristics

The wing-body configuration tests conducted as another part of these studies have demonstrated (as have other similar investigations) that appreciable interference effects result from the interaction of the vortices shed from a body of revolution at high angles of attack with any attached lifting surfaces. The nature of this interaction is well understood and methods[1] for predicting the forces acting on the wings or tails are available, provided the strength and location of the vortex are known. The major objective of this account of the investigation is to provide more basic information on this latter phase problem which has received less attention.

The body vortices and associated wake system affect the lift of a lifting surface immersed in this flow in two ways: (a) alteration of the flow inclination across the span, and, therefore, alteration of the magnitude and the spanwise distribution of the lift, and (b) changes in the local flow characteristics—i.e., Mach Number, static pressure, density, etc.—with associated changes in the magnitude and distribution of the lift.

Without an analytical procedure for determining the strength of the body vortices and the flow variations they produce, it is impossible to arrive at a reasonable estimate of the interference effects generated in a system containing such vortices.

Theoretical Considerations

The three-dimensional steady flow associated with a body of revolution at moderate angles of attack has been visually studied by means of schlieren and vapor screen photographs by many experimenters, so that sufficient evidence is available to allow approximation of this flow by the model shown in Fig. 8(a). It is also known from visual studies and total pressure surveys that the boundary layer first begins to thicken on the lee side of the body near the base of the body. This phenomenon progresses as the angle of attack increases, until the boundary layer separates and two columnar regions of concentrated vorticity are formed. The axial location at which these vortices are first formed is also known to move forward as the angle of attack is increased.

It is reasonable to assume from these observations that the flow of major interest here is completely divorced from any potential flow effects on the nose of the body. With this assumption and the omission of any effects of the feeding vortex sheet, the more tractable simplified model shown in Fig. 8 (b) may be used, and the resultant flow is that of simple line vortices symmetrically situated on the lee side of a circular cylinder in a uniform stream. At this point, it is convenient to take advantage of the well-worked out properties of incompressible cross-flow (slender-body) theory. This recourse to an expedient simplification is sanctioned because a combination of non-

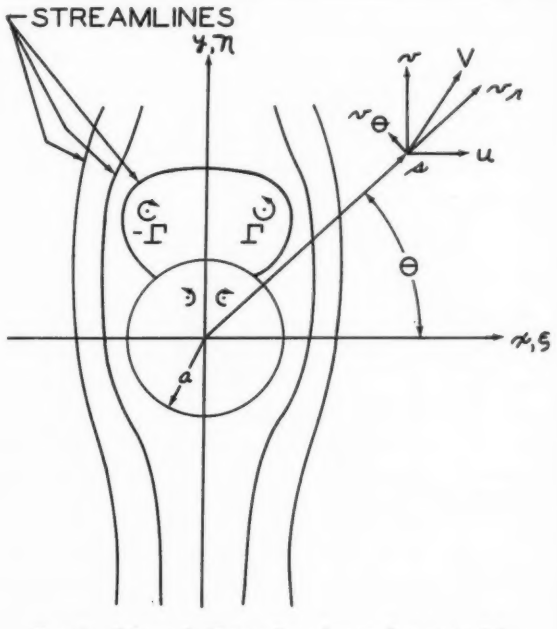

FIG. 9. Schematic illustration of cross-flow potential.

linear effects and compressibility effects would be difficult to treat. Actually, since the vortex system is of very small span, in the real case the delay of interaction between the vortices and between the vortices and the body, due to the supersonic axial flow, should not be of too great importance. This way of dealing with the cross flow does not necessarily limit the analysis to two-dimensional considerations because, as will be shown later, the effects of vortex motion and the rate of change of vortex strength on the axial velocity component may still be accounted for in a "hybrid" fashion—that is, the cross-flow velocities may be added vectorially to the axial component of the free stream, and, in addition, any axial perturbation velocities due to vortex growth and motion, as predicted by potential theory, may be superimposed.

Basic Formula

The complex potential for the cylinder and two vortices in a uniform stream, together with two image vortices placed within the body in order to satisfy the boundary condition of tangential flow at the body, is given by Lagerstrom and Graham[7] as

$$W = \Phi + i\Psi = -iV_0[s - (a^2/s)] - (i\Gamma/2\pi)\ln\left\{[(s-\sigma)(s+a^2/\sigma)]\div[(s+\bar{\sigma})(s-a^2/\bar{\sigma})]\right\} \quad (1)$$

The first term is simply the complex potential for the flow past a circular cylinder at the origin, and the second term gives the potential for four vortices; two of strength Γ located at σ, and $-a^2/\sigma$, and two of strength $-\Gamma$ located at $-\bar{\sigma}$ and $a^2/\bar{\sigma}$. A schematic illustration of such a flow is shown in Fig. 9 and serves the nomenclature used therein. The motion of the vortices in this flow may be determined simply by tracing the motion of one real vortex, since the other real vortex is symmetrically located, while the image vortices must be located so that the aforementioned boundary condition is always satisfied. For the vortex located at σ, the velocities are given by the expressions

$$d\xi/dt = -V_0[(2a^2\xi\eta)/(\xi^2+\eta^2)^2] + (\Gamma/2\pi)\times\left([\eta/(\xi^2+\eta^2-a^2)] - \left\{[\eta(\xi^2+\eta^2-a^2)]\div[(\xi^2+\eta^2-a^2)^2+4a^2\xi^2]\right\}\right) \quad (2a)$$

$$d\eta/dt = V_0\left(1+\left\{[a^2(\xi^2-\eta^2)]/[(\xi^2+\eta^2)^2]\right\}\right) - (\Gamma/2\pi)\left((1/2\xi) + [\xi/(\xi^2+\eta^2-a^2)] - \left\{[\xi(\xi^2+\eta^2+a^2)]/[(\xi^2+\eta^2-a^2)^2+4a^2\xi^2]\right\}\right) \quad (2b)$$

The path of the vortex in three dimensions may be expressed by using the following relation for the axial velocity:

$$dz/dt = U_0 \quad (3)$$

and therefore

$$d\xi/dz = (d\xi/dt)/(dz/dt) = (1/U_0)(d\xi/dt) \quad (4a)$$

$$d\eta/dz = (d\eta/dt)/(dz/dt) = (1/U_0)(d\eta/dt) \quad (4b)$$

The cross-flow velocities are u and v, which are the velocity components in the x and y directions in the cross-flow plane, and w is the axial perturbation velocity. These velocities are related to the potential equation in the following way:

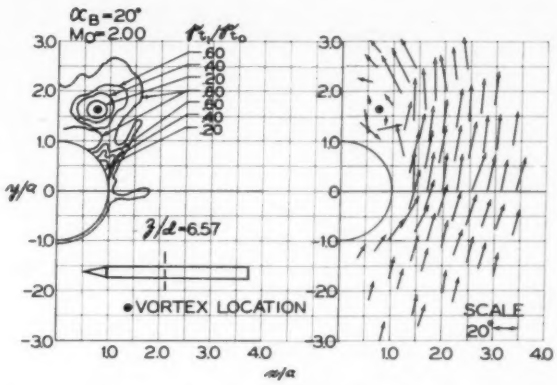

FIG. 10. Experimental total pressure ratio contours and local flow inclination (z/d = 6.57).

$$u = \partial\Phi/\partial x = \mathrm{RI}[\partial W/\partial x] \quad (5a)$$

$$v = \partial\Phi/\partial y = \mathrm{RI}[\partial W/\partial y] \quad (5b)$$

The aforementioned hybrid combination of the cross-flow velocities with the axial velocity component to obtain the resultant local velocity, U_1, may now be expressed as

$$U_1^2 = (U_0\cos\alpha_B + w)^2 + u^2 + v^2 \quad (6)$$

Using the adiabatic relationships for the flow of a perfect gas, the calculation of the other flow properties may be easily accomplished. In particular, a basic property, the local Mach Number, is given by

$$M_1^2 = [M_0^2(U_1/U_0)^2]/\left\{1 + [(\gamma-1)/2]M_0\times[1-(U_1/U_0)^2]\right\} \quad (7)$$

It should be noted that the axial perturbation velocity, w, arises from the fact that both the strength of the vortices and their positions are functions of the axial dimension z. The equation expressing this relationship is

$$w = \mathrm{RI}[\partial W/\partial z] = \mathrm{RI}[(\partial W/\partial\Gamma)(d\Gamma/dz) + (\partial W/\partial\sigma)(d\sigma/dz)] \quad (8)$$

The terms $(d\Gamma/dz)$ and $(d\sigma/dz)$ may be evaluated by using the relationships for the variation of vortex strength and the vortex trajectory. The latter is discussed above and a discussion of the former follows.

Vortex Strength

Consideration of the forces acting on the cylinder and the changes in momentum associated with the axial development of the body vortices for the simplified flow model of Fig. 8(b) results in a simple relationship between the strength of the vortices and the viscous normal force acting on the cylinder.

The simplest way to arrive at this relationship is to consider the three-dimensional flow as an unsteady two-dimensional flow—i.e., $t = z/U_0$. For the assumed model, the impulse applied to the cylinder in time t is given by the following, wherein $t = 0$ denotes

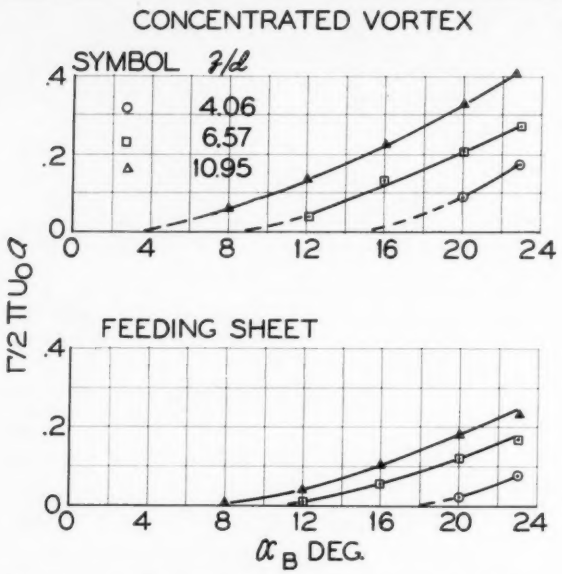

FIG. 11. Circulation strengths of concentrated vortex and feeding sheet versus angle of attack.

any point lying ahead of the point of origin of the vortices and viscous normal force;

$$I = \int_0^t n dt = \int_0^z (dN_v/dz)\,(dz/U_0) = (N_{vz}/U_0) \quad (9)$$

This impulse is equal to the change in momentum of the flow from time $t = 0$ to time t. It is evident from the choice of the station for $t = 0$ that the change in momentum of the fluid of the theoretical model is that change associated with the momentum of the vortices and the image vortices. Therefore, since it can be shown[7] that the momentum of two vortices is equal to the product of the vortex strength, density, and the span of the vortices, the change of momentum of the fluid is given by

$$\text{Change in momentum} = 2\rho_0\Gamma_z(\xi - \xi_i)_z \quad (10)$$

Thus, the finally sought result is achieved by equating the impulse to the change in momentum, or

$$N_{v_z}/U_0 = 2\rho_0\Gamma_z(\xi - \xi_i)_z \quad (11)$$

so that with some rearrangement and substitution

$$\Gamma/2\pi U_0 a = [(C_{N_v})_z\, a]/[8(\xi - \xi_i)_z] \quad (12)$$

It should be noted that $(C_{N_v})_z$ is the viscous normal force coefficient for all the viscous normal force ahead of station z.

Body Wake Surveys

Two experimental investigations pertaining specifically to the details of the body flow have been conducted as a part of this general study. One part of the part of the flow-field survey consisted of an exploratory study in which static and total-pressure measurements were taken circumferentially at various radial distances around a cone-cylinder body at $M = 1.50$ and 2.00 for two body stations and at angles of attack from 0° to 23°. The total-pressure contours thus obtained serve to indicate an approximate vortex location; this information, together with estimates of the viscous lift distribution, allows calculation of the vortex strength by means of the relationship previously derived. The values of vortex strength thus calculated are used to compute the static and total pressures on the basis of the adiabatic relationships described in the preceding section. Normal shock relationships are also applied in obtaining the pitot pressures. The close agreement of the measured pitot pressures over the greater portion of the survey plane with the predicted values calculated in the above manner provided the impetus to conduct a second investigation.

The second set of wind-tunnel tests in the series was a more complete investigation in which calibrated cone probes and pitot-pressure probes were used for the survey instrumentation. With this calibrated instrumentation it was possible to define completely the true local flow conditions, including flow inclination, within the range of the calibration. The calibration itself was rather extensive and the ranges through which the major parameters were varied are given in Table 1.

It should be noted that, since the flow-inclination instrumentation consisted of conical probes provided with four orifices (orifices located 90° apart), and since the probes were calibrated for the complete range of roll-orientations, θ_{probe}, it was possible to obtain both components of the local flow inclination—i.e., downwash and sidewash.

Vortex Strengths

The major purpose of this vector-field investigation was to confirm the hypothesis, by detailed measurements of the flow field, that the strengths of the concentrated body vortices could be estimated from the viscous normal force distributions and vortex locations. It was also intended to provide more basic knowledge of the body flow, the nature of the vortex feeding-sheet, and the vortex starting phenomenon.

The general nature of the body-alone flow is shown by the total-pressure-ratio contour plot and flow-inclination survey plot presented in Fig. 10 for $\alpha_B = 20°$. The total-pressure plots are most useful for locating the vortex core and the feeding vortex sheet in the survey plane. The flow inclination results are presented in vector form where the tail of the vector is located at the point at which data were obtained. The magnitude and direction of the vector correspond to the magnitude and direction of the local flow inclina-

TABLE 1
Range of Calibration of Instrumentation

	Minimum	Maximum
M	1.50	2.50
ϵ	0°	45°
θ_{probe}	0°	45°

tion. For the sake of clarity, all the data* are not shown in these figures.

These plots are typical of the data obtained for all cases for which a region of concentrated vorticity was in evidence. The total-pressure plots are used to determine the path of integration used in the velocity-perimeter integration performed to obtain the vortex strength, Γ. The contour of integration is chosen to consist of rays and arcs along which data were obtained. Therefore, the vortex strength is calculated using the following expression:

$$\Gamma = \oint \vec{v} \cdot \vec{ds} = \int_{r_1}^{r_2} v_r dr + \int_{\theta_1}^{\theta_2} v_\theta r_2 d\theta + \int_{r_2}^{r_1} v_r dr + \int_{\theta_2}^{\theta_1} v_\theta r_1 d\theta \quad (13)$$

In practice, the length of the integration path between the limits of integration was equally divided by the points at which data were obtained and a finite-step summation process was substituted for the indicated integrations. Several closed-contour integrations were made for each case to ensure the determination of the true vortex strength and feeding-sheet strength. For some cases, it was not possible to compute the vortex strength without resorting to an extrapolation procedure. That is to say, when the vortex lies close to the body and use of the body surface for the inboard circumferential contour is required, the measured variation of the tangential velocity component, v_θ, is extrapolated to the body surface for use in the integration procedure.

The calculated values of the circulation strength of the body vortices and of the vortex feeding sheets are presented as functions of angle of attack in Fig. 11. It may be noted that, in accordance with expectations, the circulation strengths of the vortex and feeding sheet increase with both increasing angle of attack and increasing body station.

The experimental viscous normal force distributions discussed in the preceding section and the vortex locations determined from the total pressure ratio contours are used to compute the circulation strength of the concentrated vortices for the various body stations by Eq. (12). These predictions of concentrated vortex strength are presented in Fig. 12 in comparison with the values obtained from the closed-contour integrations of the cross-flow velocities determined by the detailed flow measurements. It is seen in this figure that the theory predicts values which, in general, are in close agreement with the measured results. The cases that are not in satisfactory agreement with the theoretical predictions are those cases representing conditions near the vortex starting point for which both normal force coefficient, C_{N_v}, and the vortex span difference, $(\xi - \xi_1)$, are very small. It has been found that for these conditions the ratio of these two small numbers can vary considerably with changes in either or both of the above-mentioned quantities, even though the changes are within the accuracy of the data.

The experimentally determined values of concentrated vortex strength are generally smaller than the theoretical predictions, as attested by the comparison presented in Fig. 12. It is believed that this trend may be due primarily to the fact that the strength of the feeding sheet has been ignored while all of the viscous normal force has been used in Eq. (12). The use of a more general equation based on a finite number of discrete vortices in order to represent the feeding sheet may improve the agreement shown. It was felt, however, that there was not sufficient data available to warrant such a calculation, in view of the assumptions that would have to be made concerning the relative strengths and locations of the feeding-sheet vortices. Another reason for the generally higher theoretical prediction may be the supersonic nature of the axial flow. That is, the viscous normal force at any axial station may be related more accurately to the vortex strength existing further downstream in accordance with propagation processes at work in supersonic flow. In any event, any such effects not considered in the elementary analysis given here are indicated to be of higher order.

Local Flow Inclinations

Calculations were made of the local cross-flow velocities using the experimentally determined vortex strengths and locations for several cases for which concentrated vortices are present in the body flow. The cross-flow velocities were calculated by Eqs. (5a) and (5b), which reduce to the following specific forms of two concentrated vortices symmetrically positioned above the body:

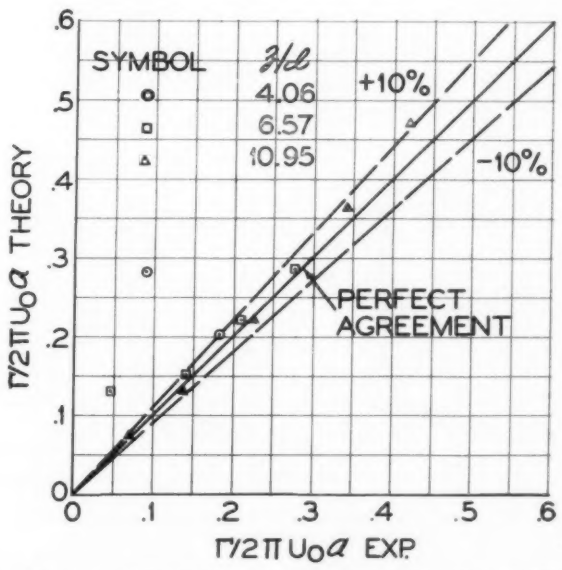

FIG. 12. Comparison of theoretical concentrated vortex strengths with concentrated vortex strengths obtained from experimental data.

* In general, for the sake of brevity, only typical selections from the data obtained are presented. A more complete documentation is presented in reference 8.

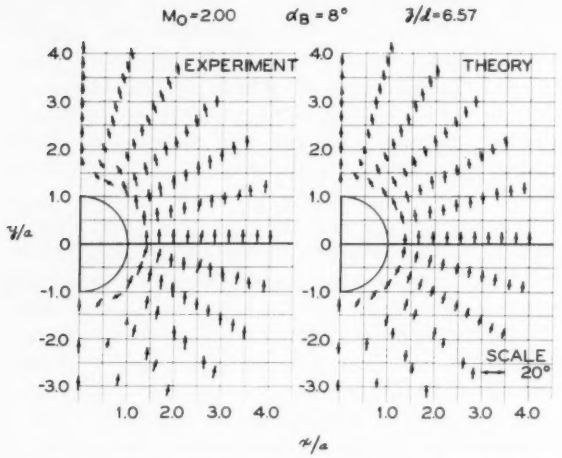

FIG. 13. Comparison of experimental and theoretical flow inclinations ($\alpha_B = 8°$).

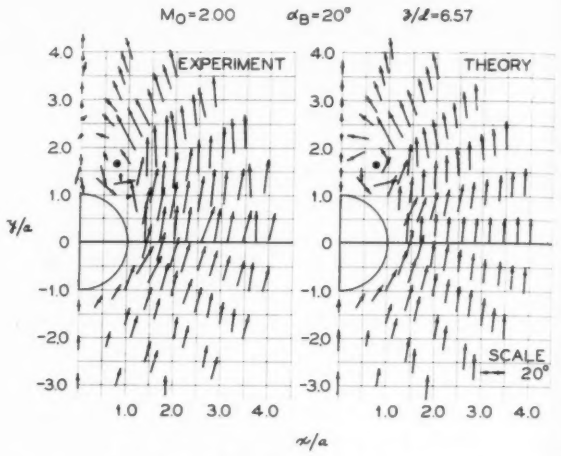

FIG. 14. Comparison of experimental and theoretical flow inclinations ($\alpha_B = 20°$).

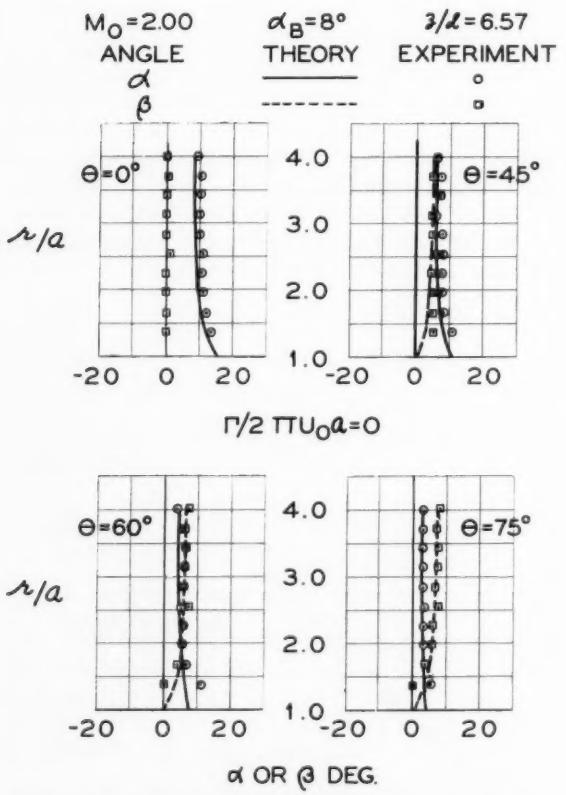

FIG. 15. Comparison of theoretical and experimental flow inclination distributions ($\alpha_B = 8°$).

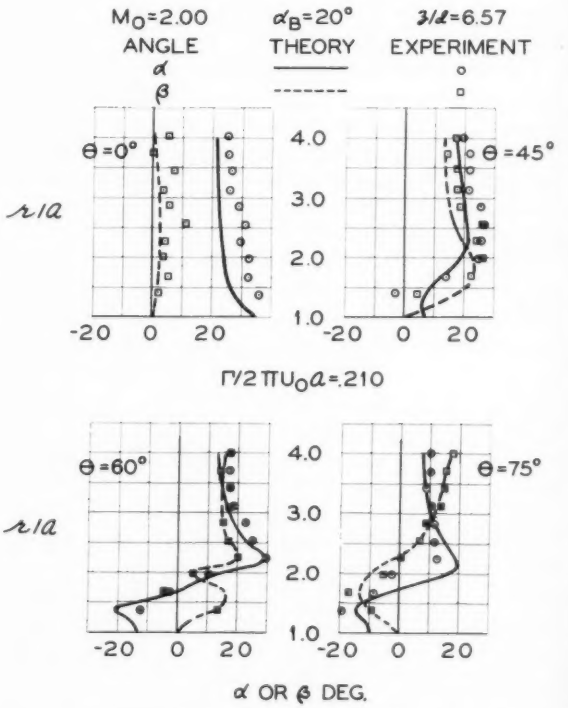

FIG. 16. Comparison of theoretical and experimental flow inclination distributions ($\alpha_B = 20°$).

$$u/V_0 = -[2a^2xy/(x^2+y^2)^2] - (\Gamma/2\pi V_0) \times \{[(y-\eta)/R_1^2] - [(y-\eta_i)/R_2^2] + [(y-\eta_i)/R_3^2] - [(y-\eta)/R_4^2]\} \quad (14a)$$

$$v/V_0 = 1 + \{[a^2(x^2-y^2)]/(x^2+y^2)^2\} + (\Gamma/2\pi V_0)\{[(x-\xi)/R_1^2] - [(x-\xi_i)/R_2^2] + [(x+\xi_i)/R_3^2] - [(x+\xi)/R_4^2]\} \quad (14b)$$

where

$$R_1^2 = (x-\xi)^2 + (y-\eta)^2$$
$$R_2^2 = (x-\xi_i)^2 + (y-\eta_i)^2$$
$$R_3^2 = (x+\xi_i)^2 + (y-\eta_i)^2$$
$$R_4^2 = (x+\xi)^2 + (y-\eta)^2$$

and (ξ, η) and (ξ_i, η_i) are the coordinates of the right-hand vortex and image vortex, respectively.

These velocities are used to obtain the resultant cross-flow velocity, V, and then the local flow inclination, ϵ, and the direction of the flow, θ. The relationships used in these calculations are:

$$(V/V_0)^2 = (u/V_0)^2 + (v/V_0)^2 \quad (15)$$

$$\epsilon = \tan^{-1}[(V/V_0)\tan\alpha_B] \quad (16)$$

$$\theta = \tan^{-1}[v/u] = \tan^{-1}[(v/V_0)/(u/V_0)] \quad (17)$$

Rigorously speaking, the local flow inclination angle, ϵ, is also influenced by the axial perturbation velocity, w, given by Eq. (8). However, it is felt that the added computational effort involved in calculating this velocity is too great to be practicable in most cases. In any event, sample calculations have shown that w is very small relative to $U_0 \cos\alpha_B$ for the greater part of the flow field.

Modification of the cross-flow velocity relationships was made in the region of the vortex core. The classical assumption that the core rotates as a solid leads to the following relationship applied to the region within the radius of the core, r_c, the extent of which is estimated from the experimental flow inclination data. These relationships are:

$$u/V_0 = -(\Gamma/2\pi V_0)[(y-\eta)/r_c^2] \quad (18a)$$

$$v/V_0 = (\Gamma/2\pi V_0)[(x-\xi)/r_c^2] \quad (18b)$$

It should be noted that these relationships do not provide for a transition region between the viscous and potential flows. The omission of such a region (usually very small) greatly simplifies the calculations and has little effect on the overall results. Comparisons between the theoretical and experimental results for two typical cases, one without and one with concentrated vortices, are presented in Figs. 13 and 14, respectively. The results are presented in vector form where the tail of the vector is located at the point for which the flow inclination was measured and calculated. The magnitude and direction of the vector correspond to the magnitude and direction of the local flow inclination. Although data were obtained along rays with sector angles chosen in increments of as small as 5° ($\Delta\theta = 5°$), the comparisons, for the sake of clarity, are made for circumferential increments of 15°. The theoretical values are presented for the locations corresponding to those for which flow inclination measurements were made.

Additional comparisons are presented in Figs. 15 and 16 for several selected circumferential rake locations ($\theta = 0°, 45°, 60°, 75°$). The conditions selected pertain to the survey station at $z/d = 6.57$ for angles of attack of $\alpha_B = 8°$ and 20°. These latter comparisons are for the components of the local flow inclination, α and β, where α and β are the local angles of inclination which correspond to the tangential and radial velocity components, v_2 and v_r, respectively (see Fig. 9).

In general, the agreement between the theoretical results and measured data is as good as may be expected in view of the fact that the theoretical methods used ignore many facets of the problem. In particular, it is noted that the two major regions for which the agreement between theory and experiment deteriorates with increasing angle of attack are near $\theta = 0°$ and 45°. For $\theta = 0°$ this discrepancy may be attributed to increasing effects of compressibility with angle of attack; this trend is exhibited most severely at the side of the body. For $\theta = 45°$ the increase in the circulation strength of the vortex feeding sheet with increasing angle of attack is primarily the cause for the noted variation in the flow inclination. The omission of the effects of the feeding sheet at the higher angles of attack is, therefore, the primary reason for the lack of agreement in this region. These effects will be discussed further in the following sections.

Agreement between experiment and theory was also noted to deteriorate with increasing axial distance from

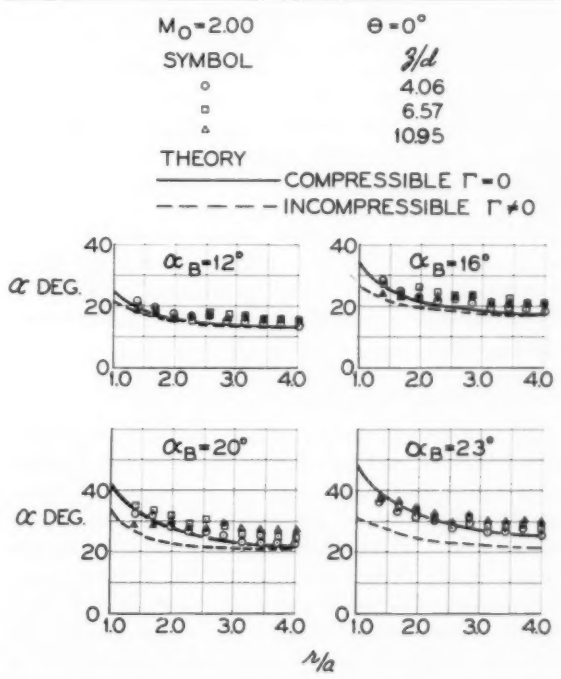

FIG. 17. The effects of compressibility on the flow inclination distribution at various angles of attack.

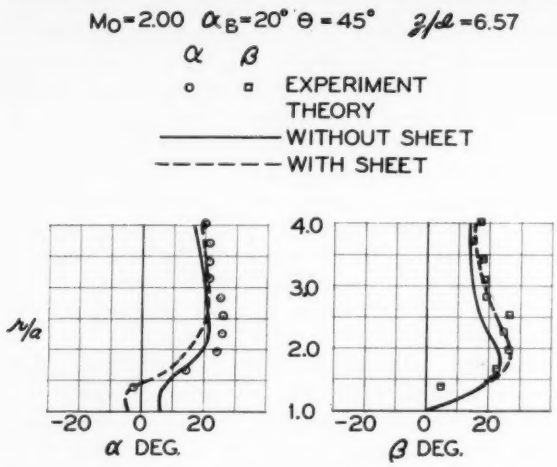

FIG. 18. Typical effects of the vortex feeding sheet on the flow inclination distributions ($\alpha_B = 20°$).

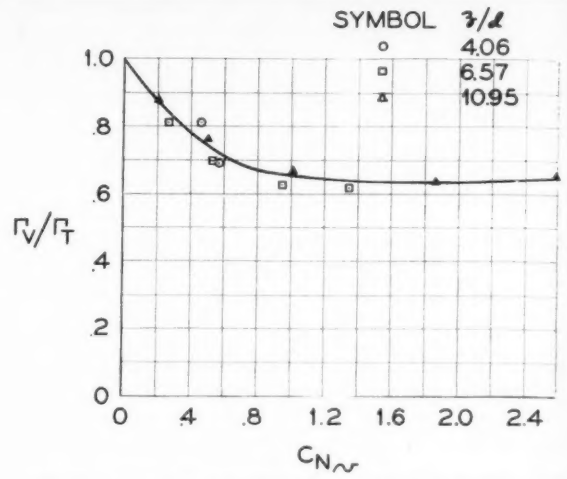

FIG. 19. Ratio of the circulation strength of the concentrated vortex to the total circulation strength versus viscous normal force coefficient.

the nose. In addition to the aforementioned phenomena, it is believed that the increasing effects of viscous flow and the elongation and spread of the concentrated vortex region have a direct bearing on the agreement to be expected.

Compressibility Effects

In the calculation of the cross-flow velocity distributions, compressibility effects can to a certain extent be accounted for in a simple manner, at least for the region to the windward of the cross-flow sonic line—i.e., the locus of points at which $M_1 \sin \epsilon = 1.00$. For this region it may be assumed that the effects of the vortices are not felt, so that the use of the compressible potential, as given by Kaplan[9] for the cylinder-alone in a uniform stream, is therefore the best representation of the flow. This procedure has been applied for $\theta = 0°$ to the previously presented data and other cases, and the results are presented in Fig. 17. Also shown for purposes of comparison are the incompressible theoretical results for the intermediate station which approximate the incompressible results for the other two body stations. It is seen that, in general, the aforementioned procedure results in some improvement in the agreement of the theoretical results with the experimental data.

Vortex Feeding Sheet Effects

The omission of the vortex feeding sheet in the cross-flow potential used to estimate the cross-flow velocity distribution naturally results in appreciable disagreement between theory and experiment in the vicinity of the sheet. It would be possible to account for the effects of the vortex sheet if the precise orientation and distribution of circulation strength along the sheet were known. Unfortunately, the probe spacing of the instrumentation used was not sufficiently small to allow a practical assessment of these physical characteristics of the sheet. However, since it is possible to determine the total circulation strength of the sheet and since the approximate locus of the sheet is indicated by the total pressure contour plots, calculation of the effects of the vortex sheet was attempted for a typical case.

The effects of the vortex feeding sheet were estimated by including in the mathematical model a number (four) of small discrete vortices and the respective image vortices for each sheet. The location of each vortex was chosen so as to provide, as nearly as possible, equal vorticity for each segment of the sheet. The total circulation strength of the sheet was equally apportioned among the vortices used to simulate the sheet. The results of the calculation are presented in Fig. 18. It is evident that for the case chosen the agreement between theory and experiment is substantially

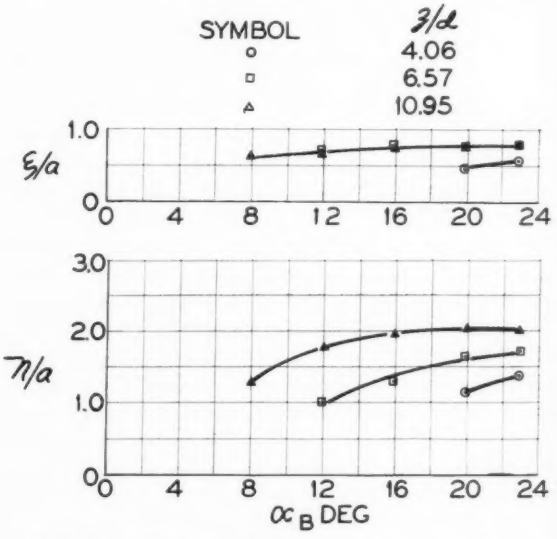

FIG. 20. Vortex-coordinates versus angle of attack.

improved in the vicinity of the vortex feeding sheet by accounting for the presence of the sheet in the manner discussed above.

The vortex feeding sheet effects were not investigated further due to the approximate nature of the method used and due to the fact that the computational work required is nearly proportional to the number of vortices included in the cross-flow potential. In addition, theoretical methods are not available for the prediction of the circulation strength of the vortex sheet. The circulation strength of the sheet, however, may be estimated empirically from experimental results, such as are available from this investigation. For example, the ratio of vortex strength to total (vortex plus feeding sheet) circulation strength is given in Fig. 19. Such a plot allows the determination of the strength of the sheet as a function of viscous lift coefficient ahead of the vortex axial station under consideration. It is evident that the data are well correlated in this manner. Additional experimental work may provide a broader correlation of this type.

Vortex Paths

The experimentally determined vortex locations for the configuration tested are presented in Fig. 20. The calculation of the vortex paths starting from a known vortex location was attempted by the use of Eqs. (2) and (4), together with the knowledge of the normal force distributions on the body. In general, contrary to the experience of Jorgensen and Perkins,[10] the vortex trajectories could not be adequately predicted. Examination of the possible reasons for this anomaly has indicated that the vortex trajectory is very sensitive to the accurate determination of the vortex location selected for starting the trajectory, although not very sensitive to vortex strength. This latter result concurs with the findings of Jorgensen and Perkins.[10] It is, therefore, reasonable to assume that the major reason why it was not possible to predict adequately the vortex trajectories in the present investigation is the lack of ability to measure the vortex locations within tolerable limits with the probe spacing used, but it is not attributable to inadequacy of the theory.

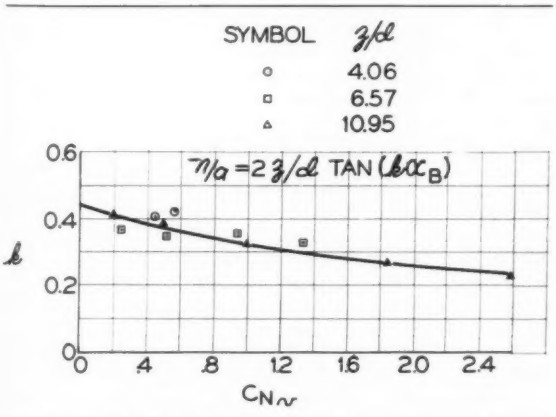

FIG. 21. Vortex location correlation constant versus viscous normal force coefficient.

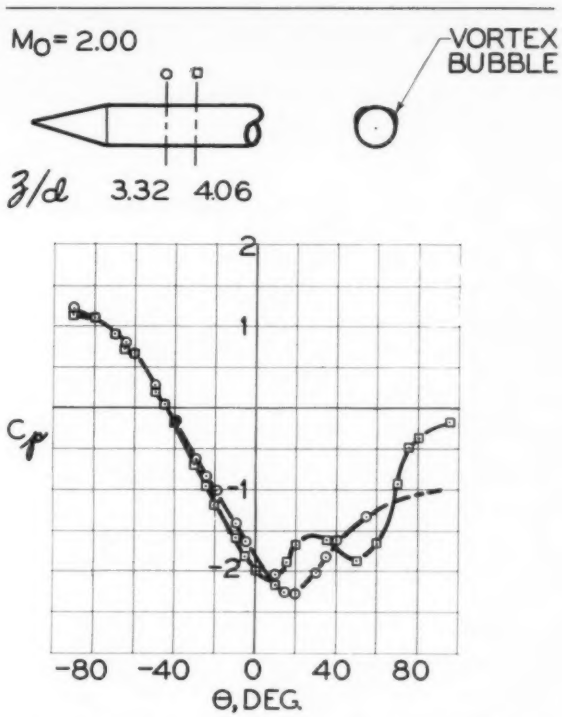

FIG. 22. Typical effects of incipient vortex formation on the circumferential variation of the static pressure coefficient.

Although a trajectory could not be adequately predicted, the vortex locations presented are sufficiently accurate for calculation of local flow properties. For this reason, any correlation of the results obtained is desirable. The vortex spanwise coordinates, ξ/a, shown in Fig. 20, are all noted to approach a value of 0.750, except near the vortex starting location. It is indicated, therefore, that $\xi/a = 0.750$ is a satisfactory spanwise coordinate for most computational purposes. An attempt was made to correlate the vortex coordinate η/a as a function of the angle of attack and the viscous lift acting on the body ahead of the axial station in question. It is found that the expression

$$\eta/a = (2z/d) \tan (k\alpha_B) \qquad (19)$$

collects the data obtained in the present investigation, where k is a function of the viscous normal force coefficient, $C_{N_{v_2}}$. This correlation is presented in Fig. 21.

Vortex Origins

The prediction of the vortex origins, like that of many other viscous phenomena, is not possible by theoretical methods at the present time. Analysis of the static pressure distributions on the body for all conditions tested indicates that the vortex formation is associated with the station at which a second minimum first appeared in the pressure coefficient curve (C_p versus θ).

This phenomena is illustrated by the pressure coeffi-

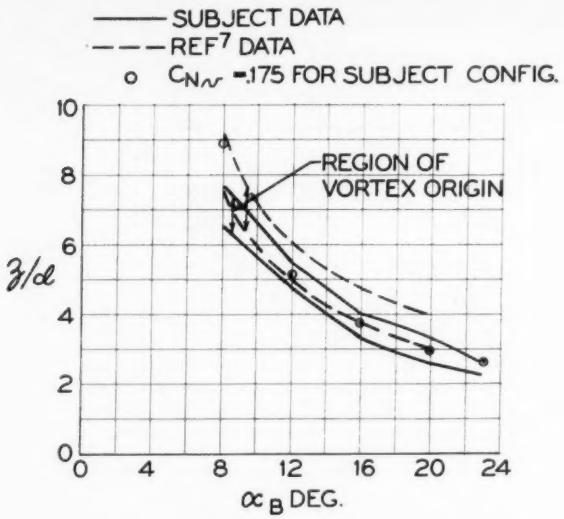

FIG. 23. Region of indicated vortex origins versus angle of attack.

cient data presented in Fig. 22. The data presented are typical of that for all conditions tested. It is seen in the data for these adjacent stations that the curve for the more forward station does not have a second minimum while the curve for the more aft station has a second minimum at $\theta = 50°$. This second minimum in the pressure coefficient data is to be expected if a vortex bubble is formed on the body at that axial location, as illustrated by the sketch in Fig. 22. It is evident, therefore, that a vortex bubble first was formed at some station intermediate to those for which data have been plotted in this instance. An area of incipient vortex formation, defined in this manner, is therefore indicated for the conditions tested. This region is presented as a function of angle of attack in Fig. 23. Included in this figure is the band presented in reference 10 as the region of vortex origins for an ogive-cylinder body. The region of vortex origin for both bodies is seen to be quite similar.

The relationship of the vortex origins to the axial development of viscous lift is indicated by the symbols denoting a value of constant viscous normal force coefficient ($C_{N_{V_z}} = 0.175$). It is seen that the station at which this value of viscous normal force coefficient is achieved is in fair correspondence with the axial location of the vortex origins.

(5) Conclusions

(1) The axial distribution of cross-flow drag coefficients for bodies of revolution at high angles of attack in supersonic flow in general will differ considerably from the distributions predicted by the methods of Allen[3] and Kelly.[4]

(2) The use of correlated experimental results for the axial distribution of cross-flow drag coefficients in conjunction with the hybrid theory of Van Dyke[2] provides a satisfactory method for estimating the normal force and pitching moment characteristics of similarly shaped bodies of revolution. Furthermore, such correlated results can be extended, within reasonable limits, to provide satisfactory estimates of the viscous force and moment characteristics for configurations and Mach Numbers other than those for which data are available.

(3) It has been confirmed by detailed flow measurements that the circulation strengths of the concentrated vortices in the body vortex wake flow can be estimated, provided the viscous normal force distributions and vortex locations are known.

(4) The flow inclination distributions in the flow field around a body of revolution, in general, can be closely predicted by the theoretical potential cross-flow model consisting of a cylinder and two symmetric vortices (plus image vortices) in a uniform stream. A closer agreement with experiment can be achieved in the vicinity of the vortex core, in the vicinity of the vortex feeding sheet, and in the regions affected by cross-flow compressibility by accounting for these phenomena with certain simple refinements to the basic theoretical model.

(5) Several of the physical properties of the body-alone wake vortex flow are found to correlate in a manner dependent primarily on the distribution of viscous lift on the body. The present methods of correlation should be applied to a wider range of body configurations and Mach Numbers to determine their limitations.

References

[1] Alden, H. L., and Schindel, L. H., *The Calculation of Wing Lift and Moments in Nonuniform Supersonic Flows*, Massachusetts Institute of Technology Meteor Report No. 53, 1950.

[2] Van Dyke, M. D., *First- and Second-Order Theory of Supersonic Flow Past Bodies of Revolution*, Journal of the Aeronautical Sciences, Vol. 18, No. 3, pp. 161–178, 216, March, 1951.

[3] Allen, H. J., and Perkins, E. W., *A Study of Effects of Viscosity on Flow Over Slender Inclined Bodies of Revolution*, NACA T.R. No. 1048, 1951.

[4] Kelly, H. R., *The Estimation of Normal-Force, Drag, and Pitching-Moment Coefficients for Blunt-Based Bodies of Revolution at Large Angles of Attack*. Journal of the Aeronautical Sciences, Vol. 21, No. 8, pp. 549–555, 565, August, 1954.

[5] Gowen, J. G., and Perkins, E. W., *Drag of Circular Cylinders for a Wide Range of Reynolds Numbers and Mach Numbers*, NACA TN 2960, June, 1953.

[6] Perkins, E. W., and Jorgensen, L. H., *Comparison of Experimental and Theoretical Normal Force Distributions (Including Reynolds Number Effects) on an Ogive-Cylinder Body at Mach Number 1.98*, NACA TN 3716, May, 1956.

[7] Lagerstrom, P. A., and Graham, M. E., *Aerodynamic Interference in Supersonic Missiles*, Douglas Aircraft Corporation, Report SM 13743, July, 1950.

[8] Mello, J. F., *Investigation of Normal Force Distributions and Wake Vortex Characteristics of Bodies of Revolution at Supersonic Speeds*, Applied Physics Laboratory, The Johns Hopkins University, Baltimore, Md., Report CM 867 (McDonnell Aircraft Corporation Report 4666), April, 1956.

[9] Kaplan, C., *Two-Dimensional Subsonic Flow Past Elliptic Cylinders*, NACA T.R. No. 624, 1938.

[10] Jorgensen, L. H., and Perkins, E. W., *Investigation of Some Wake Vortex Characteristics of an Inclined Ogive-Cylinder Body at Mach Number 1.98*, NACA RM A55E31, August, 1955.

On the Flow of a Sonic Stream Past an Airfoil Surface†

COLIN S. SINNOTT*

National Physical Laboratory, Teddington, England

SUMMARY

This study of the flow about an airfoil in a near-sonic stream indicates the important factors determining the pressure distribution on the airfoil. Analysis of the Mach wave pattern suggests that the supersonic domain of the flow can be derived from two simple-wave flows, one arising from the Mach waves reflected at the sonic line and the other from the changes in airfoil surface slope. The compressive effect of the reflected Mach waves is determined quantitatively as a function of airfoil leading-edge geometry from an analysis of measured pressure distributions for uncambered airfoils; and it is shown how this can be superimposed on the wave system from the curved surface to give an equivalent simple-wave flow over the airfoil.

An application of this scheme to the calculation of the pressure distribution over an airfoil in a sonic stream gives results in good agreement with experiment.

SYMBOLS

c = airfoil chord
H = stagnation pressure
M = Mach Number
p = static pressure
x,y = coordinates of airfoil surface
$X \equiv (x - x_{CR})/(x_{TE} - x_{CR})$
α = airfoil incidence
δ_{TE} = flow deflection at trailing edge
θ = surface slope measured from airfoil crest
ω = Prandtl-Meyer angle corresponding to local Mach Number on an airfoil surface
$\tilde{\omega}$ = effective compression angle
$\chi \equiv [y/c]_{x=0.02c}/\Delta_\theta^{\theta=4^\circ}_{\theta=2^\circ}\ (x/c)$; i.e., a function of airfoil geometry near the leading edge

Subscripts

0 = free-stream conditions
TE = conditions at trailing edge
CR = conditions at crest

(1) INTRODUCTION

THE FLOW of a sonic stream past an airfoil surface is of considerable interest, for it is known that the resultant pressure distribution on the surface is insensitive to small changes in free-stream Mach Number. Because of this, an estimate of the sonic pressure distribution over an airfoil can be a useful guide to the airfoil characteristics throughout the transonic speed range. Some typical results illustrating the phenomenon are given in Fig. 1, where the pressure distribution over an airfoil is shown for a number of free-stream Mach Numbers. It is seen that once a shock wave is established in the flow the pressure distribution head of it changes little with increase in Mach Number and the consequent rearward movement of the shock wave. When the shock wave has reached the trailing edge of the airfoil surface the pressure distribution over the whole surface is insensitive to further increase in free-stream Mach Number until some slightly supersonic value is attained. Except for very thin airfoils the surface shock wave will reach the trailing edge at a high subsonic free-stream speed, so that the range of Mach Number over which the pressure distribution is approximately constant will include the sonic value; this has been called the "sonic range." The associated independence of local Mach Number and free-stream Mach Number is known as the "Mach Number freeze." Tests on thin airfoils suggest that the surface shock does not reach the trailing edge until a slightly supersonic free-stream speed is attained. In these cases, the development of the flow is not essentially different from that described above, for although the sonic-range will be entirely supersonic the Mach Number freeze will still be established at points upstream of the shock wave at lower speeds.

A number of approximate methods of calculating sonic-range pressure distributions have been suggested, and purely theoretical results have been obtained for double-wedge and flat-plate profiles. The semiempirical method of Lindsey and Dick[1] requires a knowledge of the sonic point position, the pressures from there to the trailing edge being calculated by simple-wave theory with a modified expansion rate. Gullstrand[2]

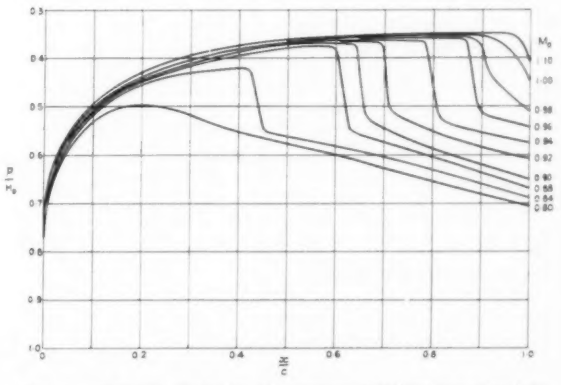

FIG. 1. Typical variation of pressure distributions with free-stream Mach Number for a 10 per cent thick airfoil at zero incidence.

Received May 12, 1958. Revised and received August 11, 1958.

† The work described in this paper has been carried out as part of the research program of the National Physical Laboratory and is published here by permission of the Director of the Laboratory.

* Senior Scientific Officer, Aerodynamics Division, Department of Scientific and Industrial Research.

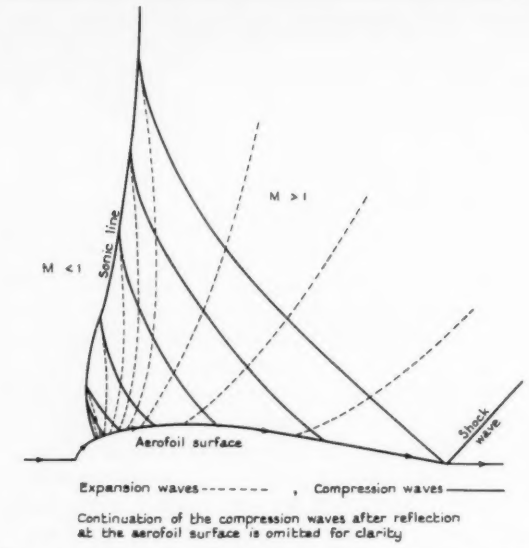
M > 1
M < 1
Sonic line
Aerofoil surface
Shock wave
Expansion waves -------- , Compression waves ——
Continuation of the compression waves after reflection at the aerofoil surface is omitted for clarity

FIG. 2. Mach wave pattern of the sonic flow past an airfoil surface.

and Bévierre[3] employ exact simple-wave theory from a chosen position on the airfoil surface and treat the upstream flow by other methods. There are important criticisms of these approaches; first, it is not yet possible to determine the sonic point on an airfoil with useful accuracy, and second, modification of the supersonic simple-wave expansion rate does not represent the physical mechanism whereby the leading-edge subsonic region affects the following supersonic flow. Also, use of exact simple-wave theory is physically incorrect. It is felt that for these reasons none of the above methods could be applied with confidence. The theoretical solutions for a double-wedge[4] and a flat plate[5] appear satisfactory but cannot be directly extended to conventional airfoil sections.

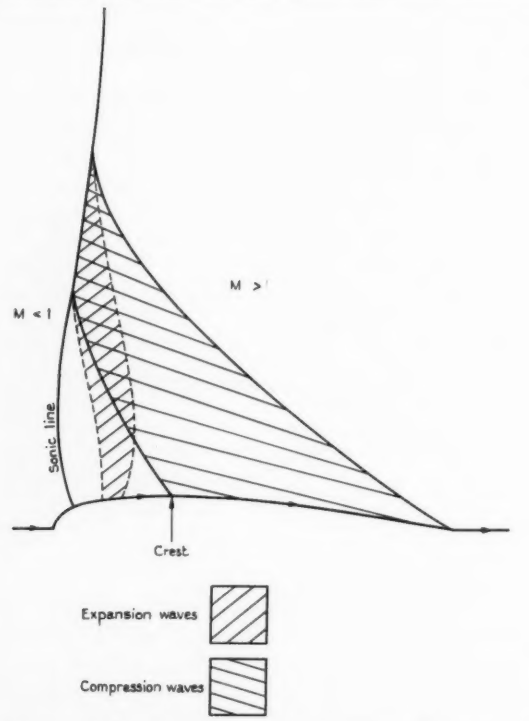

FIG. 3. Illustration of how the compression effect over the rear part of an airfoil arises from an expansion ahead of the crest.

In this paper, an alternative semiempirical method is suggested in which results obtained from an analysis of measured sonic-range pressure distributions are used in conjunction with simple-wave theory modified to represent the actual Mach wave pattern of the flow, the modification being partly derived from the theoretical solution for a double-wedge. By this means, the major part of the supersonic flow over an airfoil surface can be estimated. No method for calculating the pressure distribution near the leading edge is given, but in many cases the calculated distribution can be extrapolated forward to the stagnation point with sufficient accuracy. An example of the application of the scheme is given and the results agree well with measured values.

In Section (5) there is some discussion of the physical mechanism whereby the sonic-range flow field is established, attention being given to the relative importance of the leading and trailing edge in influencing the pressure distribution on an airfoil.

(2) Description of Flow Pattern

The flow pattern associated with the near-sonic flow about an airfoil surface is illustrated in Fig. 2. Conditions upstream of the leading edge are determined by the subsonic or supersonic nature of the free stream. In the subsonic case, there is a smooth deceleration to a stagnation point near the leading edge; alternatively, if the upstream flow is supersonic, there must first be a discontinuous deceleration to subsonic flow via a shock wave. However, in either case the flow immediately ahead of the airfoil is nonuniform normal to the free-stream direction. The flow on the airfoil surface, accelerating from the stagnation point, reaches local sonic speed at some point. Similarly, sonic speed is reached on streamlines adjacent to the surface, the locus of the sonic points forming the sonic line. Because of the nonuniformity of the flow the sonic line is curved, as are the expansion waves which originate from the curved airfoil surface bounding the supersonic flow behind the sonic line. Some of the expansion waves which meet the sonic line and are reflected as compression waves reach the airfoil surface, and so give an apparent reduction in the Prandtl-Meyer simple-wave expansion rate over the rear of the airfoil. Each of the compression waves reaching the surface is again reflected regularly as a compression; hence, the magnitude of the compressive effect is double that of the expansive effect which gave rise to the original expansion wave. It is probable that some multiple reflections occur in the neighborhood of the sonic point. The supersonic flow over the airfoil terminates in a shock wave at the trailing edge; the significance of this shock and the associated flow de-

flection in relation to the flow downstream of the trailing edge has been discussed in reference 6 and is reconsidered in the present context in Section (5) of this paper.

In a sonic stream, the Mach wave originating from the airfoil surface and meeting the sonic line at infinity defines the "limiting Mach line"; clearly disturbances behind this line cannot affect the upstream flow. Consideration of the Mach wave pattern suggests that the limiting Mach line must leave the airfoil surface ahead of the point where the surface tangent is parallel to the free stream. This point has been called the crest of an airfoil, and as the position of the limiting Mach line cannot be determined easily, the following discussion and analysis will be confined to the flow behind the crest. This flow is entirely supersonic in character and can be treated as arising from the superposition of two simple-wave flows, representing the two families of characteristics in the classical treatment of supersonic flow. One is due to changes in airfoil surface direction and the other to the compression waves coming from the sonic line. This secondary wave system is illustrated in Fig. 3, where it is shown that the origin of the compression waves which meet the surface between its crest and trailing edge is a wedge of expansion waves arising from the curved airfoil surface ahead of the crest. In Fig. 4 the contributions of the two simple-wave flows to the pressure variations of the surface of an airfoil are illustrated. Fig. 4(a) shows the pressure distribution for a double-wedge section; here the supersonic expansion takes place at a single point (the shoulder of the wedge) and there is no further change in flow direction until the trailing edge is reached. The pressure changes between the crest and trailing edge can arise only from compression waves emanating from the sonic line. Fig. 4(b) shows how the simple supersonic flow over a curved airfoil surface is modified in the same way, but in this case part of the pressure changes are due to the expansion round the curved surface of the airfoil between its crest and trailing edge.*

The factors determining the magnitude of the compression effect must be the shape and position of the sonic line, which is itself dependent on the neighboring surface shape, the airfoil shape in the region where the expansion/compression waves originate, and the change in surface direction between the crest and trailing edge, for this will affect the path of the reflected Mach waves. In the next Section it is shown empirically how the total compression between crest and trailing edge can be estimated, and that the theoretical distribution of the compression for a double-wedge[4] can be used for curved airfoils. From these results it is shown in Section (4) how the compression effect can be applied as a correction to airfoil surface slope distribution and an equivalent simple-wave flow obtained.

* In this case, of course, the flow from the sonic point onward is affected by the interaction of the sonic line and Mach waves, but, as has been stated, to simplify the problem only flow downstream of the crest is considered here.

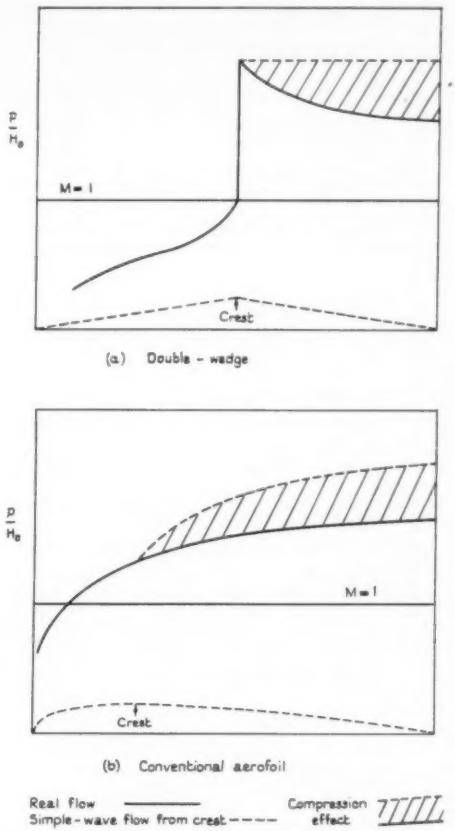

FIG. 4. The effect on airfoil pressure distributions of the compression waves coming from the sonic line.

(3) Derivation of Semiempirical Method for Estimating Sonic-Range Pressure Distributions

In the description of the sonic-range flow pattern about an airfoil surface it is noted that the flow over the surface terminates in an oblique shock wave at the trailing edge. This feature has been investigated by Holder.[6] He found that the local Mach Number ahead of the trailing-edge shock appeared to be directly related to the flow deflection at the trailing edge (determined on the assumption of no downwash). This result is illustrated in Fig. 5, where the Prandtl-Meyer

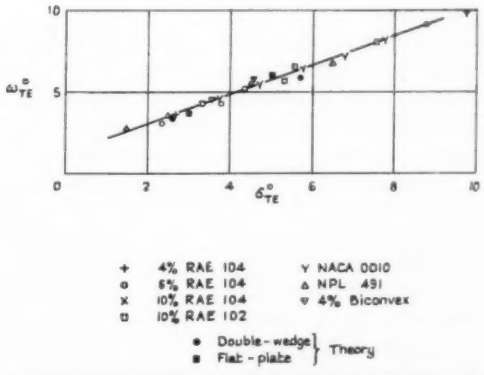

FIG. 5. Empirical relation for the flow at the trailing edge of an airfoil surface in a sonic stream.

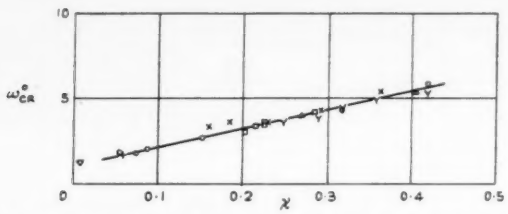

FIG. 6. Empirical relation for the flow at the crest of an airfoil surface in a sonic stream (for definition of symbols see Fig. 5).

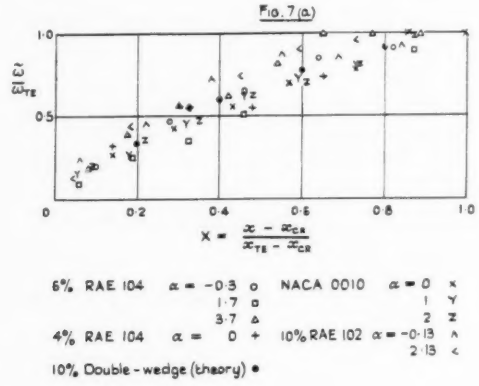

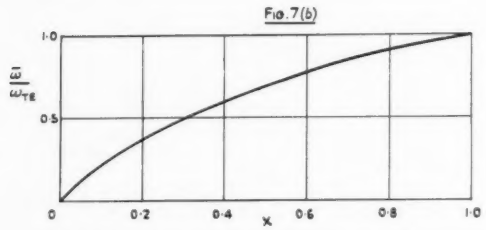

FIG. 7. Distribution of compression effect.

angle corresponding to the trailing-edge Mach Number is plotted against the assumed flow deflection for a number of airfoils at incidence. The mean curve is shown by Holder to be similar to that given by the oblique-shock relation for the assumed flow deflections and a downstream Mach Number of about 1.08, the remaining pressure recovery to free-stream conditions taking place along the wake. The relation between Holder's result and those of the present paper will be considered later.

Consideration of the Mach wave pattern has suggested that the effect of the waves reflected back to the airfoil ahead of its trailing edge can be represented as a correction to the surface slope distribution. It will be convenient to consider the compression effect of this wave system in terms of the equivalent Prandtl-Meyer flow deflection angle, as this can most easily be related to the changes in surface slope. It is noted above that the Prandtl-Meyer angle (ω_{TE}) just upstream of the trailing-edge shock wave is related to the trailing-edge flow deflection (δ_{TE})—which is also the change in surface direction between the crest and trailing edge. Hence, to determine the total compression angle from crest to trailing edge, given by $[\delta_{TE} - (\omega_{TE} - \omega_{CR})]$, it will be sufficient to determine ω_{CR}. This should be a function of the upstream geometry of the surface. Measured values of ω_{CR} for a number of airfoils were plotted against a mean of the surface curvature ahead of each airfoil crest. There appeared to be a consistent relation for each airfoil at different incidences, and the introduction of airfoil leading-edge radius as a further parameter unified the results for all the airfoils. The most consistent correlation is shown in Fig. 6; here ω_{CR} is plotted against the parameter χ, which is defined as $(y/c$ at $x = 0.02c)/[\Delta(x/c)$ for $\theta = 2°$ to $\theta = 4°]$ where θ is the surface slope measured forward from the crest. This change in x/c for a prescribed change in surface slope is a convenient measure of surface curvature. The value of y/c at $x = 0.02c$ is preferred to the nominal leading-edge radius as it takes account of the variation in leading-edge angle of biconvex and similar profiles.

From Figs. 5 and 6 the total compression from crest to trailing edge can be estimated; there remains the problem of the determination of the distribution of this compression. It has been emphasized that the pressure distribution over this part of an airfoil will be partly determined by the changes in surface direction and partly by the Mach waves reflected at the sonic line back onto the surface. To dissociate these two effects, measured pressure distributions have been analyzed to give the increment in equivalent Prandtl-Meyer angle over ω_{CR} at positions along the airfoil chord. The difference at a given point between this quantity $(\omega - \omega_{CR})$ and the surface slope is then the compression angle measured from the crest and will be denoted $\tilde{\omega}$; clearly $[\delta_{TE} - (\omega_{TE} - \omega_{CR})] \equiv \tilde{\omega}_{TE}$. To facilitate comparison of the compression distributions estimated in this way they are plotted in Fig. 7(a) in the form $\tilde{\omega}/\tilde{\omega}_{TE}$ against $(x - x_{CR})/(x_{TE} - x_{CR})$. Results taken from the theoretical solution for a double-wedge[4] are also shown on that Figure, and it is seen that these are in good agreement with the mean of the measured values. The considerable scatter of the experimental values bears no consistent relation to the parameter χ, and may be due to inaccuracies in the analysis of the experimental results. It is therefore suggested that the double-wedge distribution be used in the calculation of pressure distributions, and, for convenience, this curve is repeated in Fig. 7(b).

The method for the prediction of sonic-range pressure distributions based on the foregoing analysis is discussed in its application to a particular airfoil in Section (4).

The following points concerning the experimental results used in the analysis should be mentioned. The completeness of the Mach Number freeze within the sonic range is uncertain, and, to avoid discrepancies from this source, the results used were obtained at a nominal free-stream Mach Number of unity, with the exception of those for the 10 per cent RAE 102 airfoil. This was tested in a solid-walled tunnel which has been found to give a complete Mach Number freeze in the sonic range, so that results obtained at a high subsonic

Mach Number with the surface shock at the trailing edge should not differ from those at $M_0 = 1$. The influence of wind-tunnel wall configuration on sonic-range pressure distributions is shown to be small in references 7 and 8 for the wall shapes considered here. Because of this, it appears consistent to compare results for the 6 per cent RAE 104, 4 per cent RAE 104, and NACA 0010 airfoils, which were tested in slotted walls of 1/30th open area, with those for the 4 per cent Biconvex and NPL 491 airfoils, which were measured with 1/11th open area walls. These differences in test conditions do not appear to be important in the analysis. However, certain NACA measurements at transonic speeds do not conform with the relations established in Figs. 5 and 6. It is thought that this may partly be due to the low aspect ratio of the "two-dimensional" models used, and to other differences in test conditions.

Insofar as the theory of this paper depends on a relation between airfoil geometry and local pressure at a point, it is comparable with the well known Kármán transonic similarity law.[9] This states that, for affinely related airfoils in a sonic stream, the local pressure at a point is proportional to $\tau^{2/3}$, where τ is the thickness/chord ratio. The dependence of local pressure on τ implied by the curve of Fig. 6 cannot be easily investigated because χ is not a simple function of τ. However, it is proposed to study the relation to the transonic similarity law by testing airfoils of the same basic section (RAE 104), but with values of τ of 0.04, 0.06, and 0.10. The results for the 4, 6, and 10 per cent RAE 104 section given in Fig. 6 were obtained at different incidences.

(4) Application of Method

In this Section the calculation of a sonic-range pressure distribution for a particular airfoil (NPL 491) is described. The airfoil was designed to have a small trailing-edge angle, so that shock-induced boundary-layer separation would be absent for a range of incidence at all speeds. It is wedge shaped over the rear 60 per cent of its chord. This is of interest since consideration of the changes in airfoil surface direction only would result in the prediction of constant pressure over the wedge-tail, whereas the measured distributions show a rise in pressure towards the trailing edge. An analysis of the tests on this airfoil is given in reference 10.

The curve of airfoil surface slope θ against x/c is shown in Fig. 8. From this the trailing-edge flow deflection and the value of χ can be obtained for a given incidence; values calculated for $\alpha = 1°$ are given with Table 1, where the calculation of the sonic-range pressure distribution is set out. Column 1 gives the chordwise stations at which the pressure is to be calculated, starting at the crest corresponding to $\alpha = 1°$, Column 2 gives these positions in terms of $X = (x - x_{CR})/(x_{TE} - x_{CR})$, and, in Column 3, the corresponding values of the surface slope measured from the crest are given. The values of χ and δ_{TE} are then used to obtain ω_{CR} and ω_{TE}

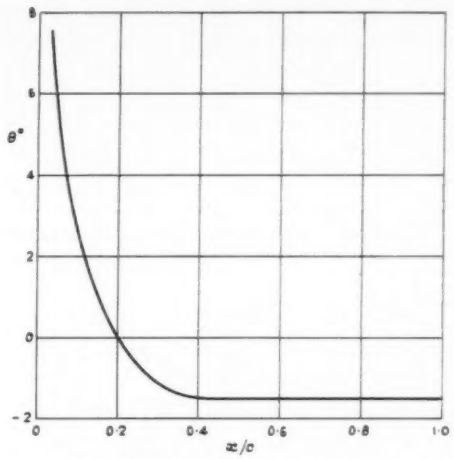

Fig. 8. Surface slope distribution for the NPL 491 airfoil.

from Figs. 5 and 6, respectively, and hence $\tilde{\omega}_{TE}$. This is the total compression from crest to trailing edge. The values of $\tilde{\omega}$ at the positions of Column 2 are calculated with the use of Fig. 7(b); Column 4 lists these values. The differences between the values of $\theta_{CR} - \theta$ and $\tilde{\omega}$ are given in Column 5; these represent the effective increments in flow deflection to be added to ω_{CR} to give Column 6, which lists the equivalent simple-wave flow deflection angles when the compression effect has been taken into account. Column 7 gives the corresponding pressure distribution.

In Fig. 9(a), the predicted and measured pressure distributions for an incidence of one degree are shown, together with that obtained on the assumption of Prandtl-Meyer flow from the crest. When the allowance for the reflected Mach waves is included, good agreement with experiment is achieved; this is fur-

Table 1

Calculation of the Sonic-Range Pressure Distribution for NPL 491 Airfoil at $\alpha = 1°$

For this airfoil $(y/c)_{x=0.02c} = 0.0096$, and from Fig. 8 it is found that

$$(x_{CR}/c)_{\alpha=1°} = 0.151$$

and $$(x/c)_{\theta=3°} - (x/c)_{\theta=5°} = 0.036$$

hence, $$\chi = 0.267; \quad \delta_{TE} = 2.51°$$

Figs. 5 and 6 give $\omega_{TE} = 3.57°$ and $\omega_{CR} = 3.90°$. The total equivalent compression angle from crest to trailing edge is then given by

$$\tilde{\omega}_{TE} = \delta_{TE} - (\omega_{TE} - \omega_{CR}) = 2.51° - (3.57° - 3.90°) = 2.84°$$

1	2	3	4	5	6	7
x/c	X	$\theta_{CR}° - \theta°$	$\tilde{\omega}°$	Col. 3 − Col. 4	ω_{CR} + Col. 5	p/H_0
0.151	0	0	0	0	3.90	0.405
0.2	0.06	1.00	0.43	0.57	4.47	0.393
0.3	0.18	2.07	0.97	1.10	5.00	0.382
0.4	0.29	2.40	1.38	1.02	4.92	0.384
0.5	0.41	2.50	1.70	0.80	4.70	0.388
0.6	0.53	2.51	2.03	0.48	4.38	0.395
0.7	0.65	2.51	2.31	0.20	4.10	0.401
0.8	0.76	2.51	2.51	0	3.90	0.405
0.9	0.88	2.51	2.75	−0.24	3.66	0.410
1.0	1.00	2.51	2.84	−0.33	3.57	0.412

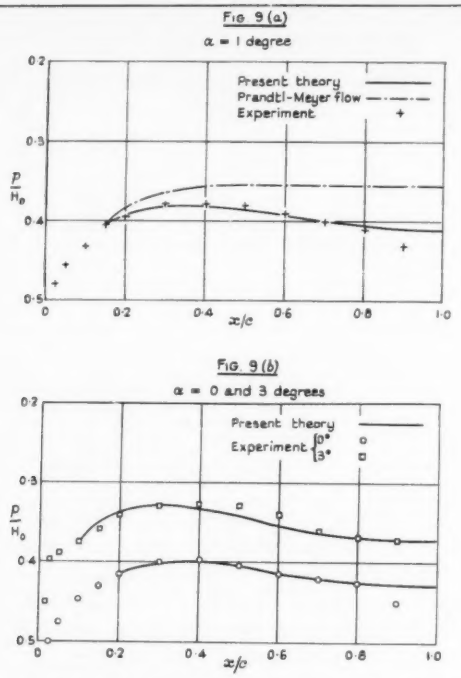

FIG. 9. Predicted and measured pressure distributions for the NPL 491 airfoil.

ther illustrated in Fig. 9(b) where results for $\alpha = 0°$ and $\alpha = 3°$ are given.

Although for this thin airfoil the surface shock wave is observed to be slightly forward of the trailing edge when $M_0 = 1$, whereas in the estimation of the pressure distribution it was assumed to be at the trailing edge, the results are comparable because of the persistance of the Mach Number freeze ahead of a shock wave when M_0 is below the sonic range (see Fig. 1). The results for the NPL 491 airfoil shown on Fig. 5 were obtained on this premise by extrapolating the measured pressure distribution to the trailing edge. Values of ω_{TE} so obtained differ little from those measured with the shock wave at the trailing edge when $M_0 > 1$.

(5) Concluding Remarks

An analysis of the Mach-wave pattern of the sonic flow about an airfoil surface has led to an understanding of the factors governing the flow, and it has been possible to represent these in a simple form so that a quantitative analysis of experimental results could be made. The empirical relations established by this analysis can be written as follows:

$$\omega_{TE} = \text{const.} + m\,\delta_{TE} \tag{1}$$

$$\omega_{CR} = \text{const.} + n\,\chi \tag{2}$$

which together give the compression angle,

$$\tilde{\omega}_{TE} = \text{const.} + n\,\chi + (1 - m)\,\delta_{TE} \tag{3}$$

Of these three relations only two appear to be independent, and it is of interest to consider which are the fundamental relations.

Earlier it is noted that the trailing-edge relation (1) appears to satisfy approximately the downstream free-stream conditions, but it is difficult to see the physical mechanism by which these can govern the supersonic flow upstream of the trailing edge, particularly for free-stream Mach Numbers above unity when the supersonic flow extends to infinity in a lateral direction.* It may be that the development of the whole flow to satisfy the trailing-edge conditions arises from the instability of alternative flows. The physical mechanism whereby airfoil leading-edge geometry plays a large part in determining the overall flow pattern is easily understood, and relations (2) and (3) demonstrate how quantitative results can be obtained from a simple representation of this geometry. It is perhaps significant that, in the theoretical studies of sonic flow, it has not been necessary to prescribe trailing-edge flow conditions nor to ensure that the downstream free-steam conditions are satisfied. In these studies, the transonic flow up to the limiting Mach line is treated as an entity, and then the supersonic flow to the trailing edge is obtained by the method of characteristics. Even so, values of ω_{TE} derived from the solutions for a double-wedge and flat plate at incidence are in fair agreement with the experimental results of Fig. 5.

The above considerations suggest that the leading-edge geometry of an airfoil is fundamental in determining the overall flow in a sonic stream and that the correlation of ω_{TE} with trailing-edge flow deflection is a consequence of this. However, there must clearly be some means whereby the downstream free-stream boundary conditions are satisfied, for the pressure rise through an oblique shock to give the required flow deflection at the trailing edge may not be sufficient to attain the appropriate downstream pressure. This difficulty can be overcome by supposing that the residual pressure rise takes place under the influence of the Mach waves reflected at the sonic line to downstream of the airfoil trailing edge. The interaction of such wave systems from the two surfaces of an asymmetric airfoil configuration may result in small changes in flow direction downstream of the trailing edge, which may be necessary to eliminate a downwash at the trailing edge. However, analysis of measured results indicates that such a downwash will be very small. Since, to satisfy the free-stream conditions downstream, it is necessary that the total effect of expansions and compressions behind the sonic line is zero, it appears that the free-stream conditions must to some extent determine the sonic-line/limiting-Mach-line configuration. It seems reasonable to conclude that (1) the free-stream conditions are dominant in determining the sonic-line configuration far above (and below) the airfoil, so that the total reflected expansion—i.e., the limiting Mach

* At the time reference 6 was written, data were available only for free-stream Mach Numbers below unity, and the physical nature of the flow at low supersonic speeds was not considered.

line position—is such as to ensure that the correct downstream velocity is attained, but (2) that the leading edge of the airfoil dominates the flow near the surface. It may be that the influence of the free-stream boundary conditions extends sufficiently towards the surface to affect the compression distribution over the surface and accounts for the small dependence of the compressive effect on δ_{TE} shown by Eq. (3). The associated correlation between trailing-edge pressure and flow deflection presumably arises from the general similarity* of the airfoil profiles considered in reference 6, and the fact that for these the bulk of the reflected Mach waves return to the plane of the airfoil ahead of the trailing edge, so that the pressure rise downstream of the trailing edge is always small. The approximate correlation between ω_{TE} and δ_{TE} would then follow from the presence of an oblique shock at the trailing edge related to trailing-edge angle and to only slightly different downstream velocities. In a real flow, the change in displacement thickness of the wake downstream of the trailing edge will also have some effect on the downstream pressure variations. Deflections of the streamlines due to reduction in the displacement thickness of the wake must in some way (at present unknown) be related to the "total effect of expansions and compressions."

These tentative conclusions do not invalidate the analysis of the preceding Sections of this paper. Without the mean curve of Fig. 5 it would be difficult to estimate empirically the influence of δ_{TE} on $\bar{\omega}_{TE}$. Indeed, because of the tentative nature of the above discussion, it is thought better to base the method for estimating sonic-range pressure distributions directly on the correlation of experimental results shown in Figs. 5 and 6, rather than to use the deduced correlation between $\bar{\omega}_{TE}$ and χ and δ_{TE}. Of course, this correlation is implied by use of Figs. 5 and 6, but the value of the method as such is not dependent on the interpretation of the flow mechanism leading to the results. However, it must be borne in mind that the scheme is based on a somewhat restricted selection of experimental results, and that certain NACA transonic tests do not accord with these. Further experimental work is being undertaken to study this difference and also to adapt the method to consideration of cambered airfoils.

Knowledge of the sonic-range pressure distribution can be a useful guide to the onset of shock-induced boundary-layer separation effects on an airfoil. Future work will be directed towards determining the pressure distribution on an airfoil with the surface shock upstream of the trailing edge.†

* In the sense that the majority of the sections considered had blunt leading edges and conventional maximum thickness positions.

References

[1] Lindsey, W. F., and Dick, R. S., *Two-Dimensional Chordwise Load Distributions at Transonic Speeds*, NACA RM L51I07, February, 1952.

[2] Gullstrand, T. R., *A Theoretical Discussion of Some Properties of Transonic Flow Over Two-Dimensional Symmetrical Airfoils at Zero Lift With a Simple Method to Estimate the Flow Properties*, K.T.H. Aero TN 25, June, 1952.

[3] Bévierre, P., *Calcul Approaché de la Résistance à l'Avancement en Transsonique d'un Profil Symétrique à la Portance Nulle*, La Recherche Aéronautique, No. 47, 1955.

[4] Guderley, G., and Yoshihara, H., *The Flow Over a Wedge Profile at Mach Number 1*, Journal of the Aeronautical Sciences, Vol. 17, No. 11, pp. 723–735, November, 1950. See also Vincenti, W. G., and Wagoner, C. B., *Transonic Flow Past a Wedge Profile With Detached Bow Wave*, NACA Report 1095, 1952.

[5] Guderley, G., *The Flow Over a Flat Plate With a Small Angle of Attack at Mach Number 1*, Journal of the Aeronautical Sciences, Vol. 21, No. 4, pp. 261–274, April, 1954.

[6] Holder, D. W., *Note on the Flow Near the Tail of a Two-Dimensional Airfoil Moving at a Free-Stream Mach Number Close to Unity*, A.R.C. C.P. 188, June, 1954.

[7] Holder, D. W., North, R. J., and Chinneck, A., *Experiments With Slotted and Perforated Walls in a Two-Dimensional High-Speed Tunnel*, A.R.C. R&M 2955, November. 1951.

[8] Marschner, B. W., *The Flow Over a Body in a Choked Wind Tunnel and in a Sonic Free Jet*, Journal of the Aeronautical Sciences, Vol. 23, No. 4, pp. 368–376, April, 1956.

[9] von Kármán, Th., *The Similarity Law of Transonic Flow*, J. Math. & Phys., Vol. XXVI, No. 3, pp. 182–190, October, 1947.

[10] Holder, D. W., *Experiments on an Airfoil Section Designed to Avoid Boundary-Layer Separation for Small Lift Coefficients at All Mach Numbers*, A.R.C. R&M 3100, August, 1957.

[11] Sinnott, C. S., *On the Prediction of Mixed Subsonic/Supersonic Pressure Distributions Over Airfoils*, A.R.C. Report Nos. 20,459, 20,460, 20,461, October, 1954.

† An extension of the semiempirical analysis to this problem has been completed recently and is reported in reference 11.

Tenth International Congress of Applied Mechanics

Stresa, Italy, August 31–September 7, 1960

Apart from a number of invited general lectures, the technical sessions of the Congress will be held in two sections: Fluid dynamics (hydrodynamics and aerodynamics); and Mechanics of solids (rigid body dynamics, vibrations, elasticity, plasticity, and theory of structures).

It should be noted that thermodynamics and computational methods as such are not included, although specific applications of computational methods to pertinent problems of one of the two sections stated above are acceptable subjects for presentation.

Abstracts should be submitted before January 1, 1960 to: *The Secretary of the International Committee, Prof. Mekelweg 2, Delft, Netherlands.* Abstracts, in four copies, should not exceed two typewritten pages (double-spaced). It is recommended that abstracts be in two of the official Congress languages (English, French, German, and Italian).

All correspondence, apart from submission of papers, should be addressed to: *The Italian Organizing Committee, Consiglio Nazionale delle Ricerche, Ufficio relazioni internazionali, Piazza delle Scienza 7, Roma.*

On the Base Pressure Resulting From the Interaction of a Supersonic External Stream With a Sonic or Subsonic Jet

W. L. CHOW*

University of Illinois

SUMMARY

It is shown that the two-dimensional base pressure problems relating to base bleed into the wake of blunt-trailing-edge airfoils, or the interaction between an external supersonic or sonic slipstream with a sonic or subsonic jet stream of a jet engine, can be calculated by theoretical considerations. Constant-pressure, isoenergetic, turbulent mixing between the streams and the stagnant fluid in the wake is assumed. The theoretical calculations are in good agreement with the experimental results.

SYMBOLS

C	$= u/u_{max} = \{1 + [2/(k-1)_M{}^2]\}^{-(1/2)}$, Crocco Number
k	$= c_p/c_v$, ratio of specific heat
G_s	= mass rate per unit width flowing between jet-boundary streamline and streamline s
H	= step height
M	= Mach Number
P	= absolute pressure
T	= absolute temperature
u	= velocity component in x direction
x, y	= coordinates in the intrinsic coordinate system
X, Y	= coordinates in the reference coordinate system
η	$= \sigma(y/x)$, dimensionless coordinate
θ	= streamline angle
ρ	= density
σ	= similarity parameter for homogeneous coordinate y/x
φ	$= u/u_{2a}$, dimensionless velocity

Subscripts

1, 2, 3, 4	refers to conditions at cross sections indicated in Fig. 3
a	refers to conditions in free stream adjacent to the dissipative regions
b	refers to conditions at the base or in the wake
d	refers to conditions along the discriminating streamline
j	refers to conditions along the jet boundary streamline
0	refers to stagnation value
s	refers to streamline

Superscript

$'$	refers to the jet stream or lower stream

INTRODUCTION

THE TWO-DIMENSIONAL FLOW MODEL, as shown in Fig. 1, simulates the problem of base bleed into the wake of blunt-trailing-edge airfoils, or the interaction between the external slipstream and the jet stream of a jet engine or rocket flying at sonic or supersonic speed. Experimental investigations dealing with a preliminary phase of such a problem, where the stagnation temperatures in both streams are nearly equal, were done notably by Fuller and Reid[1] and Wimbrow.[2] It is intended to show to what extent the base pressures for problems of this type can be calculated by theoretical considerations. Such treatment is based on concepts emerging from a theory of base pressures, as developed by Korst *et al.*, at the University of Illinois** (see references 3, 4, and 5).

Originally dealing with the problem of a two-dimensional supersonic flow past a back step, Korst devised a simple flow model which encompasses essentially as components: the approaching supersonic flow expanding around the trailing edge, constant-pressure turbulent jet-mixing along the wake,† recompression at the end of the wake, and conservation of mass within the wake. Extensions of the theory included the considerations of base bleed (see references 3, 4, 5, 7, and 8), and the interaction of two supersonic streams at the base (see references 9 and 10).

Interaction between the dissipative flow region and the adjacent free stream is such that the latter defines the pressure field in the sense of boundary-layer concepts. The free stream follows a Prandtl-Meyer relationship for the expansion around the trailing edge, and goes through an oblique-shock recompression at the end of the wake. The boundary of the corresponding inviscid jet (defined as the hypothetical frictionless jet which has the same approach Mach Number, expands

** This portion of the work was partially supported by the Office of Scientific Research under the Contract AF 18(600)-392.

† The case with laminar mixing was considered in a similar way by D. R. Chapman.[6]

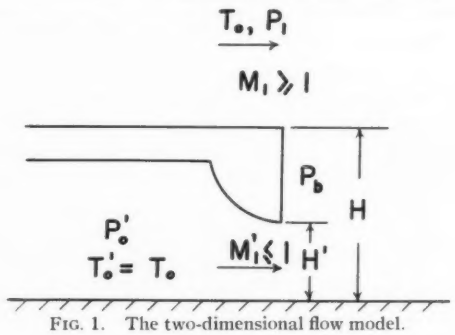

FIG. 1. The two-dimensional flow model.

Received April 7, 1958. Revised and received September 19, 1958.

* Research Assistant Professor of Mechanical Engineering.

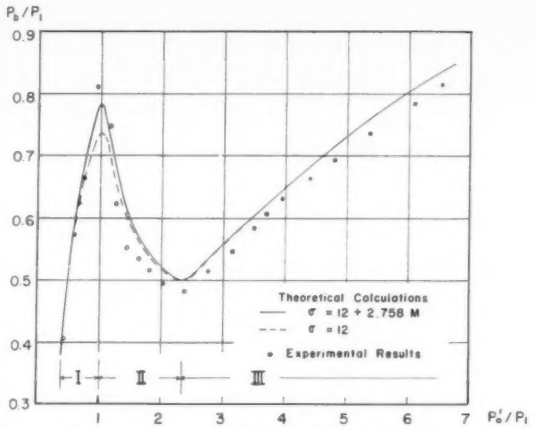

FIG. 2. The relation between P_b/P_1 and P_0'/P_1 for $M_1 = 1.92$, $H/H' = 1.94$.

through the same pressure ratio, and is influenced by the same geometry of physical boundaries as the actual viscous jet) serves as a reference system of coordinates and establishes the shape of the wake (inviscid flow model). The dissipative flow regions are superimposed on the jet boundaries of the inviscid flow model. A restriction of the flow model to a constant-pressure dead-air region is often justified, and is here assumed to be applicable to the present problem at the outset. Thus the theory of two-dimensional compressible jet-mixing at constant pressure[3,11] may now be employed.

If the thickness of the boundary layer approaching the trailing edge may be considered to be small compared to the significant wake dimensions, a considerable simplification of the problem is achieved by application of the "restricted theory"[3] which allowed a quantitative solution of the base pressure problem. Again, the applicability of the "restricted theory" is here assumed for the problem under consideration, so that the solutions may be interpreted as being reached asymptotically for high Reynolds Numbers.

Recompression at the end of the wake utilizes the concept of the discriminating streamline within the shear flow region, which attains just sufficient energy to penetrate into the high-pressure region behind the oblique shock at the end of the wake by complete isentropic (although irreversible-diabatic) conversion of its kinetic energy. The requirement of conservation of mass within the wake is here to be satisfied by balancing the contributions of both streams to the wake within the concept of an "open wake."[3, 9]

It shall be noted that an extension to nonidentical stagnation temperatures in both streams principally requires the application of nonisoenergetic mixing concepts[8] and use of an energy balance for the wake. Such a treatment, which is considerably more tedious in numerical calculation procedures, would also allow the prediction of base temperatures.

THEORETICAL FLOW MODELS

The present analysis will be applied to a fixed base geometry as shown in Fig. 1, so that for a given slip-stream approach Mach Number $M_1 \geqslant 1$, the primary variable will be the pressure ratio P_0'/P_1. As mentioned before, the stagnation temperatures in both streams are assumed to be the same; also, both streams have the same composition and identical (and constant) specific heat ratios ($k = 1.4$).

It is now instructive to inspect a typical experimental result (Fig. 2) to illustrate the appearance of three distinctly different regions—namely, region I for $P_0'/P_1 \leqslant 1$, region II for $1 \leqslant P_0'/P_1 \leqslant \sim 2.35$, and region III for $P_0'/P_1 \geqslant \sim 2.35$. While Fig. 2 represents experimental data obtained at the small supersonic facility at the University of Illinois, the same general trend was reported by Fuller and Reid[1] and Wimbrow.[2]

The different regions as shown in Fig. 2 can be associated with different idealized flow patterns as illustrated by Figs. 3 (region III), 4 (region I), and 5 (region II). It is immediately recognized that the problem associated with region III (Fig. 3) is essentially a special case ($M_1' = 1$, and the presence of the lower wall) of the one investigated by Korst and Tripp.[9] Note that in this specific case, the slipline angle θ_{4a} downstream of the oblique shocks is positive, as shown.

Region I, on the other hand, may be studied on the basis of the base-bleed concept, which was also developed before for negligible[3] and finite[7] bleed velocities. The former will be directly applicable for values of P_b'/P_1 near unity, and the influence of finite bleed velocities is disregarded here. As shown in Fig. 4, the entire mass of the jet flow is added to the wake and must be pumped out by the external slipstream.

Region II, associated with the flow model as shown in Fig. 5, is treated with the assumption that the recom-

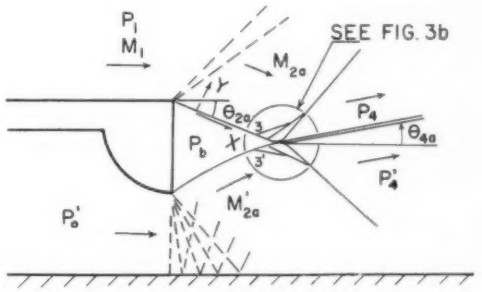

FIG. 3(a). Inviscid flow model for region III.

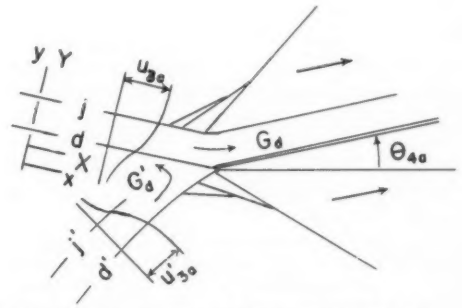

FIG. 3(b). Detail of dissipative flow near the end of the semi-dead air region.

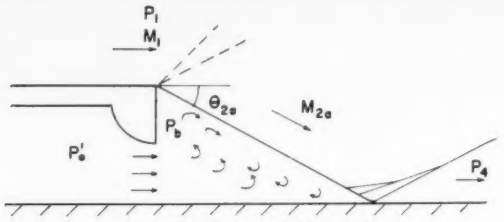

FIG. 4. The flow model for region I.

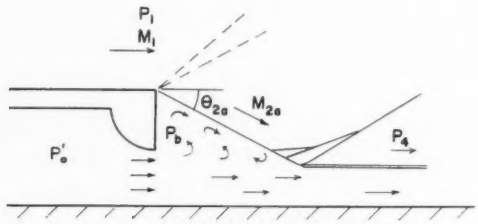

FIG. 5. The flow model for region II.

pression of the jet stream reaches the static pressure level impressed by the external slipstream turning into a direction parallel to the lower wall. Only a portion of the jet stream which is slowed down sufficiently by the mixing process along the wake will be added to the wake while the external slipstream has to pump mass out at the same rate.

THEORETICAL CALCULATION OF THE JET INTERFERENCE EFFECTS

In order to calculate the jet interference effects, it is necessary to treat the flow components within the different flow models on a quantitative basis.

(1) The streams approaching the base are considered to be uniform and parallel to the wall (symmetry line of the jet flow).

The external flow will then be specified by M_1 ($\geqslant 1$), p_1, T_0, k, while the jet flow is given by $M_1' \leqslant 1$, p_0', T_0, $k' = k = 1.4$.

(2) Expansion at the base. The external stream will undergo a Prandtl-Meyer expansion in each of the flow regions I, II, and III, while the jet flow will follow such a relation within region III only. In regions I and II, essentially parallel outflow from the jet nozzle may be assumed (although this is unimportant for cases within region I).

(3) The flow of the streams along the wake with mixing. As the wake is assumed to be of constant static pressure, the construction of the boundaries of the "corresponding inviscid jets" can be accomplished (for a given wake pressure) by potential flow concepts (method of characteristics) in the following cases:

External slipstream: regions I, II, and III
Jet stream: region III*

* Boundaries of the "corresponding inviscid jet" for the underexpanded sonic stream were calculated by the method of characteristics for two-dimensional flow on the Illiac (Electronic Digital Computer, Engineering Research Laboratory, University of Illinois).

In absence of external interference, this boundary of the external slipstream will be a straight line with the angle of θ_{2a}.

Along the jet boundaries, isoenergetic turbulent mixing at constant pressure is assumed to take place and the theoretical results obtained previously on this component are directly applied.[3, 11] The flow solution in the mixing regions is based on a highly simplified equation of motion, but is interpreted to hold within an "intrinsic system of coordinates" (x, y) which is subsequently localized with respect to the "reference system of coordinates" (X, Y) by application of the momentum integral (see Fig. 3).

Within the "restricted theory" the velocity distribution in such a case can be conveniently represented by

$$\varphi = (1/2)\,(1 + \operatorname{erf} \eta) \qquad (1)\dagger$$

The mass rate per unit width,

$$G_s = \int_{y_j}^{y_s} \rho u dy$$

flowing between the "jet boundary streamline," y_j or $\eta_j = \eta_j(C_{2a})$ (which separates the fluid of the approaching stream from the fluid in the dead-air region) and the streamline s (specified by the coordinates y_s or η_s) can be conveniently expressed in dimensionless form by

$$G_s \sigma_{2a}/x\rho_{2a}u_{2a}(1 - C_{2a}^2) = \int_{\eta_j}^{\eta_s} [\varphi d\eta/(1 - C_{2a}^2\varphi^2)] = I_1(\eta_s, C_{2a}^2) - I_1(\eta_j, C_{2a}^2) \qquad (2)$$

where

$$I_1(\eta, C_{2a}^2) = \int_{-\infty}^{\eta} [\varphi d\eta/(1 - C_{2a}^2\varphi^2)] \qquad (3)$$

has been obtained by numerical calculation on the Illiac for 21 values of the parameter C_{2a} (see reference 12), and is given in graphical form in Fig. 6 as $I_1[\varphi(\eta), C_{2a}^2]$. σ is the empirical similarity parameter in turbulent mixing supposedly dependent upon Mach Number. Here, the relation suggested by Korst and

† Equations are written for the external stream but are equally applicable to the jet stream when used with prime as superscript.

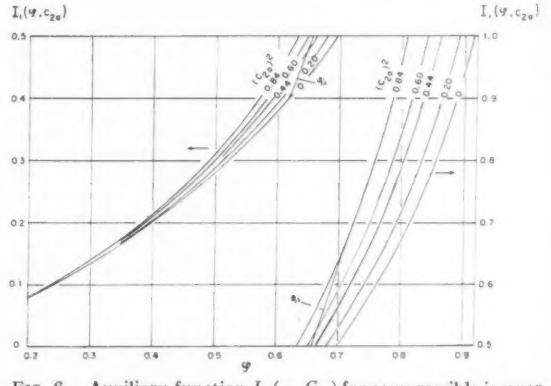

FIG. 6. Auxiliary function I_1 (φ, C_{2a}) for compressible isoenergetic turbulent jet-mixing at constant pressure (for fully developed profiles).

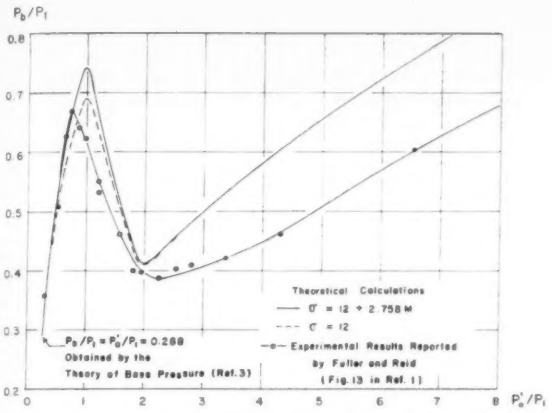

FIG. 7. Comparison of experimental results and theoretical calculations. $M_1 = 2.3$, $H/H' = 2$.

Tripp[9] $\sigma = 12 + 2.758M$ was used in the calculation.

For the treatment of the jet flow in region I, mixing concepts are not needed, since the jet velocity is assumed to be small.

(4) Recompression at the end of the wake. With the static pressure p_4 produced by the oblique shock in the external slipstream, the escape criterion[3] defines a discriminating streamline d with the dimensionless coordinate η_d, so that

$$P_{0d_3}/P_4 = 1 \tag{4}$$

where

$$P_{0d_3}/P_3 = \{1 + [(k-1)/2]M_{3d}^2\}^{k/(k-1)} \tag{5}$$

This relation, which will allow the evaluation of M_{3d} and, consequently, C_{3d} and φ_{3d},* is needed for the external flow (regions I, II, and III) and for the jet stream (regions II and III only).

Thus, for a selected base pressure $p_b = p_2 = p_3$, the streamline angles of the inviscid flow model will be determined and the static pressure behind the recompression zone will be fixed. While this is evident for regions I and II, where the shock deflection angle must be equal to θ_{2a}, a trial-and-error procedure is required for region III so that a θ_{4a} is found for which $P_4 = P_4'$.

Since the base pressure p_b was so far assumed to be known, the principle of conservation of mass within the wake must now be employed to find the correct solution.

(5) Conservation of mass in the wake. It is evident that for steady state

$$G_d + G_d' = 0 \tag{6}$$

or

$$G_d'/G_d = -1 \tag{7}$$

which can be expressed, with the help of the relations given above, by

$$\frac{G_d'}{G_d} = \frac{C_{2a}'\,\sigma_{2a}\sin\sigma_{2a}}{C_{2a}\,(1 - C_{2a}'^2)\,(H/H')\,(I_{1d} - I_{1j})} = -1 \tag{8}$$

* Note that the discriminating streamline d will coincide with the jet boundary streamline j for closed-wake problems only.

for region I, and

$$\frac{G_d'}{G_d} = \frac{C_{2a}'\,\sigma_{2a}\,x'\,(I_{1d}' - I_{1j}')}{C_{2a}\,\sigma_{2a}'\,x\,(I_{1d} - I_{1j})} = -1 \tag{9}$$

for regions II and III, where the term x'/x corresponds to the ratio of the rectified length along the mixing paths of the streams in the inviscid flow model (approximated by $\cos\theta_{2a}$ in case of region II).

Problem solutions for given height ratio H/H' and values of M_1 and P_0'/P_1, are obtained by a trial-and-error procedure where values of p_b/p_1 are assumed and the relation for mass conservation has to be satisfied as a check.

Theoretical and Experimental Results

It was first attempted to produce a theoretical solution for a flow case investigated experimentally by Fuller and Reid (test on afterbody No. 1 in reference 1). The geometry of this afterbody was similar to that of Fig. 1 with $H/H' = 2$, and the Mach Number of the external stream approaching the base was reported as being $M_1 = 2.3$. Comparison between the theoretical curve calculated by the method given in the previous sections showed good agreement within region I but only qualitative agreement for regions II and III (see Fig. 7). A careful study of the test setup used by Fuller and Reid revealed that the shock originating at the leading edge of their model, as well as the expansion fan originating at the shoulder of the leading wedge, were reflected from the tunnel wall and interfered with the wake, so that their experimental results do not seem to be representative for undisturbed conditions of the external flow.

In order to produce test conditions which were free of such a deficiency, thus allowing a better evaluation of the theory, an experimental program was conducted at the University of Illinois. The configuration of the flow channel used in this investigation is shown in Fig. 8. Air for both streams was taken from the same supply line ($T_0 = T_0'$) and the variation of P_0'/P_1 was achieved by appropriate individual throttling of the valves leading to the two streams. The external flow (upper stream in Fig. 8) was simulated by a sharp-corner nozzle designed for parallel outflow which produced an exit Mach Number of $M_1 = 1.92$ of reasonable uniformity, as checked by pressure readings in the exit cross section. The jet stream (lower stream in Fig. 8) was produced by a converging nozzle. H/H' was 1.94 as mentioned before.

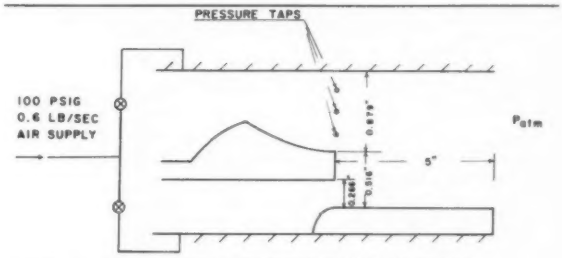

FIG. 8. Experimental configuration (1/2-in. width).

Agreement between experimental data and theoretical calculations, as evidenced by Fig. 2, is quite satisfactory, except for the region around $P_0'/P_1 = 1$, where the test configuration of the internal flow will fail to simulate correctly the condition for undisturbed external flow.*

It is noteworthy to mention that the theory does not introduce any empirical quantity other than σ. That the uncertainty in dealing with the latter is of little practical consequence is demonstrated by plotting into Fig. 2 another theoretical curve obtained for $\sigma = 12$, a value well established for $M \to 0$.

From this method of calculation, it can be predicted that the base pressure ratio would have a relative maximum for a pressure ratio of P_0'/P_1 equal unity, if one neglects the irreversibility of the shock recompression. The actual irreversibility of the shock of moderate strength will cause the relative maximum to occur for P_0'/P_1 less than but close to one. This result is at variance with the observance of Fuller and Reid[1] and Wimbrow[2] who locate the relative maximum of the base pressure ratio for values of P_0'/P_1 below unity.

It is also interesting to point out that the geometrical height ratio H/H' has little effect on P_b/P_1 in region II.

References

[1] Fuller, L., and Reid, J., *Experiments on Two-Dimensional Base Flow at $M = 2.4$*, Brit. RAE Report Aero. 2569, 1956.

[2] Wimbrow, W. R., *Effect of Base Bleed on the Base Pressure of Blunt-Trailing-Edge Airfoils at Supersonic Speeds*, NACA RM A54A 07, 1954.

* Theoretical analysis revealed that for $P_b/P_1 > 0.611$ in region I and $P_b/P_1 > 0.78$ in region II, the expansion waves reflected from the top wall interfered with the wake for a uniform nozzle flow of $M_1 = 1.92$.

[3] Korst, H. H., *A Theory for Base Pressures in Transonic and Supersonic Flow*, Journal of Applied Mechanics, Vol. 23, pp. 593–600, 1956.

[4] Korst, H. H., *Zur Theoretischen Bestimmung des Dellendruckes bei Abeglöster Strömung*, Csterreichisches Ingenieur-Archiv., Vol. 11 No. 3, pp. 227–238, 1957.

[5] Korst, H. H., Page, R. W., and Childs, M. E., *A Theory for Base Pressure in Transonic and Supersonic Flow*, Univ. of Ill. Eng. Exp. Sta. ME-TN-392-2; also OSR-TN-55-89, Contract No. AF 18(600)-392, March, 1955.

[6] Chapman, D. R., Kuehn, D. M., and Larson, H. K., *Investigation of Separated Flows in Supersonic and Subsonic Streams with Emphasis on the Effect of Transition*, NACA TN 3869, 1957.

[7] Wu, C. Y., *The Influence of Finite Bleed Velocities on the Effectiveness of Base Bleed in the Two-Dimensional Supersonic Base Pressure Problem*, Ph.D. Thesis, Univ. of Illinois, February, 1957.

[8] Page, R. H., and Korst, H. H., *Non-Isoenergetic Compressible Jet Mixing with Consideration of its Influence on the Base Pressure Problem*, Proceedings, Fourth Midwestern Conference on Fluid Mechanics, Purdue Univ., September, 1955.

[9] Korst, H. H., and Tripp, W., *The Pressure on a Blunt Trailing Edge Separating Two-Supersonic Two-Dimensional Air Streams of Different Mach Numbers and Stagnation Pressures, but Identical Stagnation Temperatures*, Paper presented at the Midwest Conference on Solid and Fluid Mechanics, Univ. of Mich., Ann Arbor, Mich., April 1–2, 1957.

[10] Tripp, W., *The Base Pressure Behind a Blunt Trailing Edge for Supersonic, Two-Dimensional Flow; Approaching Streams Having the Same Stagnation Temperature but Dissimilar Mach Numbers and Stagnation Pressures*, Ph.D. Thesis, Univ. of Illinois, 1956.

[11] Korst, H. H., Page, R. H., and Childs, M. E., *Compressible Two-Dimensional Jet Mixing at Constant Pressure*, Univ. of Illinois Eng. Exp. Sta., ME-TN-392-1; also OSR-TN-54-82, Contract AF 18(600)-392, April, 1954.

[12] Korst, H. H., Page, R. H., and Childs, M. E., *Compressible Two-Dimensional Jet Mixing at Constant Pressure—Tables of Auxiliary Functions for Fully Developed Mixing Profiles*, Univ. of Illinois Eng. Exp. Sta., ME-TN-392-3; also OSR-TN-55-99, Contract No. AF 18(600)-392, April, 1955.

Advances in Aeronautical Science

Proceedings of the First International Congress of the Aeronautical Sciences, Madrid, 1958 (2 Vols.)

In these two volumes will be published the 46 papers presented by the world's outstanding specialists in the field of aeronautics and astronautics at the First International Congress of the Aeronautical Sciences held in Madrid in September, 1958, under the leadership of Prof. Theodore von Kármán. Some 600 delegates from 25 countries, including an official delegation from the U.S.S.R., attended, and the meeting was so successful that it was decided to hold similar congresses at 2-year intervals in future.

The volumes will have a full author and subject index and number 1,200 pages. The *Proceedings*, edited by Th. von Kármán, A. M. Ballantyne, H. Blenk, R. R. Dexter, M. Roy, and H. L. Dryden, are of special interest to aerodynamicists, aeronautical engineers, rocketry research workers, and propulsion engineers.

The *Proceedings* (price, $25.00) may be obtained by writing to: *Sales Director, Pergamon Press, Inc., 122 East 55 St., New York.*

Readers' Forum

BRIEF REPORTS of investigations in the aeronautical sciences and discussions of papers published in the JOURNAL are presented in this special department. Entries must be restricted to a maximum of 1,300 words or the equivalent of one JOURNAL page including formulas and illustrations. Publication is completed as soon as possible after receipt of the material. The Editorial Committee does not hold itself responsible for the opinions expressed by the correspondents.

Contents

An Exact Solution of the Navier-Stokes Equations ..... HERBERT E. HUNTER 181

A Note on the Skin-Friction Coefficient for Compressible Couette Flow ..... ROBERT M. INMAN 182

The Stagnation-Point Boundary Layer on a Rotating Hypersonic Body ..... SINCLAIRE M. SCALA AND JOSEPH B. WORKMAN 183

On Similitude in Rarefied-Gas Aerothermodynamics ..... F. MARCEL DEVIENNE 183

Shock-Tube Testing Time ..... G. F. ANDERSON 184

Correlation of Base Pressure and Wake Structure of Sharp- and Blunt-Nose Cones With Reynolds Number Based on Boundary-Layer Momentum Thickness ..... R. LEHNERT AND V. L. SCHERMERHORN 185

The Role of Unit Reynolds Number in Boundary-Layer Transition .. JACK D. WHITFIELD AND J. LEITH POTTER 186

The Heating of Slabs With Arbitrary Heat Inputs ..... THEODORE R. GOODMAN 187

The Effects of Constant-Pressure Sound Fields on Free-Convection Heat Transfer From a Horizontal Cylinder .. JACK P. HOLMAN AND TIPTON P. MOTT-SMITH 188

A New Solution to the Laminar Boundary-Layer Equations ..... H. A. HASSAN 189

On the Supersonic Flutter of Two-Dimensional Infinite Panels .... JOHN W. MILES AND WILLIAM P. RODDEN 190

A Note on Blast-Wave Theory ..... HARVEY EINBINDER 191

Errata—"Some Panel-Flutter Studies Using Piston Theory" ..... DAVID J. JOHNS 192

An Exact Solution of the Navier-Stokes Equations

Herbert E. Hunter

Graduate Student, California Institute of Technology, Pasadena, Calif.

October 13, 1958

IN THIS NOTE the exact solution of the Navier-Stokes equations presented by W. Chester in reference 1 is generalized to include all values of γ. The notation of reference 1 will be followed, except as noted.

In rectangular coordinates the solution presented in reference 1 may be written as

$$\left.\begin{aligned} u_1 &= U(1 - y^2/a^2) \\ p_1 &= p_0 - (2\mu U/a^2)\,(x - Ut) \end{aligned}\right\} \tag{1}$$

It can be shown that Eqs. (1) are a nontrivial solution only if $\gamma = 1.5$. It seems likely that this solution is part of a more general solution which has other terms involving $(\gamma - 1.5)$. We shall assume that the more general solution is of the form: $V = [u(y, z, t), 0, 0]$, $\rho = \text{const}$. Under this assumption, the continuity equation is satisfied identically and the remaining Navier-Stokes equations reduce to

$$\left.\begin{aligned} \partial p/\partial x &= \mu[(\partial^2 u/\partial y^2) + (\partial^2 u/\partial z^2)] - \rho(\partial u/\partial t) \\ \partial p/\partial y &= \partial p/\partial z = 0 \\ (\partial p/\partial t) + u(\partial p/\partial x) &= (\gamma - 1)\,[(K/R)(\partial^2 p/\partial x^2) + \\ &\qquad \mu(\partial u/\partial y)^2 + \mu(\partial u/\partial z)^2] \end{aligned}\right\} \tag{2}$$

Integration of the momentum equations gives

$$p = p\,(x, t)$$

$$p = \{\mu[(\partial^2 u/\partial y^2) + (\partial^2 u/\partial z^2)] - \rho\,(\partial u/\partial t)\}\,x + C_1\,(t) \tag{3}$$

After examining the details of the solution presented in reference 1, we are led to trying a solution of the form:

$$u = u_1 + u' \tag{4}$$

Contributors Please Note

Readers' Forum items must be confined to the equivalent of one page in the *Journal*. Contributions that exceed this limit will be returned to the authors for condensation and rewrite. To avoid inconvenience and delay, please adhere to the following specifications:

(1) Five, double-spaced, typewritten, manuscript pages ($8\frac{1}{2}$ by 11 in.), including wide margins, formulas, and headings, equal one printed page.

(2) For every illustration, deduct at least one-half or as much as one manuscript page, depending on the size of the illustration.

and to the assumption that

$$C_1 = (2\mu U^2 t/a^2) + C_1'(\gamma, t) \tag{5}$$

where u_1 = solution from reference 1 (Eqs. 1); $u' = u'(z, t, \gamma)$; and $C_1' = C_1'(\gamma, t)$.

Combining the last of Eqs. (2) with Eqs. (3–5) and taking into account the fact that u' is independent of y, we get the following two equations:

$$\left.\begin{aligned} \mu(\partial^2 u'/\partial z^2) - \rho(\partial u'/\partial t) &= -(4\,U/a^2)\,(\gamma - 1.5)\mu \\ \partial C_1'/\partial t = (4\,U^2/a^2)\,(\gamma - 1.5)\,\mu &+ \\ (\gamma - 1)\,[(4\,\mu U/a^2)u' + \mu(\partial u'/\partial z)^2] & \end{aligned}\right\} \tag{6}$$

The last of these and Eq. (5) imply

$$(\partial u'/\partial z)\,[(\partial^2 u'/\partial z^2) + (2u/a^2)] = 0$$

Solving this we get

$$u' = n[c_3(t)z - (Uz^2/a^2)] + c_4(t) \tag{7}$$

where n is either 0 or 1.

Substituting the above equation into the first of Eqs. (6) and solving it, we get

$$u' = nU\,[C_2 z - (z^2/a^2)] + (2\mu U/a^2\rho)\,(2\gamma - 3 - n)\,t \tag{8}$$

where C_2 is a constant.

Solving the last of Eqs. (6) for C_1' we get

$$C_1' = \mu U^2\,([4(\gamma - 1)(2\gamma - 3 - n)\mu/\rho a^4]\,t^2 + \{[4(\gamma - 1.5)/a^2] + (\gamma - 1)\,C_2^2\,n^2\}\,t) \tag{9}$$

Therefore the more general solution for u is

$$u = U\{1 - [(y^2/a^2) + (nz^2/a^2)] + nc_2 z + (2\mu/a^2\rho)\,(2\gamma - 3 - n)t\} \tag{10}$$

Substituting this into Eq. (3) we get

$$p = p_0 - [4(\gamma - 1)\mu U/a^2] \times \{x - [(2\gamma - 3 - n)\mu U/\rho a^2]t^2 - [1 + (c_2 a n/2)^2]Ut\} \tag{11}$$

The case $n = 0$ is clearly a two-dimensional flow. The case $n = 1$ is best interpreted by means of cylindrical coordinates, in terms of which it becomes

$$\left.\begin{aligned} u &= U[1 - (r^2/a^2) + c_2 r \sin\theta + (4\mu/a^2\rho)\,(\gamma - 2)t] \\ p &= p_0 - [4(\gamma - 1)\mu U/a^2] \times \{x - [2(\gamma - 2)\mu U/\rho a^2]t^2 - [1 + (c_2 a/2)^2]Ut\} \end{aligned}\right\} \tag{12}$$

The solution for $n = 0$ represents plane flow between two insulated parallel flat plates which have a time-dependent distance between them. Eqs. (12) represent flow through an insulated expanding or contracting circular pipe. The direction of motion of the walls in either case is dependent on γ. It is easy to show that the above solutions reduce to those presented in reference 1 for $\gamma = 1.5$ and $\gamma = 2$, respectively. That is, the distance between the plates (or the radius of the pipe) remains fixed.

Reference

[1] Chester, W., *An Exact Solution of the Navier-Stokes Equations*, Readers' Forum, Journal of the Aeronautical Sciences, Vol. 24, No. 11, pp. 853–854, November, 1957.

A Note on the Skin-Friction Coefficient for Compressible Couette Flow

Robert M. Inman
Assistant in Engineering, Department of Engineering, University of California at Los Angeles, Calif.

October 10, 1958

Symbols

C_f = skin-friction coefficient
C_p = specific heat at constant pressure
h = distance between plates
M = Mach Number
Pr = Prandtl Number
q = heat-transfer rate
R = gas constant
Re = Reynolds Number
T = fluid temperature
u = axial component of velocity
U = velocity of moving plate
γ = ratio of specific heats
μ = viscosity of the fluid
ξ = dimensionless velocity, u/U
ρ = density of the fluid
τ = shear stress
ω = exponent for viscosity power law

Subscripts

w = conditions along stationary plate
∞ = conditions along moving plate
r = recovery conditions

It has been shown[1] that, for compressible Couette flow, the consideration of viscosity and heat-transfer effects results in the following equations for the temperature and velocity distributions within the fluid, respectively:

$$C_p(T - T_w) + (Pru^2/2) = -(q_w/\tau_w)Pru \tag{1}$$

$$(\tau_w h/\mu_\infty U) = \int_0^1 [1 + (Prq_w/\tau_w U)(\gamma - 1)M_\infty^2(1 - \xi) + (Pr/2)(\gamma - 1)M_\infty^2(1 - \xi^2)]^\omega d\xi \tag{2}$$

where the variable $\xi = u/U$ has been introduced. ω arises from the assumption that $\mu \sim T^\omega$.

Eq. (2) has been solved for the simple case of $\omega = 1$ and $q_w = 0$ in reference 1, and the solution is given as

$$(\tau_w h/\mu_\infty U) = 1 + (Pr/3)(\gamma - 1)M_\infty^2 \tag{3}$$

The skin-friction coefficient, $C_f = \tau_w/(\rho_\infty/2)U^2$, was shown to be

$$(C_f Re/2) = 1 + (Pr/3)(\gamma - 1)M_\infty^2 \tag{4}$$

where $Re = Uh\rho_\infty/\mu_\infty$.

We want to point out that a more general expression for the skin-friction coefficient can be obtained when the heat-transfer rate, q_w, is not assumed as zero. The assumption that $\omega = 1$ will again be made.

For arbitrary heat transfer, Eq. (2) is integrated easily, to give

$$(\tau_w h/\mu_\infty U) = 1 + (Prq_w/2U\tau_w)(\gamma - 1)M_\infty^2 + (Pr/3)(\gamma - 1)M_\infty^2 \tag{5}$$

Now putting the upper-wall conditions into Eq. (1) gives

$$C_p(T_w - T_\infty) = Pr(q_w/\tau_w)U + (PrU^2/2) \tag{6}$$

or

$$Pr(q_w/\tau_w U) = [C_p(T_w - T_\infty) - (PrU^2/2)]/U^2 \tag{7}$$

With Eq. (7), Eq. (5) becomes

$$(\tau_w h/\mu_\infty U) = 1 + (T_w - T_\infty)/(2T_\infty) + (Pr/12)(\gamma - 1)M_\infty^2 \tag{8}$$

where the definition $M_\infty^2 = U^2/(\gamma R T_\infty)$ has been employed.

The skin-friction coefficient becomes

$$(C_f Re/2) = 1 + (T_w - T_\infty)/2T_\infty + (Pr/12)(\gamma - 1)M_\infty^2 \tag{9}$$

Eq. (9) permits determination of C_f for all ratios of (T_w/T_∞). In particular, if the lower wall is insulated ($q_w = 0$), so that it attains recovery temperature T_r, given by

$$(T_r/T_\infty) = 1 + (Pr/2)(\gamma - 1)M_\infty^2 \tag{10}$$

then Eq. (9) reduces to Eq. (4) upon the use of Eq. (10).

Eq. (9) points out the strong dependence of the skin-friction coefficient on the heat-transfer rate as well as the Mach Number.

Reference

[1] Liepmann, H. W., and Roshko, A., *Elements of Gasdynamics*, p. 305; J. Wiley and Sons, London, 1957.

The Stagnation-Point Boundary Layer on a Rotating Hypersonic Body*

Sinclaire M. Scala and Joseph B. Workman
Missile and Space Vehicle Department, General Electric Company, Philadelphia, Pa.
October 2, 1958

Symbols

B_i	$= X_i/\bar{m}$
f	= similarity stream function
f_η	$= u/u_e$
h_i	= enthalpy of species i, including chemical
i	$= \rho\mu/\rho_w\mu_w$
L_{ij}	= Lewis Number
L_i^T	= thermal Lewis Number
m_i	= molecular weight of ith species
$\bar{m}$	$= \sum_i X_i m_i$ mean molecular weight
$\dot{M}_i$	= chemical-source term, moles per unit volume, per unit time
n	= r.p.m.
T	= temperature
Pr	= Prandtl Number
x, y, ϕ	= body-oriented coordinate system
u, v, w	= velocity components
V_∞	= flight speed
r	= radius from axis to surface of body
R_B	= nose radius
ω	= angular velocity of body, radians per sec.
X_i	= mole fraction of ith species
μ	= viscosity
ρ	= density
η	= similarity variable
$\bar{w}$	$= (w/\omega r)$ dimensionless velocity

Subscripts

crit.	= critical
e	= outer edge of boundary layer
w	= wall
η	= denotes differentiation with respect to η

PREVIOUS NOTES have reported on catalytic effects[1] and surface combustion[2] at hypersonic speeds. To date, however, the effect of the rotation of a body about its axis has been neglected. The purpose of this note is to present some results of an investigation into the effect of spin on the hypersonic laminar boundary layer.

The equations pertinent to the study of the laminar boundary layer on an axially-symmetric rotating body traveling at hypersonic speed include the conservation of mass, momentum, energy, and chemical species. For steady flow, these may be written:

Continuity

$$(\partial/\partial x)(\rho r u) + (\partial/\partial y)(\rho r v) = 0 \tag{1}$$

Momentum x

$$\rho[u(\partial u/\partial x) + v(\partial u/\partial y)] = -[(dp/dx) - \rho(w^2/r)(dr/dx)] + (\partial/\partial y)[\mu(\partial u/\partial y)] \tag{2}$$

Momentum ϕ

$$\rho\left(u\{[\partial(rw)]/\partial x\} + v\{[\partial(rw)/\partial y]\}\right) = (\partial/\partial y)\left(\mu\{[\partial(ru)]/\partial y\}\right) \tag{3}$$

Energy

$$\rho[u(\partial h/\partial x) + v(\partial h/\partial y)] = u(dp/dx) + \mu[(\partial u/\partial y)^2 + (\partial w/\partial y)^2] + (\partial/\partial y)[K(\partial T/\partial y)] - (\partial/\partial y)\{\sum_i h_i(\mu m_i/Pr)[\sum_{j\neq i}(m_j/\bar{m}^2)L_{ij}(\partial X_j/\partial y) - (L_i^T/m_i T)(\partial T/\partial y)]\} \tag{4}$$

Chemical Species i

$$\rho[u(\partial B_i/\partial x) + v(\partial B_i/\partial y)] + (\partial/\partial y)\{(\mu/Pr)[\sum_{j\neq i}(m_j/\bar{m}^2)L_{ij}(\partial X_j/\partial y) - (L_i^T/m_i T)(\partial T/\partial y)]\} = \dot{M}_i \tag{5}$$

and represent a generalization of those given, for example, by Chu and Tifford.[3]

One observes that the effects of body rotation do not appear explicitly in either the global continuity equation or in the conservation of species. Further, at a stagnation point the viscous-dissipation term $\mu[(\partial u/\partial y)^2 + (\partial w/\partial y)^2]$ vanishes. Thus, upon introducing a similarity transformation and restricting the discussion to the stagnation point, the effects of body rotation appear only in the momentum equations:

$$(lf_{\eta\eta})_\eta + ff_{\eta\eta} + 1/2\{(\rho_e/\rho) - (f_\eta)^2 + [(\omega^2\bar{w}^2)/(du_e/dx)^2]\} = 0 \tag{6}$$

$$(l\bar{w}_\eta)_\eta + f\bar{w}_\eta - f_\eta\bar{w} = 0 \tag{7}$$

for the x and ϕ directions, respectively.

In order to obtain an indication of the combination of physical and thermodynamic conditions under which the effects of body rotation can be neglected, one may take as an approximate criterion, the condition

$$|(1/2)(\omega_{\text{crit.}})^2\bar{w}^2/(du_e/dx)^2| \leqq 0.01 \tag{8}$$

It is not difficult to show that a first-order relation between nose radius R_B, flight speed V_∞, and stagnation-point velocity gradient du_e/dx, is given approximately by

$$|(R_B\, du_e/dx)^{1/2}| \simeq |5V_\infty \times 10^{-3}| \tag{9}$$

to within plus or minus 25 per cent, at flight speeds above Mach 10, regardless of altitude where all quantities in Eq. (9) are in ft. per sec. units.

Thus, since $\bar{w} \leqq 1.0$, Eq. (8) becomes

$$n_{\text{crit.}} \leqq 3.4 \times 10^{-5}(V_\infty^2/R_B)\ \text{(r.p.m. sec.}^2\text{/ft.)} \tag{10}$$

It can be immediately concluded that the effect of spin may be completely neglected in the analysis of hypersonic stagnation-point heat transfer for small vehicles, since, for example, a body having a 1-ft. nose radius when traveling at 25,000 ft. per sec., must rotate at speeds above 14,000 r.p.m. before the structure of the boundary layer is affected.

References

[1] Scala, S. M., *Hypersonic Heat Transfer to Catalytic Surfaces*, Journal of the Aeronautical Sciences, Readers' Forum, Vol. 25, No. 4, pp. 273–274, April, 1958.

[2] Scala, S. M., *Surface Combustion in Dissociated Air*, Jet Propulsion, Vol. 28, No. 5, pp. 340–341, May, 1958.

[3] Chu, S. T., and Tifford, A. N., *The Compressible Laminar Boundary Layer on a Rotating Body of Revolution*, Journal of the Aeronautical Sciences, Readers' Forum, Vol. 21, No. 5, pp. 345–346, May, 1954.

* This analysis is based upon work performed under the auspices of the U. S. Air Force, B.M.D. Contract No. AF 04(645)-24.

On Similitude in Rarefied-Gas Aerothermodynamics

F. Marcel Devienne
Director, Mediterranean Laboratory of Thermodynamic Research, Nice, France
October 8, 1958

IN RAREFIED-GAS AEROTHERMODYNAMICS, similitude is indicated by several numbers without dimensions, one of which is the Knudsen Number, K, equal to the ratio of the mean free path of the gas molecules to a characteristic dimension of the body.

When we operate in the free-molecular regime—i.e., for K values which are theoretically superior to 10*— the accommodation coefficient intervenes in the formulas. Thus, the energy received by the unit of surface of a flat plate moving perpendicularly to its plane is given by the formula:

* The researches carried out by Stalder and his collaborators and by ourselves have shown that the free-molecular flow regime takes place for Knudsen Number values inferior to 10. In the case of a cylinder, Stalder finds a Knudsen Number equal to 2; for the flat plate we have found a Knudsen Number equal to 3.[1, 2]

$$W = (a\rho v_s^3/2)[(s/2)\Phi(s) + (s^2e^{-s^2}/\sqrt{\pi}) + s^3\Phi(s)]$$

where a is the accommodation coefficient of the molecules in relation to the surface of the plate, ρ—the specific mass of gas at the pressure considered, v_s—the most probable speed of the molecules, and s—the ratio of the speed of displacement U to v_s.$\Phi(s)$—represents the error function with upper limit s.[2-4]

The accommodation coefficient depends on numerous factors and, in particular, on the pressure. The influence of the pressure moreover, is, very complex; in particular, in the case of pressures less than a few microns of mercury it depends on the outgassing, which, in turn, depends on the various physical factors to which the surface is submitted and, in particular, on the pressure. We have also brought into evidence the influence of the displacement speed of the body in a rarefied gas.[2]

It is therefore impossible to apply the results obtained in the free-molecular regime at different pressures in an absolutely certain manner. Thus, if we operate on a wire having a very small diameter under a pressure of the order of 50 microns, it is impossible to apply these results in the case of a cylinder having a diameter 500 times larger in the case where the pressure is only 1/10 of a micron. The accommodation coefficient of gas molecules can vary between these two pressures in considerable proportions—for example, 10 to 1.

This shows the indispensable precaution which should be taken with a view to generalizing the results of rarefied-gas aerothermodynamics.

References

[1] Stalder, J. R., Goodwin, G., and Creager, M. O., *Heat transfer to bodies in a high-speed rarefied gas stream*, NACA Techn. Note 2438, 1951.

[2] Devienne, F. M., *Study of Stagnation Temperature and Pressure in a Free-Molecular Flow Regime by Means of the Revolving Arm*, Technical Report AF 61(514)930, March, 1957.

[3] Devienne, F. M., *Experimental Study of the Stagnation Temperature in a Free-Molecular Flow*, Journal of the Aeronautical Sciences, Vol. 24, No. 6, pp. 403–406, 412 June, 1957.

[4] Devienne, F. M., *Frottement et Echanges Thermiques dans les Gaz Raréfiés* Gauthiers-Villars, Paris, 1958.

Shock-Tube Testing Time

G. F. Anderson
Brown University, Providence, R.I.

October 10, 1958

THE FLOW of a real gas initiated by a strong shock in a constant-diameter shock tube is complicated by the marked attenuation of the shock wave.

In a theoretical investigation of attenuation effects—it was hoped that the investigation would provide some information on the state of the gas at various locations in the test slug—the conservation of mass equation led to an explanation of the difference between the ideal theoretical test time and the experimentally obtained test time.

The result of this approach shows that for a given diameter shock tube, there is a length of tube at which the testing time reaches a maximum, and beyond this length the testing time decreases. The difference between the actual test time and the theoretical test time is explained by the loss of test gas to the boundary layer behind the interface rather than to mixing of the driver gas and test gas at the interface. This concept is important when one uses the procedure of reference 1 to determine the state of the gas at various points in the test slug.

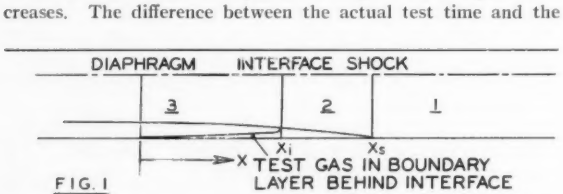

FIG. 1

x_i POSITION OF INTERFACE
x_s POSITION OF SHOCK WAVE
$\frac{dx_s}{dt}$ SHOCK WAVE VELOCITY—u_s
$\frac{dx_i}{dt}$ TEST GAS VELOCITY—u_2
1 UNDISTURBED GAS
2 TEST GAS
3 DRIVE GAS

The time rate of change of the mass of gas contained in the test slug, Fig. 1, is given by

$$(d/dt)m_2 = \pi r^2\rho_2(u_s - u_2) - \int_0^{\delta_i} 2\pi\rho(r - y)(u_2 - u)dy$$

If it is assumed that the average density $\bar{\rho}_2$ in the test slug does not vary strongly with time, it may be stated that the test time will reach a maximum when

$$\int_0^{\delta_i} 2\pi\rho(r - y)(u_2 - u)dy = \pi r^2\rho_2(u_s - u_2) = \pi r^2\rho_1 U_s$$

which reduces to

$$\rho_1 u_s/\rho_2 u_2 = (2/r)(\delta_i^* - \delta_i^\rho) \quad \text{for } r \gg \delta_i$$

where

$$\delta_i^* = \int_0^{\delta_i} [1 - (\rho u/\rho_2 u_2)]dy$$

$$\delta_i^\rho = \int_0^{\delta_i} [1 - (\rho/\rho_2)]dy$$

For strong shocks,

$$\rho_1 u_s/\rho_2 u_2 \doteq 1/(M_s - 1)$$

And, therefore, the criterion for τ_{max} is given by

$$r/2(\delta_i^* - \delta_i^\rho) \doteq M_s - 1$$

Assuming a turbulent boundary layer, let

$$\zeta = y/\delta$$
$$u/u_2 = (\zeta)^{1/7}$$
$$\rho_2/\rho = (T_w/T_2)(1 + a\zeta^{1/7} - b\zeta^{2/7})$$

Then

$$(\delta_i^* - \delta_i^\rho)/\delta_i = 7(T_2/T_w)(I_6 - I_7)$$

where

$$I_n = \int_0^1 \frac{z^n dz}{1 + az - bz^2}$$

$$a = (T_r/T_w) - 1 \doteq [(T_2/T_w) - 1]_{M_s} \gg 1$$
$$b = [(T_r/T_2) - 1](T_2/T_w) \doteq (0)_{M_s} \gg 1$$

Therefore, the criterion for τ_{max} becomes

$$(r/\delta_i)/[14(T_2/T_w)(I_6 - I_7)] \doteq M_s - 1$$

For δ_i not small compared to r, the above relationship becomes

$$(r/\delta_i)/\{14(T_2/T_w)[(I_6 - I_7) - (\delta_i/r)(I_{13} - I_{14})]\} \doteq M_s - 1$$

The test time at any tube station may be calculated if the assumption is made that M_s = constant. This is not a realistic assumption but will show the order of magnitude of the boundary-layer effect on testing time.

$$\tau \doteq m_2/\pi r^2\bar{\rho}_2\bar{u}_2$$

$$\tau_{corr}/\tau_{theo} \doteq 1 - [(M_s - 1)/x_s] \times \int_0^{x_s} 7(T_2/T_w)(I_6 - I_7)(2\delta_i/r)dx_s, \quad \delta_i \gg r$$

or for δ_i not small compared to r,

$$\tau_{corr}/\tau_{theo} \doteq 1 - [(M_s - 1)/x_s] \times \int_0^{x_s} 14(T_2/T_w)[(I_6 - I_7) - (\delta_i/r)(I_{13} - I_{14})](\delta_i/r)dx_s$$

which may be reduced to

$$\tau_{corr}/\tau_{theo} \doteq 1 - (K_1 x_s^{4/5} - K_2 x_s^{8/5})$$

where K_1 and K_2 are functions of the shock Mach Number, the tube radius, and the initial tube pressure (P_1) before the shock.

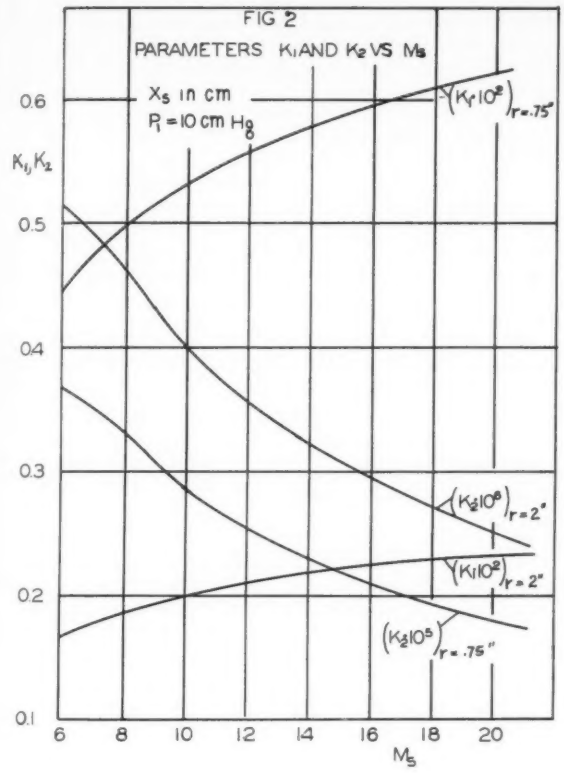

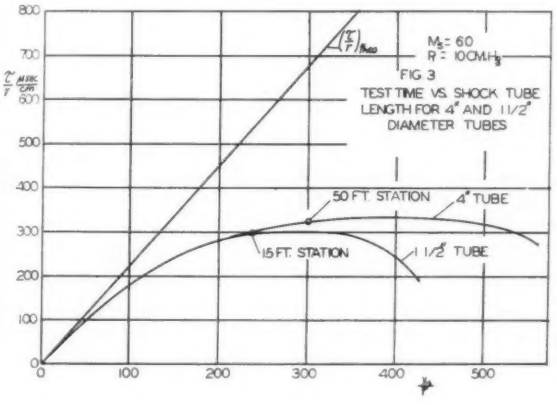

These parameters are plotted in Fig. 2 for two tube sizes and $P_1 = 10$ cm. Hg.

An example has been calculated for $M_s = 6.0$ and $P_1 = 10$ cm. for the two tube sizes and the results are plotted in Fig. 3. The 50 ft. station, measured from the diaphragm, is indicated on the result for the 4-in. tube. It is seen that little increase in test time can be expected beyond this station. This agrees well with experiments with a 4-in. tube. Furthermore, the corrected test time is approximately one half of the ideal theoretical test time which agrees with the experiment. The same holds true for the 15-ft. station in a $1^1/_2$ in. diameter shock tube.

References

[1] Rose, P. H., and Nelson, W., *On the Effect of Attenuation On Gas Dynamic Measurements Made In Shock Tubes*, AVCO Research Report 24, April, 1958.

[2] Mirels, H., *Boundary Layer Behind Shock Or Thin Expansion Wave Moving Into Stationary Fluid*, NACA TN 3712, May, 1956.

[3] Feldman, S., *Hypersonic Gas Dynamic Charts for Equilibrium Air*, AVCO Research Laboratory, January, 1957.

Correlation of Base Pressure and Wake Structure of Sharp- and Blunt-Nose Cones With Reynolds Number Based on Boundary-Layer Momentum Thickness

R. Lehnert and V. L. Schermerhorn
Naval Ordnance Laboratory, White Oak, Silver Spring, Md.
October 10, 1958

It has been established in the past that there is a certain relationship between base pressure and boundary-layer behavior.[1-3] The base-pressure and wake-flow conditions were found to be dependent upon the local flow characteristics at the surface of supersonic vehicles directly upstream of the base or of the region of wake-flow separation.

In order to use existing data on cones and other shapes to predict wake angle and base pressure on blunt bodies, an attempt was made recently at the Naval Ordnance Laboratory to establish a unique relationship between given local flow conditions at the downstream end of sharp and blunt cones at supersonic speeds and the corresponding wake-flow conditions with zero heat transfer. The models chosen for this investigation were a 10° semivertex angle, sharp-nose cone and a 10° semivertex angle, spherical-nose cone with a 0.5 bluntness ratio. The bluntness ratio is defined as the ratio of the nose radius to the base radius. Both cones had a base diameter of 6 in. They were sting mounted (1.5-in. sting diameter) in the test section of the Naval Ordnance Laboratory's 40 × 40 cm. Aeroballistics Tunnel No. 2. The sharp cone with surface finishes of 15 and 125 microinches (both designated as "smooth") was tested at Mach Numbers of 2.74 and 2.76, respectively, while the blunt cone was investigated at a Mach Number of 4.74 with different surface conditions—i.e., "smooth" (125 microinch finish) and "rough." The rough surface was achieved by application of evenly distributed carborundum powder (No. 24 grain) over the entire wetted surface area.

Surface pressure-distribution and base-pressure measurements were carried out and total pressure-wake surveys and boundary-layer profiles near the base were taken at zero angle of attack. The variation of the boundary-layer profiles immediately upstream of the cone bases was accomplished by varying the following parameters: pressure gradient (sharp cone, blunt cone). surface conditions (smooth, rough), and Reynolds Number (wind-tunnel supply pressure and temperature). The local Mach Number on the surface at the downstream end of the cones was the same for both models due to the proper choice of the ambient Mach Number.

Simultaneously with the experimental investigation, a calculation of the boundary-layer development along the cone surfaces was performed by a stepwise solution of the boundary-layer momentum equation, using the procedures from references.[4-8] Prevailing pressure gradients and surface roughness, as well as the systematic variation of supply conditions, were taken into

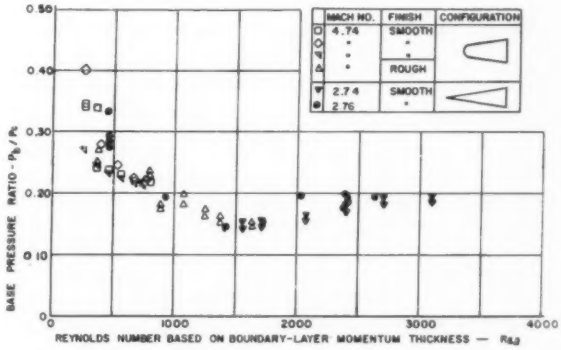

Fig. 1. Base pressure ratio of blunt- and sharp-nose 10° semivertex angle cones as a function of $R_{e\theta}$.

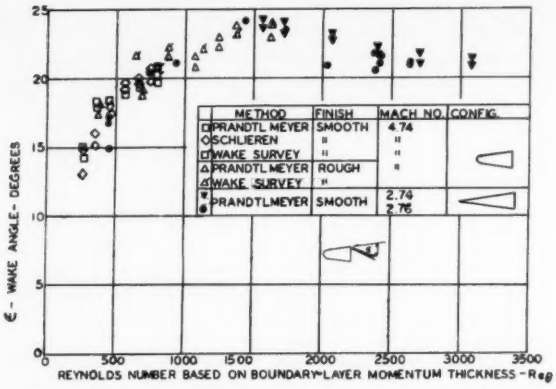

FIG. 2. Wake angle of blunt- and sharp-nose 10° semivertex angle cones as a function of Re_θ.

account for each individual case tested in the wind tunnel. The calculated Reynolds Numbers based on boundary-layer momentum thickness at the end of the cones were in good agreement with the ones obtained by evaluation of the momentum thickness from boundary-layer surveys.

The measured base pressures are presented as $p_b/p_c = f(\mathrm{R}e_\theta)$ in Fig. 1 where p_b = base pressure, p_c = static pressure on the surface at the downstream end of the cone, and $\mathrm{R}e_\theta$ = Reynolds number based on boundary-layer momentum thickness near the end of the cone. Fig. 2 shows the corresponding wake angles as a function of $\mathrm{R}e_\theta$ obtained from wake surveys, schlieren photograph evaluations, and Prandtl-Meyer expansion computations.

From these results, and in view of the model geometry and the parameters considered, it can be concluded that the base pressure ratio p_b/p_c and the corresponding wake angle are unique functions of $\mathrm{R}e_\theta$, independent of the history of the boundary-layer whenever the local Mach Number on the cone surface near the base is the same. A more detailed description of this investigation is given in reference 9.

REFERENCES

[1] Chapman, Dean R., *An Analysis of Base Pressure at Supersonic Velocities and Comparison with Experiment*, NACA TN 2137, 1950.

[2] Kurzweg, H. H. *Interrelationship Between Boundary Layer and Base Pressure*, Journal of the Aeronautical Sciences, Vol. 18, No. 11, pp. 743–748, November, 1951.

[3] Crocco, L., and Lees, L., *A Mixing Theory for the Interaction Between Dissipative Flows and Nearly Isentropic Streams*, Journal of the Aeronautical Sciences, Vol. 19, No. 10, pp. 649–676, October, 1952.

[4] Cohen, C. B., and Reshotko, E., *The Compressible Laminar Boundary Layer with Heat Transfer and Arbitrary Pressure Gradient*, NACA TN 3326, 1955.

[5] Persh, J., *A Procedure for Calculating the Boundary Layer Development in the Region of Transition from Laminar to Turbulent Flow*, NAVORD Report 4438, 1957.

[6] Schlichting, H., *Boundary Layer Theory*, 1955.

[7] Persh, J., *A Theoretical Investigation of Turbulent Boundary-Layer Flow with Heat Transfer at Supersonic and Hypersonic Speeds*, NAVORD Report 3854, 1955.

[8] Persh, J., and Lee, R., *Tabulation of Compressible Turbulent Boundary-Layer Parameters*, NAVORD Report 4282, 1956.

[9] Lehnert, R., and Schermerhorn, V. L., *Wake Investigation on Sharp and Blunt Nose Cones at Supersonic Speeds*, NAVORD Report 5668, 1958.

The Role of Unit Reynolds Number in Boundary-Layer Transition

Jack D. Whitfield and J. Leith Potter
Gas Dynamics Facility, ARO, Inc., Tullahoma, Tenn.

October 13, 1958

EXPERIMENTS HAVE DEMONSTRATED that variation of the free-stream unit Reynolds Number, U/ν, often produces changes in the usual forms of Reynolds Number used to describe the mean location of boundary-layer transition. Recognition of the possible influence of the unit Reynolds Number is important in the examination of data which are sensitive to the location of transition. There is doubt as to the status of the U/ν effect—i.e., whether it is associated with boundary-layer stability or entirely related to such factors as surface roughness or leading-edge bluntness. This note shows how a possible basis of the unit Reynolds Number effect is revealed by examination of the stability of laminar boundary layers. Subsonic flow is assumed, since it is desired to compare the results with experimental data; and data from supersonic flow experiments may include leading-edge shock-wave phenomena which confuse the search for pure U/ν effects.[1]

A measure of instability, which, we assume, is a measure of closeness to transition, may be formed by the ratio of virtual shear stress to laminar shear stress, τ^*. Thus, for a semi-infinite flat plate at zero angle of attack in a uniform subsonic stream, we define

$$\tau^* = \tau_t/\tau_1 = \rho\overline{u_i v_i}/\mu(du/dy)$$

or, from Liepmann (reference 2),

$$\tau^* = -(2/C_{fl})Kb(u'/U)_0{}^2A^2 \qquad (1)$$

where C_{fl} = laminar friction coefficient, K = correlation coefficient = $\overline{u_i v_i}/u'v'$, $b = v'/u'$, $(u'/U)_0{}^2$ = energy of frequency most amplified, and A = amplification ratio. Now, if the boundary layer is equally stable or unstable at two different conditions, (1) and (2), we may write

$$\tau_1{}^*/\tau_2{}^* = 1 \qquad (2)$$

Following Tetervin[3] and using an expression for amplification ratio given by Schlichting,[4] it can be shown[5] that Eqs. (1) and (2) result in the equation

$$[(Re_\delta{}^*)_1/(Re_\delta{}^*)_2]^2 - 1 + \left(\{\ln[(u'/U)_{0,1}/(u'/U)_{0,2}]\}/[S(Re_\delta{}^*)_2{}^2]\right) + \{\ln[(Re_\delta{}^*)_1/(Re_\delta{}^*)_2]/2S(Re_\delta{}^*)_2{}^2\} = 0 \qquad (3)$$

where $Re_\delta{}^*$ is the boundary-layer Reynolds Number based on displacement thickness and S is an amplification parameter. Eq. (3) expresses a relation between initial energy levels at the beginning of amplification of the frequency of maximum amplification and the boundary-layer Reynolds Number. One solution to Eq. (3) is obvious when $(u'/U)_{0,1} = (u'/U)_{0,2}$ then $(Re_\delta{}^*)_1 = (Re_\delta{}^*)_2$. A more general case exists when the initial energy levels are not equal, say $(u'/U)_{0,1} > (u'/U)_{0,2}$. Then it follows from Eq. (3) that

$$(Re_\delta{}^*)_1{}^2/(Re_\delta{}^*)_2{}^2 + [1/2\ S(Re_\delta{}^*)_2{}^2]\ \ln\ [(Re_\delta{}^*)_1/Re_\delta{}^*)_2] < 1 \qquad (4)$$

A necessary condition for Eq. (4) is

$$(Re_\delta{}^*)_1 < (Re_\delta{}^*)_2$$

and it follows, for the conditions initially specified, that the relationship between the transition Reynolds Numbers, based on wetted length to transition, is

$$(Re_t)_1 < (Re_t)_2 \qquad (5)$$

There is experimental evidence that the critical frequency increases with U/ν and that u'/U commonly decreases with frequency in the usual range of frequencies where maximum amplification occurs.[6, 7] Therefore, we conclude that it is possible and even most likely that $(u'/U)_{0,1} > (u'/U)_{0,2}$ when $(U/\nu)_1 < (U/\nu)_2$. Thus, if the previously undefined conditions (1) and (2) refer to $(U/\nu)_1$ and $(U/\nu)_2$, Eq. (5) results. However, it must be kept in mind that there are other factors influencing boundary-layer transition, and any one of these may dominate the process. For example, with increasing values of U/ν boundary-layer thickness becomes small and roughness is more important. If roughness dominates, then $(Re_t)_1 > (Re_t)_2$ when $(U/\nu)_1 < (U/\nu)_2$.

The effect of U/ν appears to depend on the initial energy level of the critical frequencies of oscillation which will receive maximum amplification. It seems academic whether we regard

U/ν as a fundamental factor or one only indirectly effective through its connection with frequency and energy levels of disturbances in laminar boundary layers. The significant point is the apparent probability that Re_t generally will not remain constant with varying U/ν even when the influences of all other factors are invariant.

The authors have received a report[8] including systematic, subsonic data showing variations of Re_t with U/ν in support of the writers' earlier work[5] which is the basis of this note.

References

[1] Bertram, Mitchell H., *Exploratory Investigation of Boundary Layer Transition on a Hollow Cylinder at a Mach Number of 6.9*, NACA Rep. 1313, 1957.

[2] Liepmann, H. W., *Investigation of Boundary Layer Transition on Concave Walls*, NACA-WR-W-87 (formerly NACA-ACR-4J28), 1945.

[3] Tetervin, Neal, *A Discussion of Cone and Flat Plate Reynolds Numbers for Equal Ratios of the Laminar Shear to the Shear Caused by Small Velocity Fluctuations in a Laminar Boundary Layer*, NACA-TN-4078, August, 1957.

[4] Schlichting, H., *On the Production of Turbulence in Flow Along a Plate*, translation No. 6, Council for Science and Industrial Research, Division of Aeronautics, Commonwealth of Australia, July, 1944.

[5] Whitfield, Jack D., and Potter, J. Leith, *The Unit Reynolds Number as a Parameter in Boundary Layer Stability*, AEDC-TN-58-77, September, 1958.

[6] Bennett, H. W., *An Experimental Study of Boundary Layer Transition*, Kimberly-Clark Corp., Neenak, Wis., September, 1953.

[7] Laufer, John, *Experimental Observation of Laminar Boundary-Layer Oscillations in Supersonic Flow*, Journal of the Aeronautical Sciences, Readers' Forum, Vol. 23, No. 2, p. 184–185, February, 1956.

[8] Smith, A. M. O., and Clutter, D. W., *The Smallest Height of Roughness Capable of Affecting Boundary Layer Transition in Low Speed Flow*, Douglas Aircraft Co. Inc., ES-26803, El Segundo, Calif., August 31, 1957.

The Heating of Slabs With Arbitrary Heat Inputs

Theodore R. Goodman

Senior Aerodynamics Engineer, Allied Research Associates, Inc., Boston, Mass.

October 14, 1958

THE THERMAL HEAT FLUX at the surface of airplane and missile structures may become very large at high speeds, necessitating the inclusion of thermal stresses in the structural analysis. The surface temperatures may, in fact, reach such high values that it is necessary to account for surface radiation. Furthermore, even if only aerodynamic heating is accounted for, by assuming the heat flux to be proportional to the difference between the wall temperature and an ambient temperature, nevertheless, the heat-transfer coefficient and ambient temperature will both, as a rule, be time dependent. The transient temperature distribution in the skin or near the surface can be determined by solving the linear heat conduction equation. However, if surface radiation is important, the boundary conditions are nonlinear, and if the heat-transfer coefficient and ambient temperature are time dependent, no general solution is known. The entire problem becomes even more cumbersome if the thermal properties of the skin, namely heat capacity, and thermal conductivity (and even density) must be considered temperature dependent, for then the differential equation itself becomes nonlinear.

The standard method for solving the practical problems of heat conduction for which no analytical solution is possible is to integrate the heat conduction equation numerically, using a finite difference procedure. Recently, however, the author developed an approximate analytical technique for solving unsteady heat conduction problems.[1] This technique, known as the "heat balance integral," reduces the problem to an ordinary differential equation which, for many cases of interest, can be solved in closed analytical form. In reference 1 the emphasis was placed on problems for which there was a change of phase. For aeronautical application, the heat balance integral method can be applied to heat-transfer problems in the skin when the heat flux at the surface is an arbitrary function of temperature and time. Thus, all the boundary conditions discussed in the first paragraph can be handled within the framework of a uniform theory. It will be assumed that the thermal properties are not temperature dependent, and that the solid slab is semi-infinite. Both of these restrictions can be removed, and some problems relaxing one or both of these restrictions have been set up and solved in reference 2. The present note is, in fact, a condensation of reference 2.

It is worthy of note that when the method of the heat balance integral is applied to problems whose exact solution is known, the error which is introduced by the essentially approximate nature of the method is, at the most, a few per cent.

The Heat Balance Integral Technique

The heat conduction equation for the temperature, u, with constant thermal properties is

$$\kappa(\partial^2 u/\partial x^2) = \partial u/\partial t \tag{1}$$

where κ is the diffusivity; x and t are the space coordinate and time, respectively.

Assume a semi-infinite slab extending over positive x. Initially the temperature is zero. The surface condition is

$$(\partial u/\partial x)(0, t) = -f[u(0, t), t] \tag{2}$$

The method of the heat balance integral consists in assuming a polynomial temperature profile between the surface, $x = 0$, and a thermal layer, $\delta(t)$, consistent with the boundary conditions. At $x = \delta$ the boundary conditions are:

$$u[\delta(t), t] = 0 \tag{3}$$

$$(\partial u/\partial x)[\delta(t), t] = 0 \tag{4}$$

By differentiating Eq. (3) with respect to time and applying Eqs. (1) and (4), the following conditions can be derived:

$$(\partial^2 u/\partial x^2)(\delta, t) = 0 \tag{5}$$

Eqs. (2)–(5) constitute four conditions which the temperature profile must satisfy. Assuming, therefore, a cubic profile, it must take the form,

$$u = (z/\delta^3)(\delta - x)^3 \tag{6}$$

where

$$\delta = 3z/[f(z, t)] \tag{7}$$

and z is surface temperature.

Eq. (7) expresses a relationship between the surface temperature and the thermal layer, δ. There is, therefore, still one unknown function of time in Eq. (6), and this will be obtained from the heat balance integral.

Integrating Eq. (1) from $x = 0$ to $x = \delta$ there is obtained

$$\kappa[(\partial u/\partial x)(\delta, t) - (\partial u/\partial x)(0, t)] = d\theta/dt \tag{8}$$

where

$$\theta = \int_0^\delta u dx \tag{9}$$

The left-hand side of Eq. (8) is immediately determined from Eqs. (2) and (4). The quantity, θ, may be obtained in terms of δ or z by substituting Eq. (6) into Eq. (9) and integrating. There is then finally obtained the following differential equation for z:

$$(4/3)\kappa f(z, t) = (d/dt)\{z^2/[f(z, t)]\} \tag{10}$$

The proper initial condition is $z = 0$ when $t = 0$. If the function, $f(z, t)$, is dependent on both z and t, this equation must be integrated numerically. Nevertheless, this constitutes a tremendous saving in effort when compared to the finite difference techniques which would ordinarily have to be performed on the original heat conduction equation. There are two cases for which Eq. (10) can be integrated directly, and these are when f depends solely on z, and when f depends solely on t.

Case (a)—If f is independent of t, the solution is readily obtained,

$$(4/3)\kappa t = \int_0^z \{z_1[2f(z_1) - z_1 f'(z_1)]dz_1/[f(z_1)]^2\} \tag{11}$$

Case (b)—If f is independent of z, the problem is linear and can be solved exactly by more conventional methods. Nevertheless, the simplicity of the solution given here warrants attention. The

result is

$$z = \left[(4/3)\kappa f(t) \int_0^t f(t_1)dt_1\right]^{1/2} \tag{12}$$

Applications

If f is constant Eq. (12) reduces to

$$z = \sqrt{4/3}\, f\sqrt{\kappa t} \tag{13}$$

The exact solution appears in Carslaw and Jaeger,[3] and the result is

$$z = \sqrt{4/\pi}\, f\sqrt{\kappa t} \tag{14}$$

The numerical factor $\sqrt{4/3} = 1.15$, whereas $\sqrt{4/\pi} = 1.13$. Hence, the two solutions agree to within 2 per cent.

As an example of Eq. (11), suppose $f(z) = h(V - z)$. The result is

$$(4/3)h^2\kappa t = (1/2)\{[1 - (z/V)]^{-2} - 1\} + \ln[1 - (z/V)] \tag{15}$$

The exact solution is given by Carslaw and Jaeger (reference 3, p. 53) and a plot of this solution is so given (p. 54). To the scale with which this graph is plotted, it is impossible to detect any error in Eq. (15).

Eq. (11) may be applied to a nonlinear problem. Suppose

$$f(z) = (H/k)(z + V_0)^4 \tag{16}$$

This represents a slab of absolute temperature V_0 radiating into a medium of absolute temperature zero. The result is

$$\kappa t(H^2/k^2)V_0^6 = (3/2\eta^8)[(1/6)\eta^2 - (3/7)\eta + (1/4)] + (1/56) \tag{17}$$

where $\eta = 1 + z/V_0$

This problem has been solved by Jaeger[4] by integrating the heat conduction equation numerically. On the graph which Jaeger presents it is impossible to detect any difference between his solution and Eq. (17).

References

[1] Goodman, T. R., *The Heat Balance Integral and Its Application to Problems Involving a Change of Phase*, ASME Trans. 80, No. 2, p. 335, February, 1958.

[2] Goodman, T. R., *The Heating of Slabs with Arbitrary Heat Inputs*, AFOSR-TN-58-524, May 28, 1958.

[3] Carslaw, H. S., and Jaeger, J. C., *Conduction of Heat in Solids*, Oxford University Press, London, England, First Ed., 1947.

[4] Jaeger, J. C., *Conduction of Heat in a Solid with a Power Law of Heat Transfer at Its Surface*, Cambridge Phil. Soc. Proc. 46, Part 4, p. 634, October, 1950.

The Effects of Constant-Pressure Sound Fields on Free-Convection Heat Transfer From a Horizontal Cylinder

Jack P. Holman and Tipton P. Mott-Smith

Fluid Dynamics Research Branch, WADC, Wright-Patterson Air Force Base, Ohio

October 15, 1958

The quantitative influence of strong sound fields on free-convective heat transfer was investigated by installing a 3/4 in. electrically heated cylinder in a reverberant chamber providing a constant sound-pressure field. The test results are shown in Fig. 1. Wall temperatures ranged from 208°F. to 270°F. Δh represents the increase in the free-convection heat-transfer coefficient over the value obtained without the presence of the sound field. An increase in the heat-transfer coefficient did not occur until the sound-pressure level was greater than approximately 135 db. An effect of frequency was observed at sound-pressure levels slightly greater than this value; however, at higher sound levels the effect of frequency was very small.

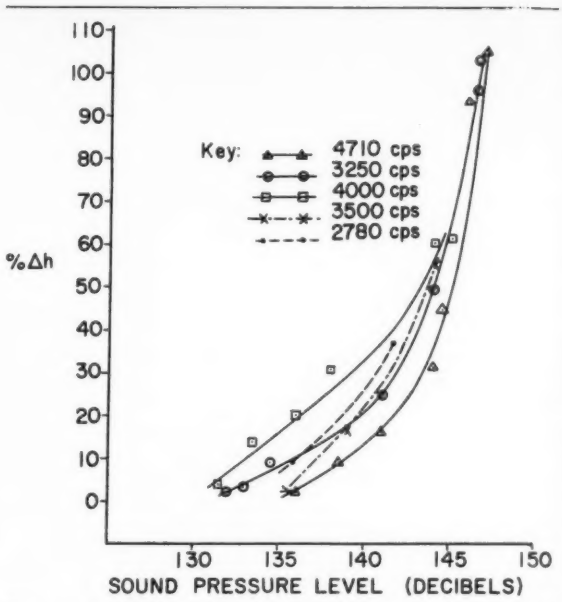

Fig. 1. Increase of heat-transfer coefficient with sound level

In an effort to explain the increase in the heat-transfer coefficient when the sound level is raised above a certain critical value, a survey of the literature on the effects of sound on the flow field about a cylinder was made. References 1–3 show that the presence of an external sound field may alter the flow field about the cylinder due to a phenomenon called acoustical streaming. The mathematical relationships that describe the detailed behavior of acoustical streaming are based on the following assumptions: a plane sound wave is propagated through the fluid, the wave length of the sound wave is large compared to the radius of the cylinder, and the amplitude of the sound wave is small compared to the diameter of the cylinder. The physical significance of the various acoustical-streaming parameters may be discussed in terms of the typical acoustical-streaming flow field shown in Fig. 2.

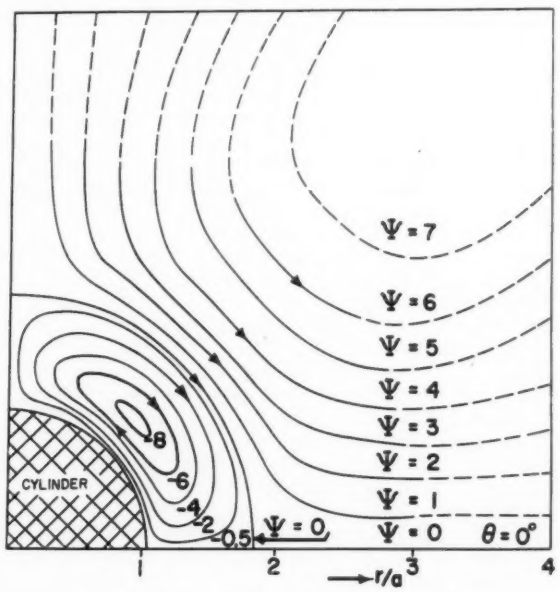

Fig. 2. Typical acoustical-streaming flow field.

Two types of acoustical streaming are usually observed: an inner vortex system and an outer vortex system, as shown in Fig. 2. The inner system is usually described in terms of its thickness corresponding to the distance from the surface of the cylinder to the streamline $\psi = 0$. This thickness is called the DC boundary-layer thickness, δ_{DC}. Raney, et al.,[2] have established the existence of a universal thickness profile defined by:

$$\delta_{DC}/a = f(a/\delta_{AC})$$

where δ_{AC} is called the AC boundary-layer thickness and is defined by:

$$\delta_{AC} = (\nu/\omega)^{1/2}$$

where ν is the kinematic viscosity of the fluid, ω is the frequency of the sound wave, and a is the radius of the cylinder. It can be shown that a/δ_{AC} is proportional to the ratio of the wave forces to the viscous forces. The essential features of the universal thickness profile are that δ_{DC} increases with an increase in ν and decreases with an increase in ω or a. The detailed acoustical-streaming profiles, as determined theoretically, are in excellent agreement with experiment as long as the amplitude of the sound wave is less than a certain critical value.[2] It has been shown[2] that if the amplitude is raised above the critical value, the thickness of the DC layer decreases very rapidly. The critical value increases with an increase in the radius of the cylinder.

The rate at which heat is transported from a cylindrical surface, due to free convection, in the presence of a sound field, is dependent on the superimposed free-convection and sound-field currents. In accordance with the above discussion, one would not expect any significant change in the heat-transfer rate with an increase in the sound intensity until a certain critical value of the amplitude of the sound field had been reached. With an increase in the sound level above the critical value, the thickness of the DC layer would be decreased with a corresponding increase in the acoustical-streaming velocity in the boundary layer. Hence, it would be expected that the heat-transfer rate would be increased. The effect of frequency on the DC layer thickness would be observed in the neighborhood of the critical sound-pressure level, but at higher sound levels the frequency effect would be very small in comparison to the amplitude effect so that the heat-transfer rate for sound levels much greater than the critical value would be relatively independent of frequency. In addition to the direct effects of the increased boundary-layer velocities, the acoustical streaming may serve as a trigger mechanism for transition to turbulent flow. Consequently, the increase in the heat-transfer rate may be dependent on the Grashof Number also and, therefore, on the surface temperature difference. This dependence will be investigated in future experiments since it may comprise an important part of the effects of sound fields on heat transfer.

The sound field in the reverberant chamber used in the above heat-transfer tests does not correspond to the plane field which has been treated theoretically in references 1–3 since it is a scalar field, as opposed to the vector field of a conventional sound wave. However, it is expected that the presence of large amplitude constant-pressure sound fields would have the same general effect on the flow field in the vicinity of the cylinder as in the case of a plane wave. Therefore, from a qualitative standpoint, the analysis of the effects of constant-pressure sound fields on the heat-transfer rate is essentially the same.

References

[1] Holtsmark, J., et al., *Boundary Layer Flow Near a Cylindrical Obstacle in an Oscillating Incompressible Fluid*, J. Acoustical Soc. of America, Vol. 26, No. 1, pp. 26–39, January, 1954.

[2] Raney, W. P., Corelli, J. C., and Westervelt, P. J., *Acoustical Streaming in the Vicinity of a Cylinder*, J. Acoustical Soc. of America, Vol. 26, No. 6, pp. 1006–1014, November, 1954.

[3] Skavlem, S., and Tjotta, S., *Steady Rotational Flow of an Incompressible, Viscous Fluid Enclosed Between Two Coaxial Cylinders*, J. Acoustical Soc. of America, Vol. 27, No. 1, pp. 26–33, January, 1955.

A New Solution to the Laminar Boundary-Layer Equations

H. A. Hassan
College of Engineering, Baghdad, Iraq

October 16, 1958

In a recent work, Görtler[1] has presented a new power series for solving plane and steady laminar boundary-layer equations for a certain class of outer pressure distributions. The object of this note is to present a solution of the same equations for a class of outer pressure distributions which has not been covered by Görtler. This is accomplished by using the transformation

$$\xi = \exp\left[-(1/\nu)\int U_\infty(x)\,dx\right], \qquad \eta = y\,U_\infty(x)/\nu$$
$$\varphi(\xi, \eta) = \psi(x, y)/\nu \tag{1}$$

and assuming a power-series solution [$U_\infty(x)$ is the given outer velocity distribution]. The new power-series solution has all the desirable qualities of Görtler's series and, in addition, its zeroth-order term, which is governed by a nonlinear total differential equation, can be given in closed form.

The differential equation for steady two-dimensional laminar boundary layer can be written as

$$\psi_{,y}\,\psi_{,xy} - \psi_{,x}\,\psi_{,yy} = U_\infty(x)\,U_\infty'(x) + \nu\,\psi_{,yyy} \tag{2}$$

with the comma denoting partial differentiation and the prime denoting total differentiation.

The boundary conditions can be written as

$$\psi(x, y) = \psi_{,y}(x, y) = \psi_{,x}(x, y) = 0 \text{ for } y = 0$$
$$\psi_{,y}(x, y) \to U_\infty(x) \text{ for } y \to \infty \tag{3}$$

Carrying out the indicated transformation in Eq. (1) and substituting in Eq. (2), one obtains

$$\varphi_{,\eta\eta\eta} + \beta(\xi)\,(1 - \varphi_{,\eta}{}^2) + \xi[\varphi_{,\eta}\varphi_{,\xi\eta} - \varphi_{,\xi}\,\varphi_{,\eta\eta}] = 0 \tag{4}$$

with

$$\beta(\xi) = -\xi\,d[\ln(U_\infty(\xi)/U_0)]/d\xi \tag{5}$$

where U_0 has the dimensions of velocity and can be chosen as the unit velocity or any other representative velocity.

The solution of Eq. (4) will be assumed as

$$\varphi(\xi, \eta) = \sum_0^\infty \varphi_n(\eta)\,\xi^n \tag{6}$$

in the region of convergence of

$$\beta(\xi) = \sum_0^\infty \beta_n\,\xi^n, \qquad \beta_0 > 0 \tag{7}$$

Substituting Eqs. (6) and (7) into Eq. (4), the following equations for the coefficients φ_n will be obtained:

$$\varphi_0''' + \beta_0(1 - \varphi_0'^2) = 0 \tag{8}$$

and

$$\varphi_n''' + (n - 2\beta_0)\varphi_0'\varphi_n' - n\,\varphi_0''\,\varphi_n = R_{n-1}, \qquad n \geq 1 \tag{9}$$

with

$$R_{n-1} = \beta_n(\varphi_0'^2 - 1) + \sum_{k=1}^{n-1}(\beta_{n-k})\varphi_k'\,\varphi_{n-k}' +$$
$$\varphi_0' \sum_{k=1}^{n-1}\beta_k\,\varphi_{n-k}' + \sum_{m=1}^{n-1}\sum_{k=1}^{n-m}\beta_n\,\varphi_k'\,\varphi_{n-k-m}' +$$
$$\sum_{k=1}^{n-1} k\,\varphi_k\,\varphi_{n-k}'' \tag{10}$$

The boundary conditions for the functions φ_n are

$$\varphi_0(0) = \varphi_0'(0) = 0, \qquad \varphi_0'(\infty) = 1;$$
$$\varphi_n(0) = \varphi_n'(0) = \varphi_n'(\infty) = 0, \qquad n \geq 1 \tag{11}$$

Eqs. (8) and (11) give

$$\varphi_0' = 3\tanh^2\left\{\left(\sqrt{\beta_0/2}\right)\eta + \tanh^{-1}\sqrt{2/3}\right\} - 2 \tag{12}$$

The functions φ_n ($n \geq 1$) satisfy the linear equations (9) and can be expressed as linear combinations of universal functions which can be tabulated once and for all for a given value of β_0. This is accomplished by letting[1]

$$\varphi_1 = \beta_1 f_1,\ \varphi_2 = \beta_1^2 f_{11} + \beta_2 f_2,$$
$$\varphi_3 = \beta_1^3 f_{111} + \beta_1\beta_2 f_{12} + \beta_3 f_3, \text{ etc.} \tag{13}$$

The governing differential equations for the functions f can be obtained as follows: letting

$$L_n(f) = f''' + (n - 2\beta_0)\varphi_0' f' - n\,\varphi_0'' f \tag{14}$$

the following differential equations for the functions result [by using Eqs. (9), (13) and (14)]:

$$\left.\begin{aligned} n = 1, \quad & L_1(f_1) = \varphi_0'^2 - 1; \\ n = 2, \quad & L_2(f_2) = \varphi_0'^2 - 1, \\ & L_2(f_{11}) = (\beta_0 - 1)f_1' + 2\varphi_0' f_1'^2 + f_1 f_1'', \text{ etc.} \end{aligned}\right\} \tag{15}$$

The boundary conditions for all the functions f are

$$f(0) = f'(0) = f'(\infty) = 0 \tag{16}$$

The class of outer velocity distributions corresponding to Eq. (7) can be easily obtained from Eqs. (1), (5), and (7). Eqs. (5) and (7) give

$$U_\infty(\xi) = U_0 \exp\left[-\int_{\xi_0}^{\xi} (\beta(\xi)/\xi)d\xi\right] =$$
$$\bar{U}\xi^{-\beta_0} \exp\left[-\sum_{n=1}^{\infty} \beta_n \xi^n/n\right],\ \bar{U} = \text{const.} \tag{17}$$

It follows from Eqs. (1) that

$$d\xi/dx = -U_\infty \xi/\nu \tag{18}$$

therefore, Eqs. (17) and (18) give

$$x = \xi^{\beta_0} \sum_0^\infty a_n\, \xi^n \tag{19}$$

or[2]

$$\xi = x^{1/\beta_0} \sum_0^\infty b_n\, x^{n/\beta_0} \tag{20}$$

Combination of Eqs. (17) and (20) leads to the desired expression for $U_\infty(x)$—i.e.,

$$U_\infty(x) = x^{-1} \Sigma\, c_n\, x^{n/\beta_0}, \qquad c_0 \neq 0 \tag{21}$$

References

[1] Görtler, H., *A New Series for the Calculation of Laminar Boundary Layer Flows*, J. Math. & Mech., Vol. 6, No. 1, pp. 1–66, January, 1957.

[2] Bromwich, T. J. I., *An Introduction to the Theory of Infinite Series*, 2nd Ed., pp. 156–158, Macmillan and Co., London, 1947.

On the Supersonic Flutter of Two-Dimensional Infinite Panels

John W. Miles* and William P. Rodden**
University of California at Los Angeles, and North American Aviation, Inc., Respectively

October 16, 1958

SUPERSONIC FLUTTER of infinite, flat panels on two-dimensional periodic supports was studied originally by Hedgepeth, Budiansky, and Leonard.[1] Miles,[2] comparing their results with those for an infinite *unsupported* panel, questioned several of their basic assumptions. Leonard and Hedgepeth[3] then offered further justification of these assumptions on the basis of a "static air force approximation." The problem has since been reviewed by Rodden.[4] The primary purpose of this note is to emphasize that much of the apparent conflict among the discussions of references 1–3 may be resolved by distinguishing between (α) *single-degree-of-freedom instability* and (β) *coupled-mode instability*.

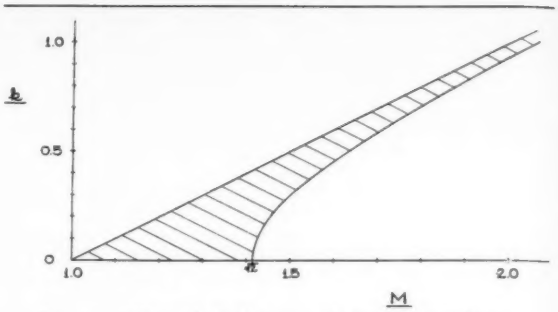

FIG. 1. Region of single-degree-of-freedom instability.

To define our terms, let the panel motion $w(\mathbf{r}, t)$ be approximated by a set of N *primitive modes* $w_n(\mathbf{r})$ according to

$$w(\mathbf{r}, t) = \sum_1^N A_n(t)\, w_n(\mathbf{r}) \tag{1}$$

let $\bar{a}_n$ denote the Laplace (or Fourier) transform of a_n, and let the equations of motion be reduced to the algebraic set

$$\sum_1^N c_{mn} a_n = 0\ (m = 1, \ldots, N) \tag{2}$$

by any of the usual methods—e.g., Galerkin's; the character of the permissible motions then will be determined by the N eigenvalues (usually complex frequencies) for which the determinant of c_{mn} vanishes—viz., $|c_{mn}| = 0$. If the motion determined by the (single-degree) approximation $c_{nn} = 0$ is unstable, we define the instability as type α, while if the primitive motions corresponding to each of two or more modes are stable but the resulting, coupled motion is unstable, we define the instability as type β. To be sure, these definitions—although mutually exclusive—are not comprehensive, but we may cover all possibilities in the designation (N, P, R), where P denotes the number of primitive modes that are unstable and R the resulting number of unstable eigenvalues for the coupled set; types α and β then are (1, 1, 1) and (N, O, R) with $N \geq 2$ and $R \geq 1$. We remark that the coupling of two or more unstable modes may yield only stable motions; e.g., (2, 2, 0); but then it seems likely that an improved approximation based on a greater number of modes would yield unstable motions. We also remark that if N is too small β-instability may be predicted where, in fact, it cannot exist.

The instability considered in reference 2 is associated with a harmonic, traveling wave (waves of different wave number being uncoupled) and is, therefore, type α. The analysis of reference 3, on the other hand, rules out α-instability *a priori* by its neglect of aerodynamic damping; accordingly, it can predict only β-instability.

It is established in reference 4 that a *necessary* condition for α-instability of the fundamental mode $\sin(\pi x/c)$ is

$$(k + 1)^2 < M^2 < k^2 + 1 + \sqrt{4k^2 + 1} \tag{3}$$

where $k = \omega c/\pi a$, M = Mach Number, ω = angular frequency, c = support spacing, and a = sonic velocity; the k, M region described in Eq. (3) is shaded in Fig. 1. We emphasize, however, that Eq. (3) is not *sufficient* for α-instability, since the allowable values of k depend on the equations of motion; moreover, the linearized aerodynamic theory breaks down as $k \to M - 1$ (but the equations of motion may bound k away from $M - 1$ in such a way as to prevent this breakdown—e.g., reference 2). Similar boundaries may be established for other modes,[4] and we conclude that α-instability is especially likely in (although not restricted to) $1 < M < \sqrt{2}$ if $k < M - 1$.

The analysis of reference 4 achieves an explicit stability boundary for a two-mode analysis of a periodically supported panel

* Professor of Engineering, University of California at Los Angeles, and Consultant, Thompson Ramo Wooldridge Inc.

** Research Specialist, Vibration and Flutter, North American Aviation, Inc., Los Angeles, and Lecturer in Engineering, University of California at Los Angeles.

by neglecting the (still) air beneath the panel (see Nelson and Cunningham[5] with regard to this approximation). The results are in agreement with those of reference 1 but permit rather more insight by virtue of their greater simplicity; in particular, they demonstrate that the second stability boundaries of Fig. 9, reference 1, correspond to transition to a stable motion of type (2, 2, 0), thereby affording a probable explanation for the destabilizing effect of structural damping (but, as noted above, these second loops are not likely to be significant approximations).

An analysis of a two-bay continuous panel at $M = 1.56$ and 2.00 also is presented in reference 4 and tends to support the choice of modes for the periodically supported panel in reference 1, the spectra of the two configurations being somewhat similar. The mean stiffness requirement found at $M = 1.56$ and 2.00 was

$$\{[B/(1-\nu)]\,(E/q)\}^{1/3}\,(t/c) = 0.5156 \qquad (4)$$

where $B = (M^2-1)^{1/2}$, ν = Poisson's ratio, E = Young's modulus, q = dynamic pressure, and t = panel thickness. At $M = 1.3$ and $\sqrt{2}$, on the other hand, α-instability was found and no stability boundary obtained. The detailed analysis of this configuration will be published following the completion of a similar investigation for a four-bay panel, for which the frequency spectrum more closely resembles that of the periodically supported panel.

We conclude that the problem of single degree of freedom instability warrants further investigation, especially with respect to the approximation of two-dimensional flow.[6]

References

[1] Hedgepeth, John M., Budiansky, Bernard, and Leonard, Robert W., *Analysis of Flutter in Compressible Flow of a Panel on Many Supports*, Journal of the Aeronautical Sciences, Vol. 21, No. 7, pp. 475–486, July, 1954.

[2] Miles, John W., *On the Aerodynamic Instability of Thin Panels*, Journal of the Aeronautical Sciences, Vol. 23, No. 8, pp. 771–780, August, 1956.

[3] Leonard, Robert W., and Hedgepeth, John M., *On the Flutter of Infinitely Long Panels on Many Supports*, Journal of the Aeronautical Sciences, Readers' Forum, Vol. 24, No. 5, pp. 381–383, May, 1957.

[4] Rodden, William P., *The Flutter of Two-Dimensional Flat Panels with Equally Spaced Supports in a Supersonic Flow*, Ph.D. Thesis, University of California, Los Angeles, October 1, 1957.

[5] Nelson, Herbert C., and Cunningham, Herbert J., *Theoretical Investigation of Flutter of Two-Dimensional Flat Panels with One Surface Exposed to Supersonic Potential Flow*, NACA TN 3465, July, 1955.

[6] Luke, Y. L., and St. John, A. D., *Panel Flutter at Supersonic Speeds*, Midwest Research Institute Report under Contract AF 33(616)-2897, October 31, 1956.

A Note on Blast-Wave Theory

Harvey Einbinder
Consultant, Advanced Electronics Center, Light Military Electronic Equipment Department, General Electric Company, Ithaca, N. Y.

October 21, 1958

BLAST-WAVE THEORY, first developed by G. I. Taylor[1] to describe the shock wave produced by an atomic explosion, has been applied to the flow about slender blunt-nosed bodies traveling at hypersonic velocities. As Hayes[2] has shown, the equations of this theory are equivalent to those of hypersonic small-disturbance theory. The theory is valid for distances downstream that are not too close to the stagnation region but where the strong-shock conditions hold. It is, therefore, suitable for analyzing the inviscid flow that occurs outside the boundary layer along the body. The simplicity of the theory is due to the assumption of flow similarity, which requires that the variation in the transverse flow field be independent of the distance downstream. When this assumption is satisfied, the equations of motion can be reduced to ordinary differential equations, whose solution is much simpler than the more general equations.

Of special interest is the case of constant energy release which corresponds to a blunt-nosed body of constant drag, such as a hemispherically-capped cylinder, where the drag of the body provides the transverse velocity field. For this case, the equations of motion were first integrated numerically by Lin.[3] Recently they have been integrated analytically by Kubota,[4] by following the procedure of Latter,[4] who solved the equations for the spherical blast wave.

The purpose of this note is to draw attention to some of the consequences that can be derived from Kubota's analytic solution. According to his solution for the axially symmetric case,

$$\phi = sz \qquad (1)$$

$$F = \{[\alpha(\gamma\phi - z)^{\gamma-1}]/[z(z-\phi)\phi^{2(\gamma-1)}]\}^{1/\beta} \quad \text{where} \begin{cases} \alpha = 2^{\gamma}(\gamma-1)/(\gamma+1)^{\gamma+1} \\ \beta = 2-\gamma \end{cases} \qquad (2)$$

$$\psi = \{\epsilon(\gamma\phi - z)/z(z-\phi)\phi^{2}\}^{1/\beta} \quad \text{where } \epsilon = 4(\gamma-1)^{\gamma-1}/(\gamma+1)^{\gamma+1} \qquad (3)$$

where ϕ, F, and ψ are dimensionless variables that represent the

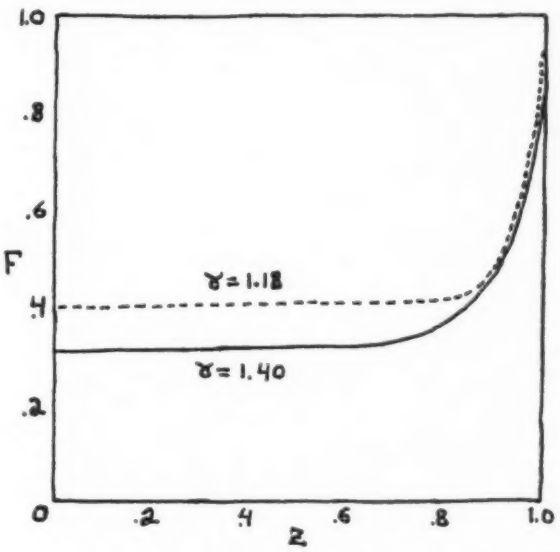

FIG. 1. The transverse variation of the pressure.

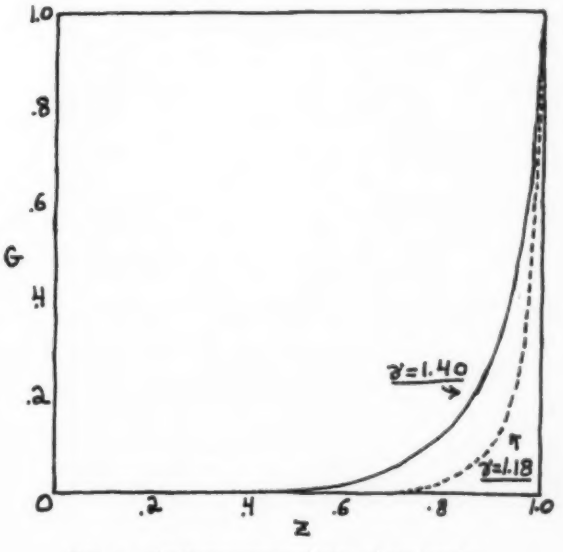

FIG. 2. The transverse variation of the density.

transverse variation of the velocity, pressure, and density, respectively. $\gamma = C_p/C_v$, s is an auxiliary variable, and $z = y/R$, where y is the transverse distance from the axis of the body and R is the distance to the shock front. When $0 \leq z \leq 1$, then $1/\gamma \leq s \leq 2/(\gamma + 1)$. The variable s is defined implicitly by the equation

$$z = \sqrt{\zeta}[\gamma s - 1)/\sigma_m]^{(\gamma - 1)2\gamma} \tag{4}$$

where $\zeta = 4/[(\gamma + 1)^2 s(2 - \gamma s)]$ and $\sigma_m = (\gamma - 1) \div (\gamma + 1)$

The expressions for F and ψ can be simplified by expressing them in terms of s by eliminating ϕ and z with the aid of Eqs. (1) and (4). Thus,

$$F = s\{[(\gamma - 1)(2 - \gamma s)]/[2(1 - s)]\}^{\gamma/(2 - \gamma)} \tag{5}$$

$$G = (F/s)^{2/\gamma}\,[(\gamma s - 1)/\sigma_m]^{1/\gamma} \tag{6}$$

where $G = \sigma_m \psi$, so that at the shock front where $z = 1$, $G = 1$ and $F = 2/(\gamma + 1)$. These functions are shown in Figs. 1 and 2 for $\gamma = 1.40$ and $\gamma = 1.18$, corresponding to normal and dissociated air, respectively. It can be seen from these figures that there is a slow decrease in the pressure, F, in going from the shock toward the body. In contrast, there is an exceedingly rapid decrease in G, the density. The form of this decrease can be exhibited explicitly by means of an approximate formula for G valid when $z < 0.8$.

When $z = 1$, $\sqrt{\zeta} = 1$, while when $z = 0$, $\sqrt{\zeta} = 2\sqrt{\gamma}/(\gamma + 1) \approx 1$. Therefore, $\sqrt{\zeta}$ can be replaced by unity in Eq. (4). Using this equation to eliminate $(\gamma s - 1)/\sigma_m$ in Eq. (6), and replacing F/s by its value at $z = 0$, yields the desired expression for G.

$$G \approx (\gamma/2)^{2/(2 - \gamma)}\, z^{2/(\gamma - 1)} \quad (z \lesssim 0.8) \tag{7}$$

Now the exponent of z in this equation, $2/(\gamma + 1)$, will be large. For $\gamma = 1.40$, it equals 5, while for hypersonic flow where γ is closer to unity, it will be even larger. Thus, when $\gamma = 1.18$, G varies as the eleventh power of z. This extreme variation in the density between the shock front and the body does not seem plausible. Furthermore, as γ approaches unity, the exponent tends toward infinity so that the solution breaks down.

The rapid decrease in the density implies a corresponding increase in the temperature since by the equation state, $T \sim P/\rho \sim F/G$. Thus, according to blast-wave theory there is a very low-density, high-temperature layer in the inviscid flow just outside the boundary layer.

The solution for the flow field which has been obtained is based on a constant γ, which is reasonable as long as the flow does not depend critically on the value of γ. However, according to the theory, the density and the temperature are very sensitive to the value of γ in the hypersonic regime. Therefore, it is not justified to neglect its variation with temperature.

Kubota[4, 6] has attempted to confirm blast-wave theory by measuring the shape of the shock front and the pressure along the surface of a hemispherically-capped cylinder for $M = 7.7$. However, these quantities are relatively insensitive predictions of the theory. Consequently, such measurements do not provide a very adequate test of the theory.

Because of the complex interaction that occurs between the body and the shock front, blast-wave theory fails to provide an adequate description of the hypersonic flow about blunt-nosed slender bodies. The presence of such interaction is demonstrated by the characteristic lines which are reflected a number of times between the body and the shock front in passing from the stagnation region downstream. This is the primary cause of the failure of blast-wave theory.

References

[1] Taylor, G. I., *The Formation of a Blast Wave by a Very Intense Explosion Part I. Theoretical Discussion. Part II. The Atomic Explosion of 1945*, Proc. Royal Soc. (A), Vol. 201, pp. 159–186, March, 1950.

[2] Hayes, W. D., *On Hypersonic Similitude*, Quart. Appl. Math., Vol. 5, No. 1, pp. 105–106, April, 1947.

[3] Lin, S. C., *Cylindrical Shock Waves Produced by Instanteneous Energy Release*, J. Appl. Physics, Vol. 25, No. 1, pp. 54–57, January, 1954.

[4] Kubota, T., *Investigation of Flow Around Simple Bodies in Hypersonic Flow*, GALCIT Memo. No. 40, Calif. Inst. Tech., June 25, 1957.

[5] Latter, R., *Similarity Solution for a Spherical Shock Wave*, J. Appl. Physics, Vol. 26, No. 8, pp. 954–960, August, 1955.

[6] Lees, L., and Kubota, T., *Inviscid Hypersonic Flow Over Blunt-Nosed Slender Bodies*, Journal of the Aeronautical Sciences, Vol. 24, No. 3, pp. 195–202, March, 1957.

Errata—"Some Panel-Flutter Studies Using Piston Theory"*

David J. Johns

Department of Aircraft Design, The College of Aeronautics, Cranfield, Bletchley, Bucks., England

January 20, 1959

I WOULD LIKE to point out an omission and an error in my recent paper.

On page 681, the definition of $p_n(x)$ should be: $p_n(x) = p_{(x,\,t)}e^{-i\omega t}/\rho c\omega^2$ with Z replaced by Z_n in $P_{x,t}$.

On page 684, the values of $2qc^3/MD$ in Fig. 5 should be factored by $(80\sqrt{3}/9)$.

* Johns, David John, *Some Panel-Flutter Studies Using Piston Theory*, Journal of the Aero/Space Sciences, Vol. 25, No. 11, pp. 679–684, 715, November, 1958.

Midwestern Conference on Fluid and Solid Mechanics

University of Texas, September 9–11, 1959

Although the Conferences are held on a regional basis, there are no restrictions on attendance or on the residence of authors of technical papers.

Abstracts and titles of proposed papers should be submitted before April 1, 1959, to the Chairman: *Dr. Milton J. Thompson, Professor of Aeronautical Engineering, University of Texas.* Complete manuscripts will be required by June 1, 1959, to make possible the distribution of the Proceedings at the opening of the Conference. Inquiries concerning other details of the Conference should also be addressed to Professor Thompson.

A number of technical societies and research organizations, including the IAS, have joined with The University of Texas in cosponsoring this Midwestern Conference.

REQUIREMENTS *for* CONTRIBUTIONS
to the publications of the
INSTITUTE *of the* AERONAUTICAL SCIENCES

The Institute of the Aeronautical Sciences invites both members and nonmembers from any country to submit papers for publication in the JOURNAL OF THE AERO/SPACE SCIENCES and AERO/SPACE ENGINEERING. The Institute, following the practice of other societies, does not pay for contributions.

The following directions for the preparation of papers, if followed by authors, will save correspondence, avoid the return of papers for changes, minimize the work of preparation for the printer, and save the expense due to the charges made for "author's corrections."

MANUSCRIPTS: The original typewritten copy of the paper is desired. **To expedite review, an additional copy of both the manuscript and figures should be submitted.** The manuscript must be double or triple spaced on one side of white paper sheets, consecutively numbered. There should be wide margins to allow for the marking of directions to the printer. Correcting, changing, or adding to papers after they are in type is costly. It is, therefore, imperative that papers submitted be in final form. Typographical errors may be corrected on proofs, but if authors wish to add material, they may do so at their own expense. In mailing, drawings may be rolled, but manuscripts should be sent flat. Send by first-class mail (register if you wish for your own protection) to the Editorial Office, Institute of the Aeronautical Sciences, 2 East 64th Street, New York 21, N.Y. All manuscripts will be examined by the Editorial Committee and by the Editor. Authors will be advised as promptly as possible whether the paper is acceptable for publication.

TITLES: The title of the paper should be brief. The name and initials of the author should be written as he prefers. The use of the full name of an author is advocated because of the frequent duplication of initials and surnames which sometimes makes it difficult to establish the identity of the author. This is particularly important for large annual indexing and abstracting services. All titles and degrees or honors are omitted. The name of the organization with which the author is associated should be placed after his name on a separate line. The date on which the paper is received will be inserted by the Editor. The author's title or position should be indicated in a footnote.

SUMMARIES OR ABSTRACTS: An abstract to be printed at the beginning should accompany each article. It should be adequate as an *index* and as a *summary*. It should contain a statement of major conclusions reached, since summaries in many cases constitute the only source of information used in compiling scientific reference indexes. Abstracts printed in other journals, especially foreign, in most cases consist of summaries from printed papers. The summary should explain as adequately as possible the major conclusions to a nonspecialist in the subject and should contain from 100 to 300 words, depending on the length of the paper.

SUBHEADINGS: Subheadings should be inserted by the author at frequent intervals. The work of editorial preparation will be simplified by the author's provision of many subheadings.

MATTER USUALLY DELETED: Photographs or illustrations of little technical interest and not showing advances in general practice. Too detailed tabular matter (general results of such tables may be included in the text). Lengthy descriptions of materials or processes or of preliminary experiments or theories that preceded final results; salient features only are of interest.

REFERENCES: References should be numbered consecutively and grouped together at the end of the manuscript, with only the corresponding number being mentioned in the text. The arrangement should be as follows. For books: [1] Durand, W. F., *Aerodynamic Theory*, 1st Ed., Vol. 1, p. 23; Julius Springer, Berlin, 1934. For magazines: [1]England, C. R., Crawford, A. B., and Mumford, W. W., *Some Results of a Study of Ultra-Short-Wave Transmission Phenomenon*, Proc. IRE, Vol. 20, No. 12, pp. 481–482, March, 1933. Please give author, title, edition, volume, number, page, publisher, and place and date of publication as indicated. Omission of one required fact causes much extra editorial work and possible inaccuracies.

ILLUSTRATIONS: Illustrations should accompany manuscripts, and each should always be referred to in the text by number. Drawings or graphs should not be larger than 12 × 16 inches, and must be made with jet black India ink on white paper or tracing cloth, the latter being preferred. *Do not use typewriter for lettering.* The smallest lettering on 8 × 10 inch figures should be no less than $^1/_4$ inch high. Cross-section paper (white with black lines) may be used, but it should not have more than 4 lines per inch. If finer ruled paper is used, the major division lines should be drawn in with black ink, omitting the finer divisions. In the case of finely ruled paper, only blue-lined paper can be accepted. *Tracing paper and blueprints* are not acceptable. Lettering and all markings must be large enough to be readable after reduction to single-column width ($3^3/_{16}$ in.). Mail rolled or flat; never fold. Drawings that cannot be reproduced (including pencil drawings) will be returned to the author for redrawing, thus delaying publication of the paper. Photographs should be distinct and show clear black and white contrasts. They must be on glossy white paper. Avoid round and oval photographs.

CAPTIONS AND LEGENDS: Legends or captions must accompany each drawing or photograph submitted. If written on the drawing or photograph, they should be placed below and well outside the part to be reproduced. Each table should have a caption such as Table 1, Table 2, Table 3, etc. Captions should be complete in themselves so as to make the data intelligible to the reader without reference to the text. A duplicate list of captions for figures should be included as the last page of the manuscript. Use "Fig. 1" (not Figure 1), "Figs. 3 and 4," etc., in both the text and the numbering of illustrations. In the text, "Eq. (1)" or "Eqs. (1) and (2)" is used, not "Equation (1)." In captions, legends, and in table headings, write all words in full; do not abbreviate, except for "Fig." and "Eq."

MATHEMATICAL WORK: Formulas may be typewritten or carefully written in pen and ink, the writing to be large enough so that it can be marked for the printer. Considerable space for marking should be allowed above and below all equations. All complicated equations should be repeated on separate sheets with plenty of space left for marking. The solidus should be used for simple fractions appearing within the text. Make all expressions clear to the typesetter. Greek letters used in formulas should be clearly designated by name in the margin of the manuscript. The difference between capital and lower-case letters should be clearly distinguished and care taken to avoid confusion between zero (0) and the letter (o), between the numeral (one) and the letter (ell) and the prime (′), between alpha and a, kappa and k, u and mu, v and nu, n and eta. All subscripts and exponents should be clearly distinguished. Avoid complicated exponents and subscripts. Dots and bars over letters or mathematical expressions should also be avoided. When it is necessary to repeat a complicated expression, it should be represented by some convenient symbol.

SYMBOLS AND ABBREVIATIONS: The symbols recommended in the American Standard Association "Letter Symbols for Aeronautical Sciences," ASA Y10.7—1954, should be used wherever practicable. All symbols should be clearly written and carefully checked. Standard abbreviations should be used, and it should be noted that most abbreviations are lower case, such as m.p.h., b.m.e.p., i.h.p., b.hp., hp., etc.

Corporate Members

OF THE

Institute of the Aeronautical Sciences

AC SPARK PLUG DIVISION, GENERAL MOTORS CORPORATION
ACADEMY OF AERONAUTICS
ADAMS RITE MANUFACTURING COMPANY
AEROJET-GENERAL CORPORATION
AEROLAB DEVELOPMENT COMPANY
AERONCA MANUFACTURING CORPORATION
AERONUTRONIC SYSTEMS, INC.
AEROQUIP CORPORATION
AGAWAM AIRCRAFT PRODUCTS, INC.
ALLIED RESEARCH ASSOCIATES, INC.
ALLIS-CHALMERS MANUFACTURING COMPANY
ALLISON DIVISION, GENERAL MOTORS CORPORATION
ALUMINUM COMPANY OF AMERICA
AMERICAN AIRLINES, INC.
AMERICAN BOSCH ARMA CORPORATION
AMERICAN NON-GRAN BRONZE COMPANY
AMERICAN STEEL & WIRE DIVISION, UNITED STATES STEEL CORPORATION
AMOCO CHEMICALS CORPORATION
AMPHENOL-BORG ELECTRONICS CORPORATION
ANDERSON, GREENWOOD & CO.
ARDE ASSOCIATES
ASSOCIATED AVIATION UNDERWRITERS
AVCO RESEARCH LABORATORY
AVIEN, INC.
AVRO AIRCRAFT LIMITED
BAKER STEEL & TUBE COMPANY
BEECH AIRCRAFT CORPORATION
BELL AIRCRAFT CORPORATION
BENDIX AVIATION CORPORATION
THE BG CORPORATION
BOEING AIRPLANE COMPANY
BOOZ, ALLEN & HAMILTON
THE BRISTOL AEROPLANE COMPANY (U.S.A.) INC.
BULOVA RESEARCH AND DEVELOPMENT LABORATORIES, INC.
CANADAIR, LTD.
THE CESSNA AIRCRAFT COMPANY
CHANCE VOUGHT AIRCRAFT, INCORPORATED
THE CHASE MANHATTAN BANK
CHICAGO AERIAL INDUSTRIES, INC.
THE CLEVELAND PNEUMATIC INDUSTRIES, INC.
CONSOLIDATED CONTROLS CORPORATION
CONTINENTAL MOTORS CORPORATION
CORNELL AERONAUTICAL LABORATORY, INC.
CURTISS-WRIGHT CORPORATION
THE DECKER CORPORATION
DEL MAR ENGINEERING LABORATORIES
DELCO-REMY DIVISION, GENERAL MOTORS CORPORATION
DOAK AIRCRAFT COMPANY, INC.
DOUGLAS AIRCRAFT COMPANY, INC.
DZUS FASTENER COMPANY, INC.
EASTERN AIR LINES, INC.
EDO CORPORATION
ELASTIC STOP NUT CORPORATION OF AMERICA
ELECTROL INCORPORATED
ENGINEERING SUPERVISION COMPANY
ESSO STANDARD OIL COMPANY
FAIRCHILD CAMERA AND INSTRUMENT CORPORATION
FAIRCHILD ENGINE AND AIRPLANE CORPORATION
THE FIRESTONE TIRE & RUBBER COMPANY
THE GARRETT CORPORATION
GENERAL DYNAMICS CORPORATION
GENERAL ELECTRIC COMPANY
GENERAL PRECISION EQUIPMENT CORPORATION
G. M. GIANNINI & CO., INC.
GIANNINI PLASMADYNE CORPORATION
THE B. F. GOODRICH COMPANY
GOODYEAR AIRCRAFT CORPORATION
GRUMMAN AIRCRAFT ENGINEERING CORPORATION
HYDRO-AIRE, INC.
INSURANCE COMPANY OF NORTH AMERICA COMPANIES
INTERNATIONAL BUSINESS MACHINES CORPORATION
THE INTERNATIONAL NICKEL COMPANY, INC.
ITT LABORATORIES, DIVISION OF INTERNATIONAL TELEPHONE AND TELEGRAPH CORPORATION
JANITROL AIRCRAFT DIVISION, SURFACE COMBUSTION CORPORATION
JOHNS-MANVILLE SALES CORPORATION
EARLE M. JORGENSEN CO.
KELSEY-HAYES COMPANY
WALTER KIDDE & COMPANY INC.
KOLLSMAN INSTRUMENT CORPORATION
KOPPERS COMPANY, INC. SOUND CONTROL DEPARTMENT
LAVELLE AIRCRAFT CORPORATION
LEAR, INCORPORATED
C. W. LEMMERMAN, INC.
LIBRASCOPE, INCORPORATED
THE LIQUIDOMETER CORPORATION
LOCKHEED AIRCRAFT CORPORATION
LOEWY-HYDROPRESS DIVISION OF BALDWIN-LIMA-HAMILTON CORPORATION
LONGINES-WITTNAUER WATCH COMPANY, INC.
MARQUARDT AIRCRAFT COMPANY
THE MARTIN COMPANY
MARTIN STEEL PRODUCTS CORPORATION
McDONNELL AIRCRAFT CORPORATION
MELETRON CORPORATION
MID-CONTINENT MANUFACTURING, INC.
MINNEAPOLIS-HONEYWELL REGULATOR COMPANY
NATIONAL CREDIT OFFICE, INC.
NORTH AMERICAN AVIATION, INC.
NORTHROP CORPORATION
NUCLEAR DEVELOPMENT CORPORATION OF AMERICA
PAN AMERICAN WORLD AIRWAYS, INC.
THE RALPH M. PARSONS COMPANY
PESCO PRODUCTS DIVISION, BORG-WARNER CORPORATION
PHILLIPS PETROLEUM COMPANY
PIASECKI AIRCRAFT CORPORATION
RADIO CORPORATION OF AMERICA DEFENSE ELECTRONIC PRODUCTS
REPUBLIC AVIATION CORPORATION
ROHR AIRCRAFT CORPORATION
PAUL ROSENBERG ASSOCIATES
RYAN AERONAUTICAL COMPANY
SANDBERG-SERRELL CORPORATION
SHAFER BEARING DIVISION, CHAIN BELT COMPANY
SHELL OIL COMPANY
SIMMONDS AEROCESSORIES, INC.
SOCONY MOBIL OIL COMPANY, INC.
SOLAR AIRCRAFT COMPANY
SOUTHWEST PRODUCTS CO.
R. DIXON SPEAS ASSOCIATES
SPERRY GYROSCOPE COMPANY DIVISION OF SPERRY RAND CORPORATION
STANDARD OIL COMPANY OF CALIFORNIA
STANDARD OIL COMPANY (INDIANA)
STANDARD-THOMSON CORPORATION CLIFFORD MANUFACTURING DIVISION
STANLEY AVIATION CORPORATION
THIOKOL CHEMICAL CORPORATION
THOMPSON RAMO WOOLDRIDGE INC.
TRANS WORLD AIRLINES, INC.
TURBO PRODUCTS, INC.
UNION CARBIDE CORPORATION
UNITED AIR LINES, INC.
UNITED AIRCRAFT CORPORATION
UNITED STATES AVIATION UNDERWRITERS, INC.
VARD, INC.
VERTOL AIRCRAFT CORPORATION
VITRO CORPORATION OF AMERICA
WESTERN GEAR CORPORATION
WESTINGHOUSE ELECTRIC CORPORATION
WESTON INSTRUMENTS DIVISION OF DAYSTROM, INC.
WYMAN-GORDON COMPANY
YOUNG RADIATOR COMPANY